Department of Materials Science and Engineering

The reaction mechanism and operating window for the decomposition of hydrated magnesium sulfate under reducing conditions

Madeleine Scheidema

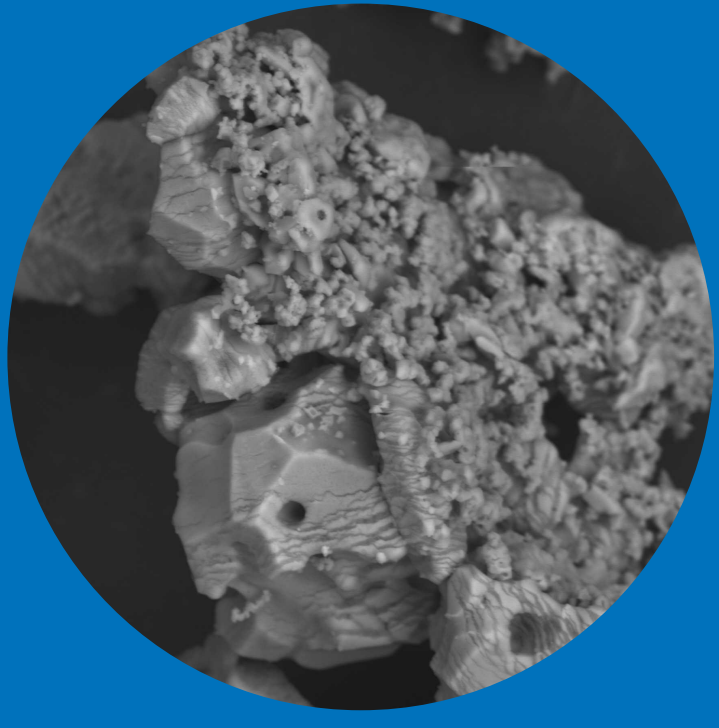

Aalto University

DOCTORAL DISSERTATIONS

Aalto University publication series
DOCTORAL DISSERTATIONS 120/2015

The reaction mechanism and operating window for the decomposition of hydrated magnesium sulfate under reducing conditions

Madeleine Scheidema

A doctoral dissertation completed for the degree of Doctor of Science (Technology) to be defended, with the permission of the Aalto University School of Chemical Technology, at a public examination held at the lecture hall V1 of the school on 16 October 2015 at 12.

Aalto University
School of Chemical Technology
Department of Materials Science and Engineering
Metallurgical Thermodynamics and Modelling

Supervising professor
Professor Pekka Taskinen

Thesis advisor
Dr. Maija-Leena Metsärinta

Preliminary examiners
Professor Caisa Samuelsson, Luleå University of Technology, Sweden
Professor Tomáš Havlík, Technical University of Kosice, Slovakia

Opponent
Professor Emeritus Ilkka Turunen, Lappeenranta University of Technology, Finland

Aalto University publication series
DOCTORAL DISSERTATIONS 120/2015

ISBN 978-952-60-6346-1 (printed)
ISBN 978-952-60-6347-8 (pdf)
ISSN-L 1799-4934
ISSN 1799-4934 (printed)
ISSN 1799-4942 (pdf)
http://urn.fi/URN:ISBN:978-952-60-6347-8

Unigrafia Oy
Helsinki 2015

Finland

441 697
Printed matter

Aalto University

Abstract

Aalto University, P.O. Box 11000, FI-00076 Aalto www.aalto.fi

Author
Madeleine Scheidema

Name of the doctoral dissertation
The reaction mechanism and operating window for the decomposition of hydrated magnesium sulfate under reducing conditions

Publisher School of Chemical Technology

Unit Department of Materials Science and Technology

Series Aalto University publication series DOCTORAL DISSERTATIONS 120/2015

Field of research Metallurgy

Manuscript submitted 2 June 2015 **Date of the defence** 16 October 2015

Permission to publish granted (date) 26 August 2015 **Language** English

☒ **Monograph** ☐ **Article dissertation (summary + original articles)**

Abstract

Magnesium compounds commonly occur in ores that are treated hydrometallurgically for the recovery of valuable metals. The metals of interest can be recovered by pH control, using a neutralizing agent. Magnesium sulfate remains in the waste leach solution when sulfuric acid is used as the leaching medium. The magnesium sulfate can be crystallized from the solution and decomposed into magnesium oxide and sulfur dioxide. The magnesium oxide can be utilized as a neutralizing agent, thus avoiding the need for additional materials such as lime, in the process, whereas the sulfur dioxide can be used for the production of sulfuric acid, which is then used for leaching of the ore.

The decomposition of magnesium sulfate is a strongly endothermic reaction, but the decomposition temperature can be lowered by using a reducing agent. The effect of different reductants on the decomposition mechanism of magnesium sulfate and on the operating window for decomposition of magnesium sulfate was tested experimentally. Sulfur was used as the main reductant in the experimental work, as it does not produce any carbon-containing off gases; carbon and carbon monoxide were used for comparison. The main equipment for the experimental work was a fluidized bed reactor, as the heat and mass transfer rates are high in this type of reactor. The intermediate samples and products were analyzed using XRD analysis, total sulfur analysis and extensive SEM/EDS analysis of both powder samples as well as polished sections.

Several factors affecting the reaction kinetics were tested and evaluated, including temperature, the type of magnesium sulfate raw material, amount of reductant, particle size and the presence of minor amounts of manganese sulfate, iron sulfate, and calcium sulfate. It was found that sulfur as the reductant not only strongly increases the reaction rate, but that it also forms a protective magnesium oxide layer around the magnesium sulfate particles, which prevents fluidization problems. A clear reaction front was observed for the majority of the particles with SEM/EDS analysis. Kinetic model fitting showed that the rate-controlling step with magnesium sulfate monohydrate and sulfur as the reductant was chemical reaction control at the unreacted interface, and the control shifted to ash layer diffusion control when dried magnesium sulfate heptahydrate was used instead. Gas film diffusion was found to be the rate-controlling step with carbon and carbon monoxide as the reductant, due to carbon deposition on the surface of the particles.

Keywords Magnesium sulfate, decomposition, fluidized bed, reductant, kinetics

ISBN (printed) 978-952-60-6346-1 **ISBN (pdf)** 978-952-60-6347-8

ISSN-L 1799-4934 **ISSN (printed)** 1799-4934 **ISSN (pdf)** 1799-4942

Location of publisher Helsinki **Location of printing** Helsinki **Year** 2015

Pages 139 **urn** http://urn.fi/URN:ISBN:978-952-60-6347-8

Preface

The research work for this thesis has been carried out in the period 2010-2015, at the department of Materials Science, Metallurgical Thermodynamics and Modeling (TDM) research group and the experimental work has been carried out at the Outotec Research Center in Pori. The graduate school of Advanced Materials and Processes supported me financially and enabled the participation in courses and international conferences. The experimental work was supported by TEKES project 'Fluidisaatioteknologia – kiinteän tilan pasutusprosessit', as well as by Outotec.

Firstly, I would like to thank Professor Pekka Taskinen for his support and giving me the possibility to carry out the work at the Outotec Research Center. I would like to thank my thesis advisor Dr. Maija-Leena Metsärinta for her support and advice on the experimental work. I would also like to thank Dr. Jarkko Partinen for encouraging me to start with the PhD work. I would like to thank Dr. Satu Jyrkönen for her support, especially during the first years. I am thankful for the support I received at the Outotec Research Center in Pori, and special thanks to Karoliina Köykkä for carrying out the main part of the fluidized bed tests and Tuija Nieminen and Veikko Kukkonen for teaching me how to operate the scanning electron microscope. I would like to thank Prof. Dr. Markus Reuter for encouraging me to overcome the last difficulties in my work. Finally, I would like to thank Fred, who has taken the time to listen to me, read my thesis and helped me with the modeling part.

Pori, August 26, 2015

Madeleine Scheidema

Author's Contribution

The author had the responsibility for planning the work, interpretation of the results and writing the monograph, as well as the following publications and conference presentations, under the supervision of Prof. Pekka Taskinen and Dr. Maija-Leena Metsärinta:

Decomposition Thermodynamics of Magnesium Sulfate
Scheidema, Madeleine; Taskinen, Pekka
Industrial & Engineering Chemistry Research **2011**, *16*, 9550-9556

Reductive Decomposition of Magnesium Sulfate
Scheidema, Madeleine; Taskinen, Pekka, Metsärinta, Maija-Leena
EMC 2011, Düsseldorf 26-29.6.2011

Regeneration of Magnesium Sulfate by Decomposition
Scheidema, Madeleine; Taskinen, Pekka, Metsärinta, Maija-Leena
SRCR'11, Falmouth 10-12.5.2011 (published on conference CD only)

The experimental work was carried out at the Outotec Research Center in Pori, and it was planned and supervised by the author. The high-temperature experiments and analysis of the samples were carried out by personnel of the Research Center, but the author carried out all SEM/EDS analysis, after receiving training at the Outotec Research Center.

List of Abbreviations and Symbols

Abbreviations

EDS	Energy Dispersive X-ray Spectroscopy
FB	Fluidized Bed
FBR	Fluidized Bed Reactor
FTIR	Fourier Transform Infrared Spectroscopy
H, Heptahydrate	Magnesium sulfate heptahydrate (epsomite)
ICP	Inductively Coupled Plasma
M, Monohydrate	Magnesium sulfate monohydrate (kieserite)
MW	Molecular weight
R^2	R-squared, coefficient of determination
SATP	Standard Ambient Temperature and Pressure
SEM	Scanning Electron Microscope
SS	Sum of squares
St.	Stoichiometric requirement
STP	Standard Temperature and Pressure
TG/DSC	Thermogravimetry/Differential Scanning Calorimetry
XRD	X-Ray Diffraction

Symbols

A	Surface area [m^2]
g	Gas
k	Rate constant [s^{-1}]
K	Equilibrium constant [-]
M_P	Molecular weight of solid product [$gmol^{-1}$]

M_R	Molecular weight of solid reactant [$gmol^{-1}$]
RH	Relative Humidity [%]
s	Solid
t	Time [min]
T	Temperature [°C]
V	Volume [m^3]
X	Conversion fraction [-]
z	Ratio, with $z < 1$: porous; $z > 1$ non-porous
α	Stoichiometry factor [-]
ΔG	Gibbs free energy of reaction [kJ]
ΔH_f	Enthalpy of formation [$kJmol^{-1}$]
ΔH	Enthalpy of reaction [kJ]
ΔS	Entropy of reaction [JK^{-1}]
ρ_P	Density of solid product [kgm^{-3}]
ρ_R	Density of solid reactant [kgm^{-3}]
τ	Time for completion of the reaction [min]

Contents

1. Introduction

1.1 Background

Magnesium is the eighth most common element in the earth's crust and is found as compounds in seawater, brines, rocks, and minerals [1]. Ores or concentrates can contain high concentrations of magnesium compounds, such as magnesium oxide or magnesium carbonate. An example of a magnesium-rich ore is nickel laterite ore. Lateritic ores can be divided into different zones: overburden, limonite layer, transition layer, saprolite layer, and base rock [2]. The limonite layer is generally low in magnesium oxide (around 3%), the nickel content is 1-1.5% and the iron content is high, generally >40%, but limonite ores lower in iron exist as well. Saprolite ores are higher in magnesium oxide and nickel, but lower in iron, compared with limonite ore. The magnesium oxide content is around 25%, the nickel content 2-2.5%, and the iron content below 15%. [2, 3, 4]

One of the main leaching media in the hydrometallurgical route for recovery of the valuable metals from saprolite ore is sulfuric acid [3, 5]. The acid consumption tends to be high due to the high magnesium content of the ore [5, 6] and the waste leach solution tends to be high in dissolved magnesium. The waste sulfuric acid should be concentrated either by evaporation or by addition of strong sulfuric acid, so that the metals are precipitated from the solution. The magnesium sulfate that is crystallized from the solution is most likely to contain minor impurities, such as iron sulfate, manganese sulfate, and/or calcium sulfate. Under atmospheric conditions, magnesium sulfate will precipitate as heptahydrate [6, 7, 8]; the monohydrate form can be crystallized under elevated temperature and pressure [7].

Hydrated magnesium sulfate can either be dried first (in the case of heptahydrate) or decomposed directly into magnesium oxide and sulfur

dioxide, which can be used as a neutralizing agent in the leaching process and for the production of sulfuric acid, respectively. The advantage is that the waste products of the hydrometallurgical process are recycled internally instead of being disposed of, which also lowers the need for feed materials such as neutralizing agents and acid into the process. Not only is this beneficial from an economic point of view, it also reduces the environmental footprint of the plant. A general flowsheet to illustrate this process is shown in Figure 1. It is advantageous to use magnesium sulfate with low crystal water content as the feed material, as the energy requirement for decomposing the material will be lower and the sulfur dioxide content in the off-gas will be less diluted.

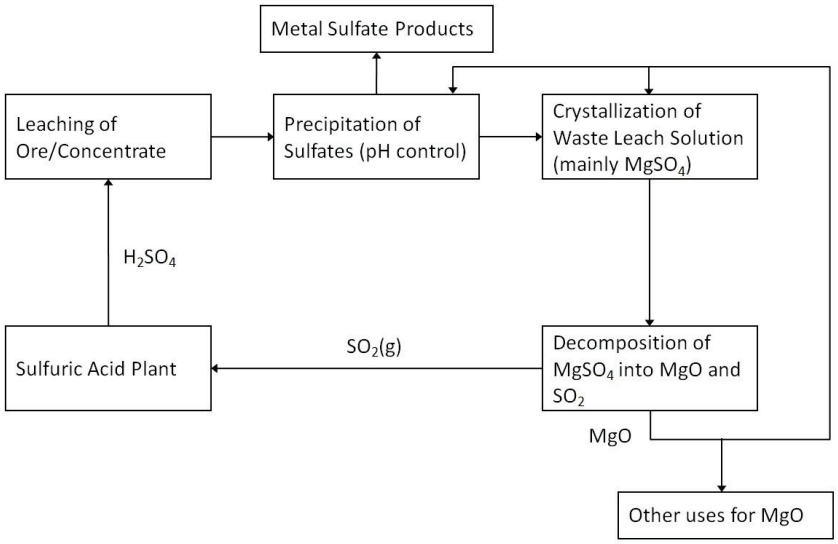

Figure 1. General flowsheet for a hydrometallurgical treatment process and the recycling of magnesium oxide and sulfur to the process.

Processes for the decomposition of magnesium sulfate from waste sulfuric acid solutions have been proposed [9, 10, 11], but the focus of these processes is on the production of sulfuric acid from the sulfur dioxide formed during the decomposition of magnesium sulfate. The quality of the magnesium oxide product was not considered in these processes. Recycling of the magnesium oxide would both reduce the volume of the waste stream and limit the need for additional substances into the leaching process [12, 13]. There are also other potential uses in addition to using the magnesium oxide as a neutralizing agent, for example for the production of refractory materials and for the

formation of magnesium chloride, which can be used to produce electrolytic magnesium.

1.2 Objectives and scope

This work concentrates on the part of the process where the crystallized magnesium sulfate is decomposed into magnesium oxide and sulfur dioxide. The aim is to decompose magnesium sulfate in the presence of a reductant so that a magnesium oxide product with low sulfur content is formed, which has a high surface area and an off-gas rich enough in sulfur dioxide for the production of sulfuric acid. The two main research questions are:

'How is the decomposition mechanism of $MgSO_4$ affected by the use of a reductant and does the mechanism depend on the choice of reductant?'

'What is the operating window for the decomposition of magnesium sulfate in the presence of different reductants?'

2. Theory

In this chapter, the properties of magnesium sulfate and its hydrates are described in section 2.1, which includes the stability of magnesium sulfate hydrates, different magnesium sulfate polymorphs, and the thermodynamic properties of magnesium sulfate. This section is followed by consideration of the decomposition of magnesium sulfate in section 0, including the decomposition reactions and kinetics of magnesium sulfate decomposition, together with the theory of fluidization.

2.1 Magnesium sulfate and its hydrates

2.1.1 Magnesium sulfate hydrates and their stability

Magnesium sulfate ($MgSO_4$) only occurs in hydrated form in nature. The two most abundant magnesium sulfate hydrate minerals are kieserite and epsomite. Kieserite is a colorless, grayish-white or yellowish mineral, with a (Mohs) hardness of 3.5 and a monoclinic crystal structure. It occurs as massive salt deposits of oceanic origin and crystals are uncommon [14]. Epsomite is a white, grey, colorless, pink, or greenish mineral with a (Mohs) hardness of 2-2.5 and an orthorhombic crystal structure. It is found for example on the walls of mines or caves, in salt deposits and on outcrops of dolomitic or calcareous rocks, usually occurring as crusts. Synthetic epsomite crystals are short prismatic to equant (the crystallographic axes a, b, and c have nearly similar lengths) [15].

The magnesium sulfate minerals recognized by the International Mineralogical Association are meridianiite ($MgSO_4 \cdot 11H_2O$), epsomite ($MgSO_4 \cdot 7H_2O$), hexahydrate ($MgSO_4 \cdot 6H_2O$), pentahydrate ($MgSO_4 \cdot 5H_2O$), starkeyite ($MgSO_4 \cdot 4H_2O$), and kieserite ($MgSO_4 \cdot H_2O$). Leonhardtite has been

renamed starkeyite and the existence of sanderite ($MgSO_4 \cdot 2H_2O$) is regarded as questionable. [16] Meridianiite was earlier often reported as $MgSO_4 \cdot 12H_2O$, but it has been renamed [17]. In addition, metastable hydrates of magnesium sulfate can also exist. Stable and metastable forms of magnesium sulfate hydrate crystallized from solutions reported in the literature are hydrates with 1-11 moles of crystal water [18]. Magnesium sulfate can be crystallized from a solution containing sulfuric acid under atmospheric conditions as heptahydrate [6, 7, 8]. In order to crystallize magnesium sulfate as the monohydrate, elevated temperature and pressure are required. [7]

Magnesium sulfate hydrate will lose its crystal water when it is heated up to form anhydrous magnesium sulfate, according to eq. (1). Different temperatures for complete dehydration to anhydrous magnesium sulfate have been reported in the literature: over 300°C [19], 320 [20], 330-380°C [21], and 400-500°C [22]. Stepwise dehydration of a higher hydrate, for example epsomite, can produce hydrates with 6, 4, 3, 2, 1.25, and 1 moles of crystal water [22]. Emons et al. [21] found that the repeatability of dehydration tests was not very good, due to the possible formation of metastable hydrates. The stable hydrates that were formed when epsomite was dehydrated were $MgSO_4 \cdot 3H_2O$ at 105°C, $MgSO_4 \cdot 2H_2O$ at 140°C, and $MgSO_4 \cdot H_2O$ at 190°C. Natural kieserite dehydrates in a single step, whereas the synthetic kieserite ($MgSO_4 \cdot 1.25H_2O$) gradually releases its crystal water. [21]

$$MgSO_4 \cdot xH_2O \leftrightarrow MgSO_4 + xH_2O(g) \quad (1)$$

Anhydrous magnesium sulfate is highly hygroscopic: at Standard Atmospheric Temperature and Pressure (SATP), it will attract water. The amount of water that is attracted depends on the relative humidity (RH): below 39% RH, starkeyite is formed, between 39-52% RH hexahydrate is the stable hydrate, and at a relative humidity above 52%, epsomite is the stable hydrate. Metastable phases are an unknown 2.4 hydrate in the range of 7-22% RH and pentahydrate between 22-39% RH. [23] Another recent publication on the stability of magnesium sulfate hydrates, at relatively low temperatures and varying relative humidity, was made by Grevel and Majzlan [18]. According to these authors, at SATP, kieserite is stable in the area up to 50% relative humidity, hexahydrite is stable in the area of 49-54 (RH%), and heptahydrate is stable at 54-90% RH. At higher humidity, the aqueous solution is stable. The boundary of the stability areas of hexahydrite and metastable starkeyite lies at

a relative humidity of 43%. [18] The stability diagram has been updated with new data and the stability area of starkeyite at SATP is now defined as below 41% RH [24]. According to Steiger et al., the boundaries are in good agreement with the latest data that was reported by Grevel et al. [25]

2.1.2 Magnesium sulfate polymorphs

Anhydrous magnesium sulfate is reported in the literature to exist in different forms: α-magnesium sulfate, β-magnesium sulfate, γ-magnesium sulfate and magnesium sulfate without any prefixes. The different prefixes appear to be used both to indicate variations in the crystal lattice and to make a distinction between the phase that is stable at high and low temperature. However, a distinction has not been made between the different structural forms of $MgSO_4$ in all literature sources.

In crystallographic literature sources, the prefix α or β is used to make a distinction between structural variations in the crystal lattice [26, 27]. This difference is often a result of the production method that is used to obtain the crystals. The α-phase is grown from an aqueous solution of MgO and H_2SO_4; the β-phase can be formed either by dehydration of magnesium sulfate hydrates or by heating α-$MgSO_4$ to 595°C followed by quenching to room temperature, where it persists as β-$MgSO_4$ (possibly metastable) [21, 26]. In the crystal data book [27], two polymorphs of magnesium sulfate are reported, both orthorhombic in crystal structure, but with different space groups. It is claimed that the β-phase is the form that is commercially available [26]. Fortes et al. [26] mention a third form: γ-$MgSO_4$, which is said to be the same material as the high-temperature form in the article by Rowe et al. [28] that is obtained when heating β-$MgSO_4$. The α-$MgSO_4$ and β-$MgSO_4$ can co-exist below 527°C, according to Fortes et al. [26]. These two phases can also co-exist according to Du [29], having a difference in enthalpy of formation of 3.0 kJ/mol. Different values for the transition temperature from the low-high temperature forms are given by different literature sources: the transition seems to take place between 997-1095°C [26, 27, 28].

For clarity, the two different forms of magnesium sulfate identified in this thesis are distinguished by their Bravais crystal lattice and axis length. The powder diffraction file [30] does not give a prefix for the base-centered

orthorhombic form of magnesium sulfate, but in order to distinguish between the different forms, the prefix α is added in this work.

α-$MgSO_4$: base-centered orthorhombic, a = 5.18100, b = 7.88500, c = 6.50100

β-$MgSO_4$: primitive orthorhombic, a = 4.75000, b = 8.59000, c = 6.71000 [30]

2.1.3 Thermodynamic properties of magnesium sulfate

The thermodynamic properties of anhydrous magnesium sulfate that are found in the literature are in agreement with each other, except for the enthalpy of formation. The choice of standard enthalpy of formation has a large impact on the calculated stability of $MgSO_4$ as a function of temperature. Table 1 shows an overview of the different values for the enthalpy of formation (ΔH_f) of magnesium sulfate available from the literature.

The value of the standard enthalpy of formation of magnesium sulfate is generally between -1255 and -1289 kJ/mol [29, 31-38]. The two most frequently used values are -1261.8 kJ/mol [31, 33] and -1284.9 kJ/mol [29, 35, 36, 37]. A recent value reported by Landolt-Börnstein (2000) [32] is −1288.8 kJ/mol, which was accepted in the SGTE database (MTDATA [39]). This value may, however, refer to α-$MgSO_4$, since the value is similar to the α-forms reported by Pankratz [34] and Ko & Daut [36]. Du [29] has shown that the use of an enthalpy of formation of -1288.8 kJ/mol is internally consistent with the properties of the K_2SO_4-Na_2SO_4-$MgSO_4$-$CaSO_4$ system, using the Calphad approach. The Calphad approach combines thermochemical data with data from phase diagrams. This value is for the alpha polymorph, but it is claimed that the beta polymorph with an enthalpy of formation of -1284.9 kJ/mol is the commercially available form [26].

Table 1. Enthalpy of formation of $MgSO_4$ from various literature sources.

Source	Species	ΔH_f (kJ/mol)	Year	Reference used
Binnewies 02 [31]	$MgSO_4$	-1261.8	2002	-
Landolt 01 [32]	$MgSO_4$	-1288.76	2001	V.P. Glushko et al., unpublished results.
Du [29]	α-$MgSO_4$	-1288.8	1999	SGTE data for pure elements, Calphad, 1991, *15* , 317-425.
	β-$MgSO_4$	-1285.79	1999	
JANAF 98 [33]	$MgSO_4$	-1261.8	1998	Knopf, H. J., Staude, H., Z. Physik. Chem., Leipzig, 1955. *204* , 265-275.
Pankratz 95 [34]	α-$MgSO_4$	-1288.8	1995	DeKock, C. W., Thermodynamic Properties of Selected Metal Sulfates and their Hydrates. USBM IC 9081, 1986, 59pp. Based on Ko and Daut, correction for sulfate ion.
	β-$MgSO_4$	-1284.95	1995	
Barin 93 [35]	$MgSO_4$ (cr)	-1284.91	1993	Wagman, D. D., Evans, W. H., Parker, V. B., Schumm, R. H., Halow, I., Bailey, S. M., Churney, K. L., Nuttall, R. L. The NBS Tables of Chemical Thermodynamic Properties, Washington D.C., 1982.
Ko and Daut [36]	α-$MgSO_4$	-1288.46	1980	-
	β-$MgSO_4$	-1284.61	1980	-
	$MgSO_4$	-1309.84	1937	Kelley, K. K, Contributions to the Data of Theoretical Metallurgy. The Thermodynamic Properties of Sulfur and its Inorganic Compounds, BuMines Bull. 406, 1937, 154 pp.
	$MgSO_4$	-1258.97	1897	Berthelot, M.P., Thermochimie. Gauthier-Villars Fils, Paris, France, 1897. p. 261.
	$MgSO_4$	-1264.87	1883	Thomsen, J., Termochemische Untersuchungen. Johann Ambrosium Barth, Leipzig, 1883, 567 pp.
Parker, V.B, Wagman, D.D. Evans, W.H. [37]	$MgSO_4$	-1284.91	1971	-
Rossini, F.D., Wagman, D.D., Evans, W.H., Levine, S., Jaffe, I. [38]	$MgSO_4$	-1278.21	1952	Averaged values: Thomsen, Berthelot and Ilosvay, Pickering and Kelley.

2.2 Decomposition of magnesium sulfate

2.2.1 Thermodynamics of magnesium sulfate decomposition

Magnesium sulfate will start to decompose spontaneously into magnesium oxide and sulfur trioxide gas at elevated temperatures. The material starts to decompose below its melting point. The melting point is not easy to define, but is reported in literature to be between 1120-1185°C in Gmelins Handbook [40] and at approximately 1177°C, when heated in a closed container [26]. The exact temperature of decomposition depends on the atmosphere under which the decomposition is carried out. In the absence of any reducing agent, magnesium sulfate starts decomposing in the temperature range of 900-1100°C. [41] It was proven by Lau et al. that SO_3 is the gaseous product of magnesium sulfate decomposition and not SO_2 and O_2, as is the case for example for the decomposition of calcium sulfate [42, 43, 44]. The decomposition reaction thus proceeds in two steps. The reaction for the decomposition of anhydrous magnesium sulfate to magnesium oxide and sulfur trioxide by heat alone is given in eq. (2). Sulfur trioxide is not stable at elevated temperatures, i.e. >700 °C, and spontaneously forms sulfur dioxide and oxygen, as shown in eq. (3). The two-step reaction is illustrated in Figure 2.

$$MgSO_4 \rightarrow MgO + SO_3(g) \quad (2)$$

$$SO_3(g) \rightarrow SO_2(g) + \frac{1}{2}O_2(g) \quad (3)$$

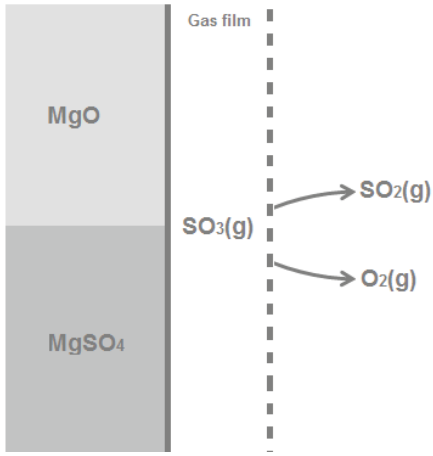

Figure 2. Illustration of the two-step decomposition reaction of magnesium sulfate according to reaction equations (2) and (3).

The sulfur trioxide partial pressure in the gas film surrounding the particles may be high; it may even be close to unity when the heat and mass transfer in the system is poor. Magnesium sulfate is stable up to high temperatures when the sulfur trioxide pressure is high, as shown in Figure 3, in which reaction equation (2) was used, with the two different enthalpies of formation for magnesium sulfate, as described in section 2.1.3. This figure shows that magnesium sulfate in an atmosphere of sulfur trioxide is no longer stable above 1190°C and 1327°C, calculated with an enthalpy of formation of magnesium sulfate of -1261.8 kJ/mol, and -1284.9 kJ/mol, respectively. It was reported by Hulbert [45] that the sulfur trioxide gas pressure in powdered compacts would build up, retarding the decomposition reaction.

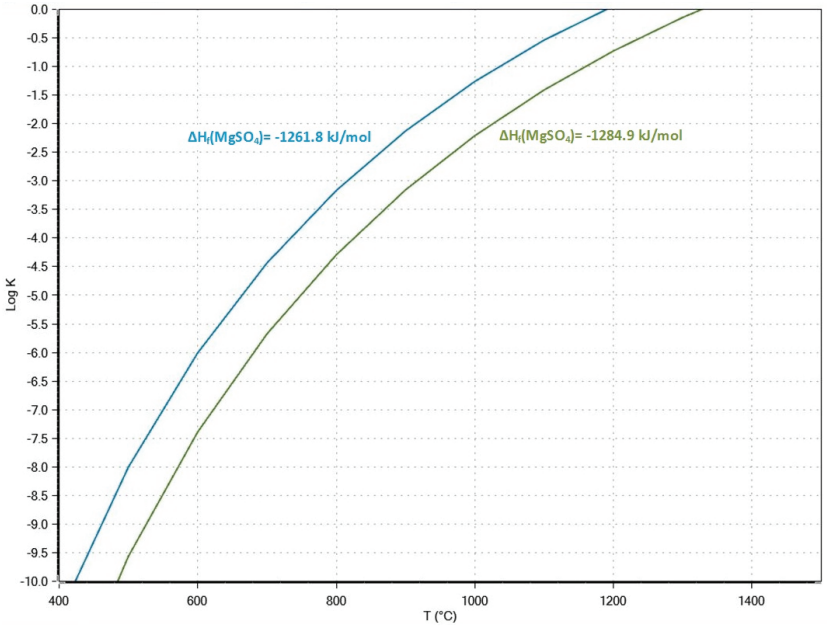

Figure 3. The reaction $MgSO_4$ = MgO + SO_3(g) calculated with HSC Chemistry 8.0 [46] using two different enthalpies of formation for $MgSO_4$.

The equilibrium diagram in Figure 4 shows that the choice of the standard enthalpy of formation has a large impact on the calculated stability of $MgSO_4$ as a function of temperature. With an enthalpy of formation of $MgSO_4$ of -1261.8 kJ/mol, $MgSO_4$ starts to decompose at 857°C and is fully decomposed at 993°C. With an enthalpy of formation of -1284.9 kJ/mol, $MgSO_4$ starts to decompose at 931°C and is fully decomposed at 1081°C. The start of decomposition was defined as >0.5% of decomposed $MgSO_4$. The choice of enthalpy of formation for $MgSO_4$ thus results in a difference of the calculated

decomposition temperature of 88°C. The equilibrium diagram showing all phases for magnesium sulfate with an enthalpy of formation of -1284.9 kJ/mol is shown in Figure 5. This diagram shows that the gas phase that is formed due to decomposition of magnesium sulfate is composed of sulfur dioxide, oxygen, and a minor amount of sulfur trioxide when in equilibrium. These calculations were carried out with one kmol of anhydrous magnesium sulfate and 0.1 kmol of N_2 gas in a closed system, in the absence of any reductants.

The phase stability diagram in Figure 6 shows the line of stability between magnesium oxide and magnesium sulfate at different temperatures with oxygen and sulfur dioxide partial pressure as the variables. The area of stability for magnesium sulfate decreases with increasing temperature. This diagram shows that decreasing the oxygen pressure at a fixed temperature will move the point towards the stability area of magnesium oxide and that lowering the sulfur dioxide partial pressure will move the balance towards the magnesium oxide region as well. Lowering the oxygen and/or the sulfur dioxide partial pressure thus lowers the decomposition temperature of magnesium sulfate.

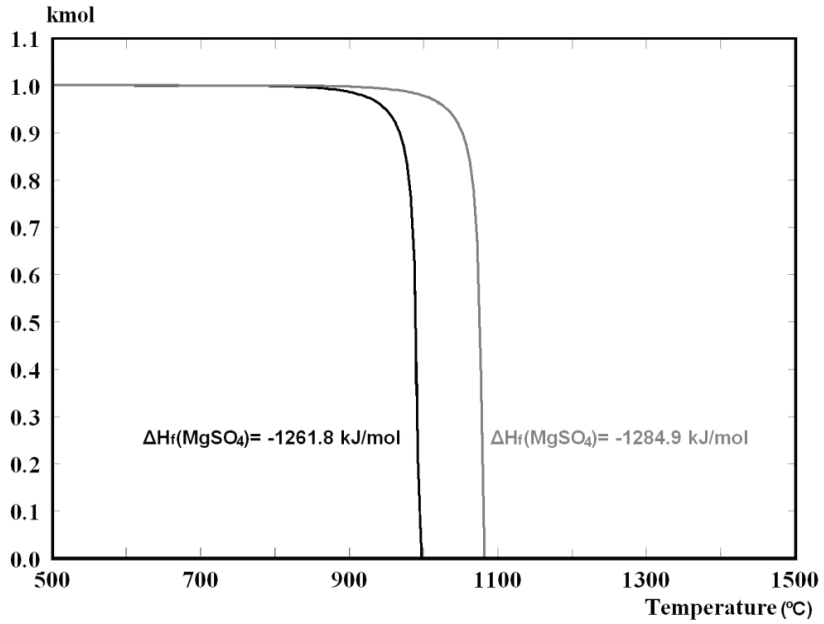

Figure 4. Comparison of calculated decomposition temperature of magnesium sulfate in its own atmosphere with an enthalpy of formation of -1261.8 kJ/mol and -1284.9 kJ/mol, calculated using HSC Chemistry 7 [47].

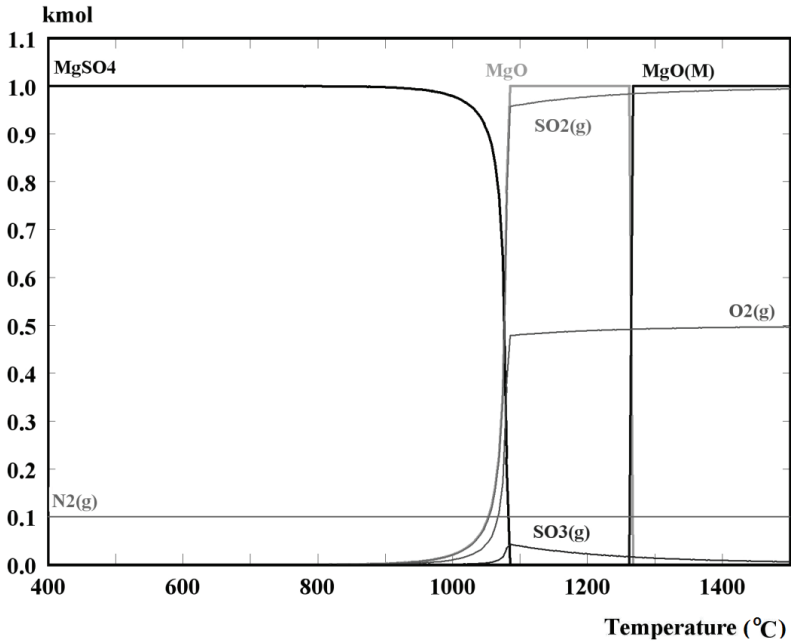

Figure 5. Equilibrium diagram for 1 kmol $MgSO_4$ and 0.1 kmol N_2 with $\Delta H_{f(MgSO4)}$= -1284.9 kJ/mol, calculated using HSC Chemistry 7 [47].

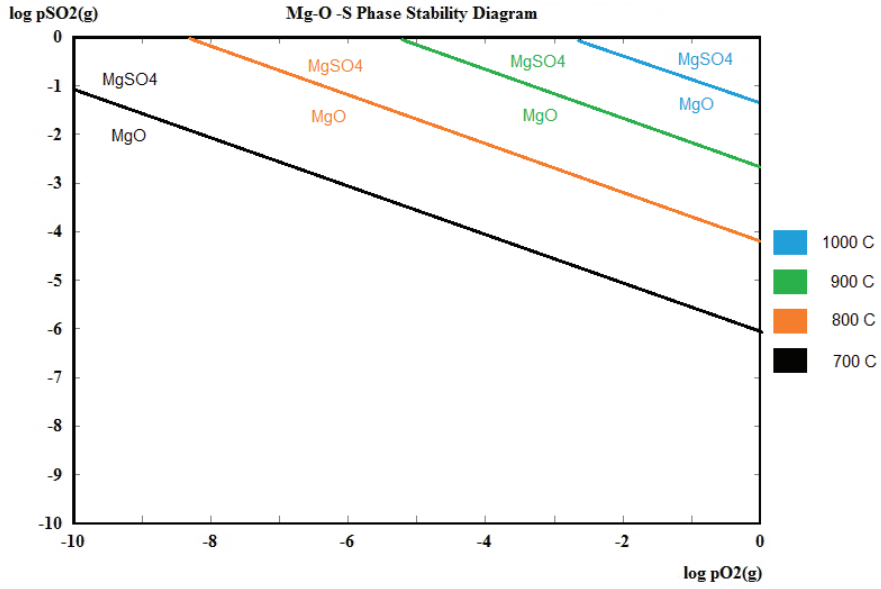

Figure 6. Mg-S-O phase stability diagram for 700, 800, 900, and 1000°C, calculated using HSC Chemistry 7 [47].

A reductant can be used in order to decompose magnesium sulfate at lower temperatures. It will only lower the decomposition temperature when the sulfur trioxide film, as illustrated in Figure 2, is removed efficiently (i.e. in an environment with high gas flow velocities). The decomposition temperature will be higher when sulfur trioxide is not transported from the gas film efficiently, as shown in Figure 3. The reducing agents used in current research are solid carbon or an atmosphere containing carbon monoxide gas, obtained from incomplete combustion of a carbonaceous fuel [48, 49]. The decomposition products are magnesium oxide, sulfur dioxide, and carbon dioxide, assuming that stoichiometric amounts of the feed materials are used. The overall reactions are given in eq. (4) [12] and eq. (5) [48, 49] for solid carbon and carbon monoxide, respectively. The use of a deficiency of carbon leads to the partial decomposition of $MgSO_4$. On the other hand, with the use of an excess of carbon, species such as COS, CS_2, and S_x may form in the gas phase. When a hydrated form of magnesium sulfate is used, H_2S might be formed when the decomposition gases react with the evaporated crystal water. [50]

Alternative reducing agents to carbon that may possibly be used are sulfur (gas) [7, 13] or hydrogen gas [48, 51]. The decomposition with sulfur takes place according to eq. (6), in which magnesium sulfate decomposes to form MgO and SO_2. With hydrogen as the reductant, MgO is formed together with SO_2 and H_2O, according to eq. (7). The use of these reducing agents instead of a carbon-containing reducing agent prevents the presence of CO and CO_2 in the off-gas, which is unwanted. In the reaction with hydrogen, water vapor is formed, which may be corrosive in the off-gas line when it reacts with for example sulfur dioxide.

$$MgSO_4 + \frac{1}{2}C \rightarrow MgO + SO_2(g) + \frac{1}{2}CO_2(g) \quad (4)$$

$$MgSO_4 + CO(g) \rightarrow MgO + SO_2(g) + CO_2(g) \quad (5)$$

$$MgSO_4 + \frac{1}{4}S_2(g) \rightarrow MgO + \frac{3}{2}SO_2(g) \quad (6)$$

$$MgSO_4 + H_2(g) \rightarrow MgO + SO_2(g) + H_2O(g) \quad (7)$$

The Gibbs Free Energies for the decomposition reactions at 900°C in Table 2 show that decomposition of magnesium sulfate only occurs in the presence of a reductant. The heats of reaction also show that the reactions are strongly endothermic. The molar heat capacity of magnesium sulfate at constant

pressure and a temperature of 298.15 K is 96.5 J mol^{-1} K^{-1} [52]. The strongly endothermic reaction results in the cooling of the particles as well as the surrounding gas when magnesium sulfate decomposes.

The equilibrium diagram of magnesium sulfate with sulfur as the reductant is shown in Figure 7, in order to illustrate that the decomposition temperature is lowered in the presence of a reductant, which can be easily seen when comparing Figure 7 with Figure 5.

Table 2. Decomposition reactions of magnesium sulfate, in the presence and absence of reductants at a temperature of 900°C, calculated with an enthalpy of formation of -1284.9 kJ/mol using HSC Chemistry 7 [47].

Reaction	ΔG kJ	ΔH kJ	ΔS J/K	K
$MgSO_4=MgO+SO_3(g)$	70.884	272.26	171.654	6.98E-04
$MgSO_4+0.5S=MgO+1.5SO_2(g)$	-87.028	213.956	256.561	7.50E+03
$MgSO_4+0.5C=MgO+SO_2(g)+0.5CO_2(g)$	-138.408	172.336	264.88	1.46E+06
$MgSO_4+CO(g)=MgO+SO_2(g)+CO_2(g)$	-120.698	87.812	177.735	2.37E+05

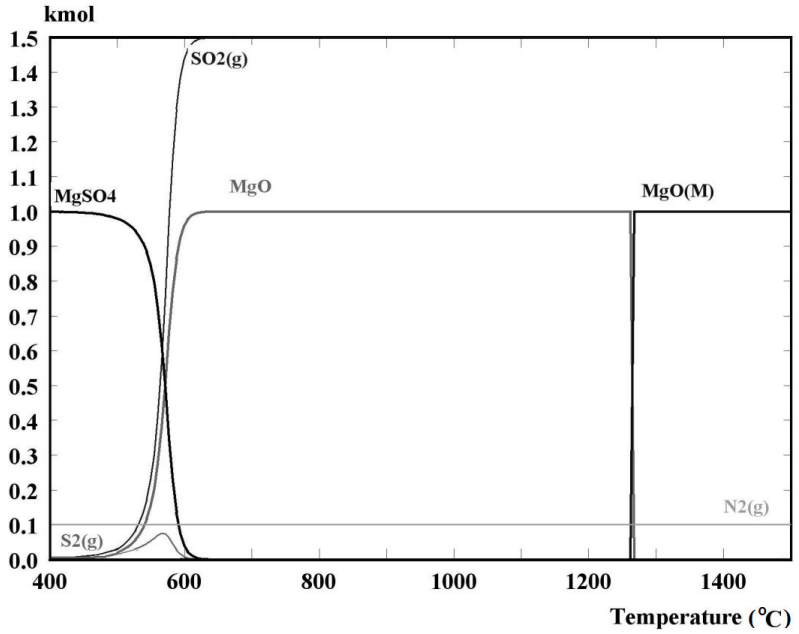

Figure 7. Equilibrium diagram of 1 kmol $MgSO_4$, 0.5 kmol S, and 0.1 kmol $N_2(g)$ with $\Delta H_{f(MgSO4)}$= -1284.9 kJ/mol, calculated using HSC Chemistry 7 [47].

2.2.2 Reaction kinetics of porous particles

The decomposition of magnesium sulfate in the presence of a reductant can be regarded as a gas-solid reaction: the reaction between magnesium sulfate and a solid reductant takes place through gaseous intermediates.

Generally, gas-solid reactions are a combination of part or all of the following steps:

- Mass transfer from the bulk to the reaction interface of the gaseous reductants
- Diffusion of the reactants and products in the pores of the solid
- The chemical reaction between the reactants
- Heat conduction within the solid
- Heat transfer from the solid surface to the bulk gas [53]

Two commonly used models to describe reaction kinetics are the shrinking core model and the uniform reaction model [54, 55, 56, 57]. The uniform reaction model describes control by chemical reaction, where the particles react uniformly throughout the particle, as illustrated in Figure 8. In the shrinking core model the reactions take place at the interface of the unreacted core, as illustrated in Figure 9. [55, 56] These two models are extreme cases; in reality, mixed control often occurs.

The reaction according to the shrinking core model is composed of all or some of the following five steps, which are illustrated in Figure 10:

1. Diffusion of gas through the gas film to the particle surface
2. Diffusion of gaseous reductant through the ash layer
3. Reaction of the gas at the solid interface
4. Diffusion of gaseous products through the ash layer
5. Diffusion of gaseous products through the gas film

These steps are generally summarized as: diffusion through the gas film (steps 1 and 5), diffusion through the ash layer (steps 2 and 4) and chemical

reaction at the interface (step 3). The integrated functions for the shrinking core/contracting sphere model of these steps are expressed in equations (8)-(10). The Jander model (equation (11)) is sometimes used to express ash layer diffusion, but it is only applicable at low conversions. Another diffusion model is the Ginstling-Brounshtein model (equation (12)).[54, 56, 58] Rearranging the integrated function of this model shows that it is in the same form as the ash layer diffusion model, only with a factor three difference.

Reaction at the unreacted interface $\frac{t}{\tau} = 1 - (1 - X)^{1/3}$ (8)

Film diffusion: $\frac{t}{\tau} = X$ (9)

Ash layer diffusion: $\frac{t}{\tau} = 1 - 3(1 - X)^{2/3} + 2(1 - X)$ (10)

Jander $\frac{t}{\tau} = [1 - (1 - X)^{\frac{1}{3}}]^2$ (11)

Ginstling-Brounshtein $\frac{t}{\tau} = 1 - \frac{2}{3}X - (1 - X)^{2/3}$ (12)

Where:

t	=	Time	[min]
τ	=	Time for completion of the reaction	[min]
X	=	Conversion fraction	[-]

These steps may have different resistances; the greatest resistance is the rate-determining step. It is possible that the rate-controlling step changes during the reaction, for example due to a change in temperature, atmosphere, or particle size [54, 55].

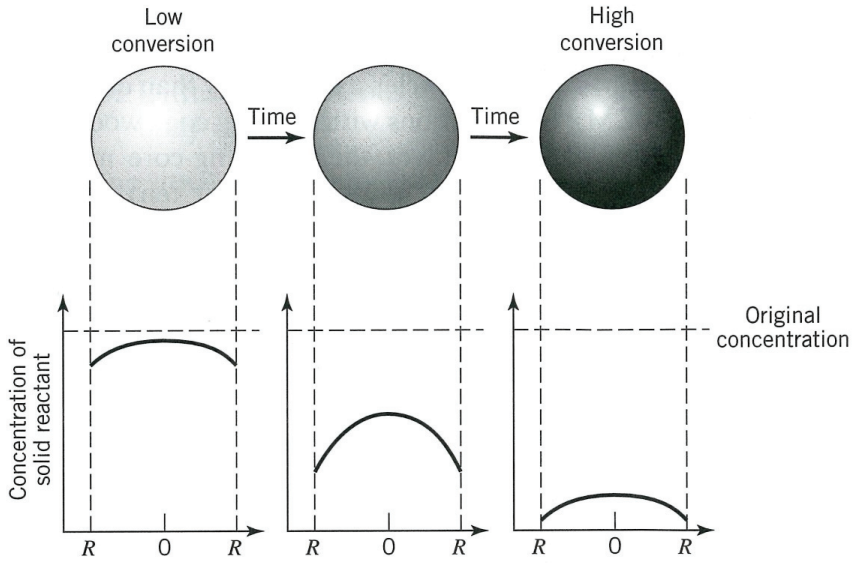

Figure 8. Uniform reaction model, reused with permission [54].

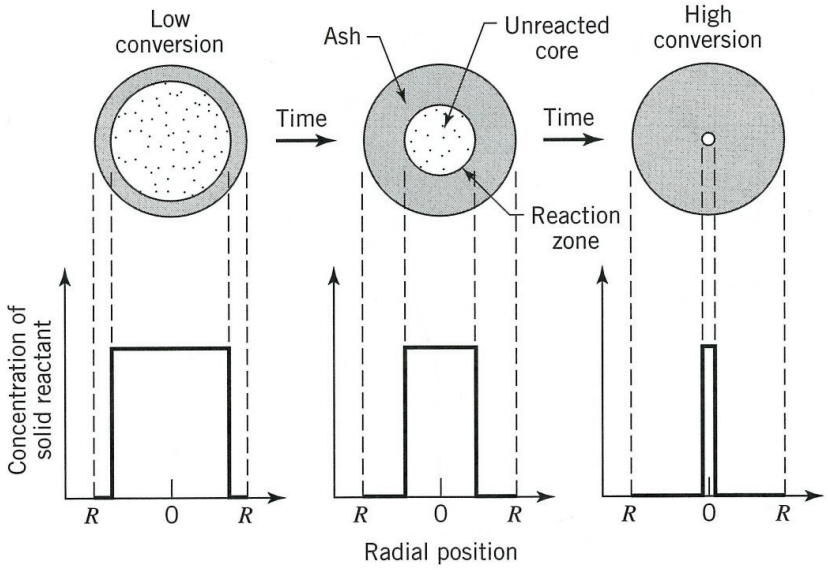

Figure 9. Shrinking core model, reused with permission [54].

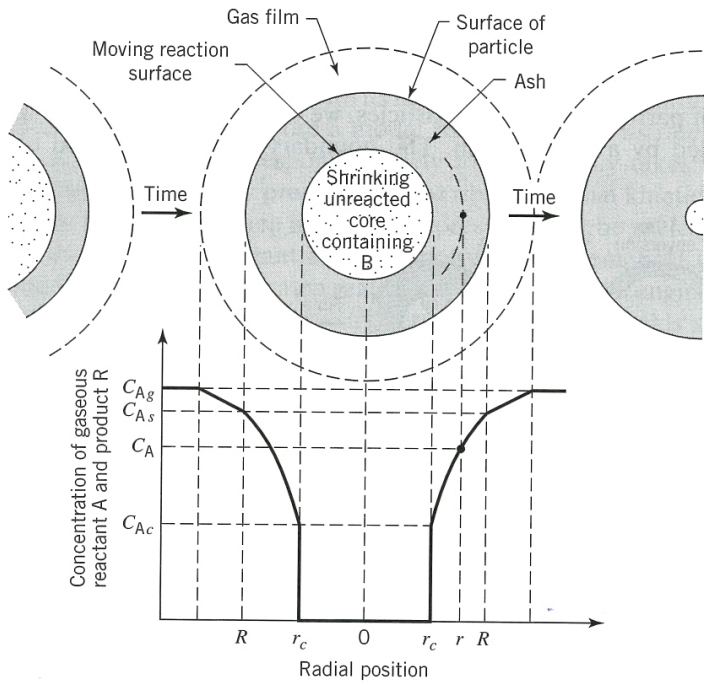

Figure 10. The shrinking core model, with possible rate controlling phenomena illustrated, reused with permission. [54]

The reaction kinetics of porous particles is affected by the porosity, pore size distribution, and specific surface area [56], in addition to factors such as temperature and atmosphere. For porous particles, the grain model is used. Within the grain model, there are two models, which are similar to the shrinking core model and the uniform reaction model, although in this case they apply to porous solids.

The reaction kinetics of the decomposition reaction is also affected by the product layer formation. The product gases can easily diffuse through a porous product layer, but a non-porous product layer may hinder the diffusion of gases. Equation (13) defines whether a product layer is porous or non-porous, based on molar volumes. [59]

$$\mathrm{z} = \frac{1}{\alpha}\left(\frac{M_p/\rho_p}{M_R/\rho_R}\right) \qquad (13)$$

Where:

z	=	ratio, with $z < 1$: porous; $z > 1$ non-porous	[-]
α	=	stoichiometry factor	[-]
M_P	=	molecular weight of solid product	[$gmol^{-1}$]
M_R	=	molecular weight of solid reactant	[$gmol^{-1}$]
ρ_P	=	density of solid product	[kgm^{-3}]
ρ_R	=	density of solid reactant	[kgm^{-3}]

The following z-values were found for magnesium sulfate heptahydrate, monohydrate, and anhydrous magnesium sulfate: 0.077, 0.209, and 0.249, respectively, using data from the HSC Chemistry database [47]. These values show that a porous MgO product layer is formed for both hydrated and anhydrous magnesium sulfate.

2.2.3 Fluidizing conditions

The experimental work in this thesis was carried out using a fluidized bed reactor. In this type of reactor, the heat and mass transfer rates are high compared to other reactors, because the particles are in suspension in the fluidized bed. The gas bubbles that are formed take solids along in the bubble wake and the solids move downwards when the surface of the bed is reached because of gravity, which results in good heat and mass transfer [55]. The good heat transfer in fluidized beds ensures an even temperature distribution throughout the bed; hot and cold spots are thus avoided [56]. Overheating of the magnesium oxide product decreases its surface area, making it less efficient as a neutralizing agent for pH control in the leaching process.

Carrying out experiments using fluidizing conditions ensures that the sulfur trioxide gas film, described in section 2.2.1, is removed more efficiently than under conditions with low gas velocities in which the particles remain static instead of fluidized.

Different phases exist in the fluidized bed reactor: a dense phase directly above the grate and a lean phase or freeboard, where the solids density is much lower than in the dense phase. In these phases, both coarse and fine particles are present. [55] The fluidizing behavior is strongly affected by the

properties of the solids; Geldart has made a classification of solids based on particle size and density, which is illustrated in Figure 11 and described below.

The solids of group C are fine grained (mean size < 30 μm) and/or particles with a low density, which are very difficult to fluidize due to their cohesive behavior; the inter-particle forces are greater than those from the gas. Channeling is therefore likely to occur and heat and mass transfer is poor. Fluidization can be improved by means of mechanical equipment such as stirrers or vibrators.

The solids of group A have a particle diameter of around 100 μm and/or a density of around 1.4 g/cm^3. These particles can be fluidized easily, and rapid mixing takes place so heat and mass transfer is good. Back-mixing of gas into the dense phase occurs. Inter-particle forces, however, still play a role with these types of particles. The bed expands uniformly at low gas flow velocities; at increased velocities, bubbles of a limited size start to form and the bed is highly expanded with a surface that resembles a boiling liquid. The bed collapses relatively slowly when the gas flow is stopped.

The solids of group B typically have a density of 1.4-4.0 g/cm^3 and a particle size of 50-500 μm. Gas bubbles start to form at gas flow rates above the minimum fluidization point, and may grow into large bubbles. The bed expansion is less stable compared to group A particles and the bed collapses quickly when the gas flow is stopped. Little back-mixing of gas into the dense phase occurs. Inter-particle forces do not play a role with these particles.

Group D solids generally have large particle sizes (> 600 μm) and/or a high density. The mixing of solids for these particles is poor and back-mixing of gas is low. The bed expansion is low and the bed collapses rapidly when the gas flow is stopped. The bed behaves turbulently and channels may form in deep beds; therefore, low bed heights are often used for this type of particle. [55, 57, 60, 61]

The bed can become defluidized for various reasons: the inter-particle forces become excessive for fine particles, particles can soften when heated, or fluidization problems may also occur when crystal water is released from the feed material [57]. As a result, the heat and mass transfer is significantly lower, and therefore the reaction kinetics is much slower. An inert bed can be used

when particles tend to get sticky, in order to dilute the bed or act as a separator [62].

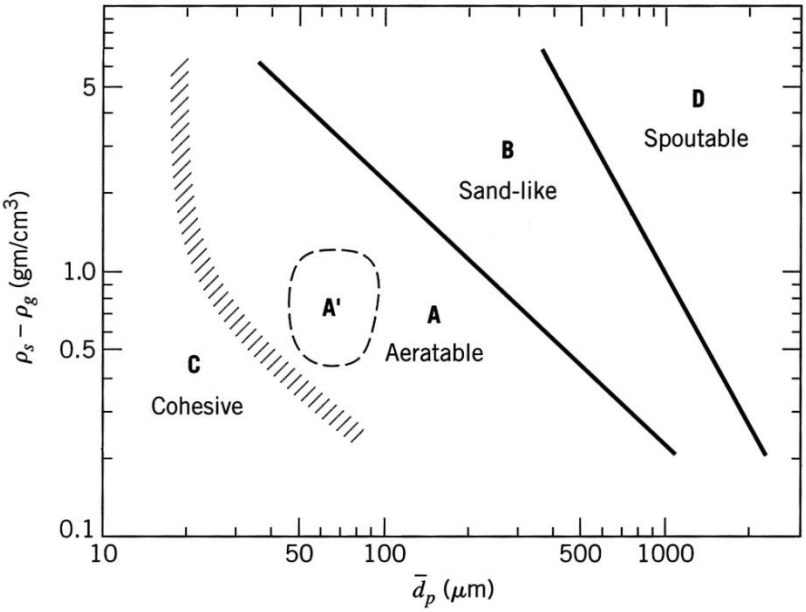

Figure 11. Geldart particle classification, reused with permission. [54]

2.2.4 Kinetics of magnesium sulfate decomposition

The thermal decomposition of anhydrous magnesium sulfate in the absence of any reductants was studied by Hulbert [45]. The decomposition was carried out using thermogravimetric analysis, both with loose magnesium sulfate powder and compacted powder. The anhydrous magnesium sulfate was obtained by drying magnesium sulfate heptahydrate for two hours at 400°C. The sample size had an effect on the reaction kinetics; the smaller the size of the sample, the shorter the reaction time. The reaction kinetics is strongly affected by the temperature in experiments carried out with a sample mass of 25 mg. At 1060°C full decomposition took place in 65 minutes, whereas full decomposition at 1000°C took 148 minutes. At lower temperatures, decomposition was incomplete; at 950°C approximately 34% decomposed, and at 920°C only 12% of the magnesium sulfate decomposed. The kinetics was also affected by whether the powder was loosely packed or a pressed powder; for example at 1060°C with packed powder it took 114 min to reach full

decomposition of magnesium sulfate, compared with 65 minutes for loosely packed powder. Compacted powder at 1000°C did not fully decompose, whereas it decomposed completely when it was loosely packed. The difference in kinetics between packed and loose powder is explained by the difficulty of SO_3 gas escaping from the packed powder. [45]

The kinetics of anhydrous magnesium sulfate decomposition in the presence of carbon monoxide by means of a thermobalance was studied by Plewa and Steindor [49]. Magnesium sulfate was dried at 400°C and was used in the experiment with a residual moisture content of 0.7%. The experiments were carried out in an atmosphere of 100% CO. The sample size had a similar effect on the reaction kinetics to that described by Hulbert. The thermogravimetric experiments with different temperatures were carried out with a sample mass of 300 mg. Full decomposition was achieved at 675°C after 60 minutes and at 660°C full decomposition was achieved after 72 minutes. The conversion was only 95% at 635°C after 125 minutes. It was also found that the composition of the products or intermediates was dependent on the temperature. Magnesium sulfide was found to be stable between 550-625°C, together with magnesium sulfate and magnesium oxide. Magnesium oxide was the only stable phase at temperatures above 625°C. [49]

3. Experimental

The equipment is described in section 3.1, followed by information on the materials that have been used in section 3.2. The experimental procedure for the initial reaction tests as well as the fluidized bed reactor tests are described in section 3.3.

3.1 Equipment

The majority of the experiments were carried out in a fluidized bed reactor but other experimental equipment was also used to study the decomposition behavior of magnesium sulfate, such as TG/DSC equipment and a chamber furnace.

Fluidized bed reactor

The experiments were carried out in a 38 mm inner diameter lab-scale fluidized bed reactor. A sintered quartz disc with a thickness of 4-6 mm and a pore size of 40-90 microns was used as the grate. The reactor tube is placed in a 610 mm high Trans-Temp furnace (Thermcraft Inc., USA), with electrical spiral heating with a maximum power of 2.5 kW and a maximum temperature of 1000°C. The temperature is measured in the bed and between the reactor tube and the furnace, using a type S Pt-Rh thermocouple, which is calibrated and has an error of ±1.5°C. The experimental set-up is shown in Figure 12. The Trans-Temp furnace is made of quartz and has a thin gold film deposited on the inside, which becomes transparent at elevated temperatures, as shown in Figure 13. [63, 64] The transparent reactor makes it possible to see the bed height and observe the fluidizing behavior. Fluidizing gases enter the furnace from below the grate and solids are fed from the top. The off-gas is removed freely by means of ventilation. It needs to be borne in mind that the behavior in a lab-scale fluidized bed may be very different from the behavior in larger-scale equipment. In reactors with a diameter smaller than 0.1 m, the tendency

for slugging is increased and the wall effects also play a more significant role, resulting in larger electrostatic forces between the solids and the wall [57].

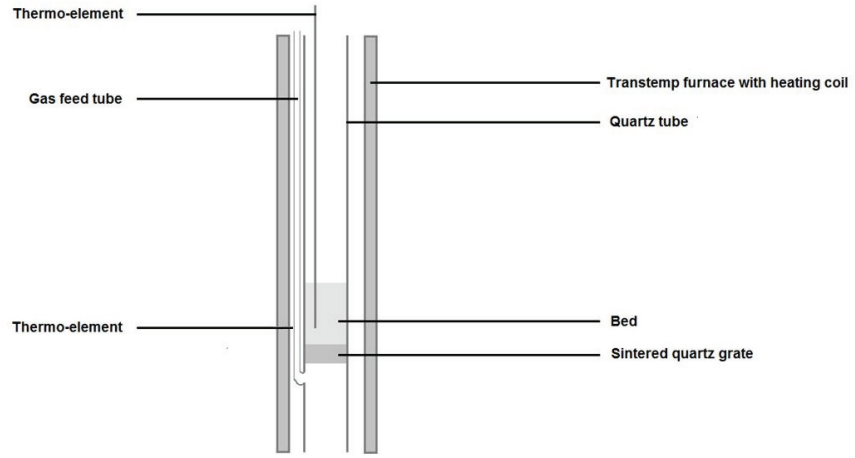

Figure 12. Schematic drawing of the experimental set-up.

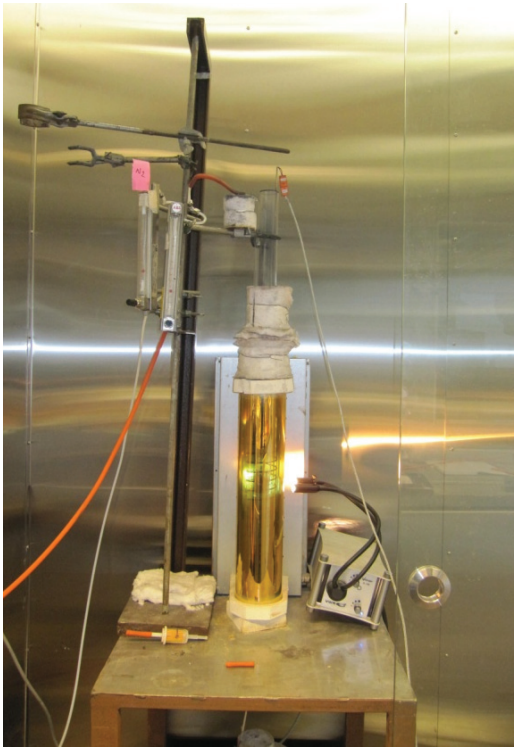

Figure 13. Laboratory scale fluidized bed reactor with off-gas measurements.

Themogravimetry and Differential Scanning Calorimetry (TG/DSC)

Thermal analysis was carried out in the preliminary experiments using a Netzsch STA 409 C/3/F (Netzsch, Germany). In this device, thermogravimetry (TG) and Differential Scanning Calorimetry (DSC) are carried out simultaneously [65]. This method was used to identify at which temperatures weight loss and the accompanying phase changes took place as a result of dehydration or decomposition.

Chamber furnace

A chamber furnace (Carbolite CSF 1100, Carbolite Limited, UK) with a volume of five liters was used in the initial reaction experiments. It can reach a maximum temperature of 1100°C at the maximum heating power of 2.75 kW. [66, 67]

Sample analysis and measurements

In some of the experiments, the off-gas composition was analyzed using Fourier Transform Infrared Spectroscopy (Gasmet FTIR dx4000, Gasmet Technologies Oy, Finland) and oxygen measurements (Spectracap oxygen transmitter OMT355, Vaisala, Finland).

A diffractometer (Bruker AXS D8 Focus, Bruker Corporation, Germany) was used for X-ray diffraction (XRD) analysis. Copper is used as the source for (K-β) X-rays. The measurement was done from 6.000°-70.00° on the theta scale, with a step size of 0.050° and a step time of 1 second. The type used was 2Th/Th locked, which refers to the 2θ measurement angle between the incident beam and detector. The different species in a material can be identified by XRD with a detection limit- of approximately 3 wt%.

The microstructures and local chemical compositions were determined using SEM/EDS equipment (JEOL JSM-6490LV, Jeol Ltd, Japan). EDS analysis was carried out using the backscattered electron mode. All samples, both cross sections and powder samples, were covered with carbon and analyzed using the high vacuum mode, except for the raw material samples, where the low vacuum mode was used, in order to prevent loss of crystal water.

Chemical analysis of the samples was carried out using ICP (Thermo scientific iris intrepid, Thermo Fisher Scientific Inc., USA). The analyzer has

an error of ±3%. The sulfur and carbon content was analyzed using the combustion method, using an Eltra device (CS2000, Eltra GmbH, Germany).

3.2 Materials

Three types of magnesium sulfate were used in the experimental work: kieserite, epsomite, and dried epsomite. The kieserite was technical grade material from Sigma Aldrich (USA), with a purity of >97%. The chemical analysis is shown in Table 3. XRD analysis, shown in Figure 14, indicates that the material is mainly composed of well-crystallized monoclinic magnesium sulfate monohydrate. In addition to this, minor amounts of amorphous $MgSO_4 \cdot 1.25H_2O$ and $MgSO_4 \cdot 2H_2O$ may form when the material is exposed to the air. The epsomite was from Kali (Germany), containing >99% $MgSO_4$, calculated with reference to the dried substance. The chemical analysis is shown in Table 3. The XRD analysis of the epsomite shown in Figure 15 indicates that the sample contains both $MgSO_4 \cdot 6H_2O$ and $MgSO_4 \cdot 7H_2O$. The hexahydrate has a monoclinic crystal structure and the heptahydrate is orthorhombic. The dried magnesium sulfate heptahydrate was obtained by drying the material in a chamber furnace at 200°C with a residence time of 17 hours, after which it was placed in a closed container in order to prevent the rehydration of magnesium sulfate to a higher hydration stage. XRD analysis of the dried heptahydrate, see Figure 16, shows that the material is mainly composed of kieserite ($MgSO_4 \cdot H_2O$) and amorphous $MgSO_4 \cdot 1.25H_2O$, with a minor amount of $MgSO_4 \cdot 2H_2O$. The shape of the XRD graph indicates that the material is not well crystallized. Magnesium oxide was used a bed material, in order to improve fluidization. The chemical analysis of this material shown in Table 3.

The structure of kieserite and dried heptahydrate is shown in Figure 17; it was not possible to analyze heptahydrate by SEM, due to its high amount of crystal water. The materials were sieved and the following particle size groups were used: 420-595 μm (group 1), 297-420 μm (group 2), 105-210 μm (group 3), and -150 μm (group 4).

Elemental sulfur, activated carbon, and carbon monoxide gas were used as reducing agents in the experiments. The elemental sulfur was composed of 99.64% S. The composition was determined by evaporating the sulfur away and analyzing the remaining ash. The main metal component in the ash was

iron (approximately 13.5%). The activated carbon was extra pure quality from Merck (Germany), with a maximum heavy metal content of 0.01%, a zinc content of below 0.01%, iron below 0.05%, and lead below 0.005%. The fixed carbon content was 89.5%, the sulfur content 0.91%, the ash content 4.7%, and 4.9% volatiles.

Manganese sulfate, calcium sulfate, and iron sulfate were used as impurities in some of the tests. The manganese sulfate from Riedel-de-Haen (Germany) was composed of mainly $MnSO_4 \cdot H_2O$ and a very minor amount of MnS according to XRD analysis. The technical grade calcium sulfate from J. T. Baker (USA) consisted entirely of gypsum, $CaSO_4 \cdot 2H_2O$, according to XRD analysis. The iron sulfate was from J. T. Baker and consisted mainly of $FeSO_4 \cdot 7H_2O$, with minor amounts of $FeSO_4 \cdot 4H_2O$, according to XRD analysis.

Table 3. The chemical analysis of kieserite, epsomite, and MgO bed material.

	Kieserite	Epsomite	MgO bed
Na	< 0.02	< 0.02	0.04
Mg	16.1	9.6	54.2
K	< 0.02	0.029	< 0.01
Ca	0.015	0.004	0.762
Mn	< 0.004	< 0.002	0.015
Fe	< 0.004	< 0.002	0.142
S	21.5	12.4	0.01
SO_4^{2-}		39.3	< 0.12

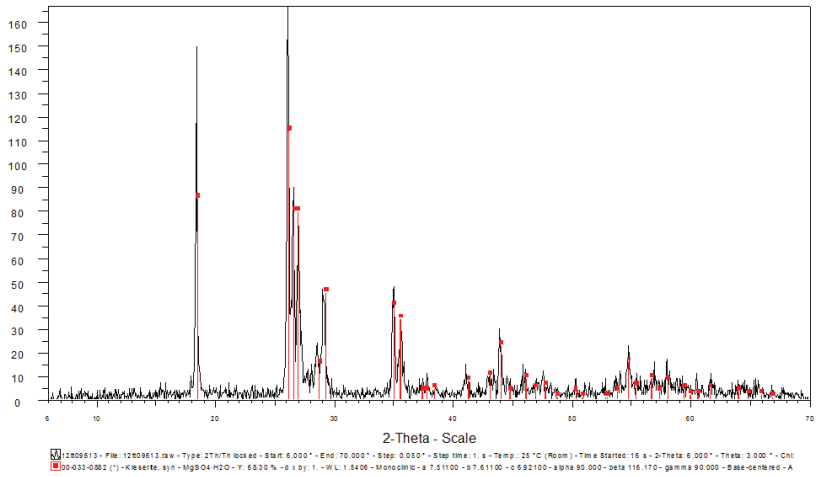

Figure 14. XRD analysis of kieserite feed material

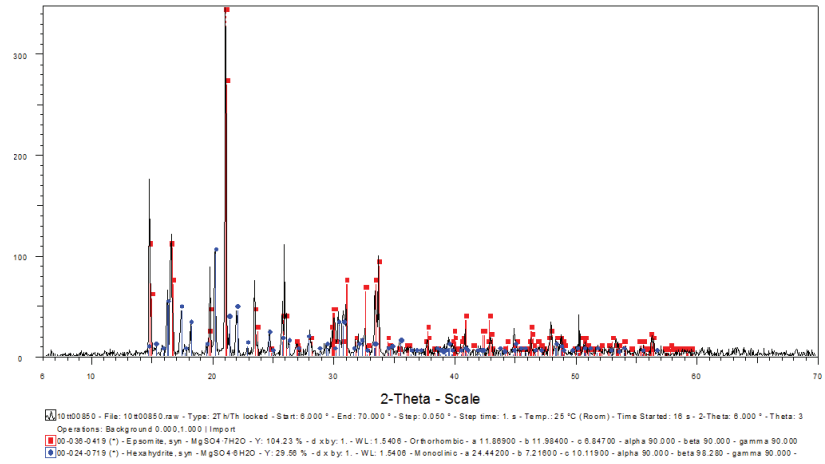

Figure 15. XRD analysis of epsomite feed material.

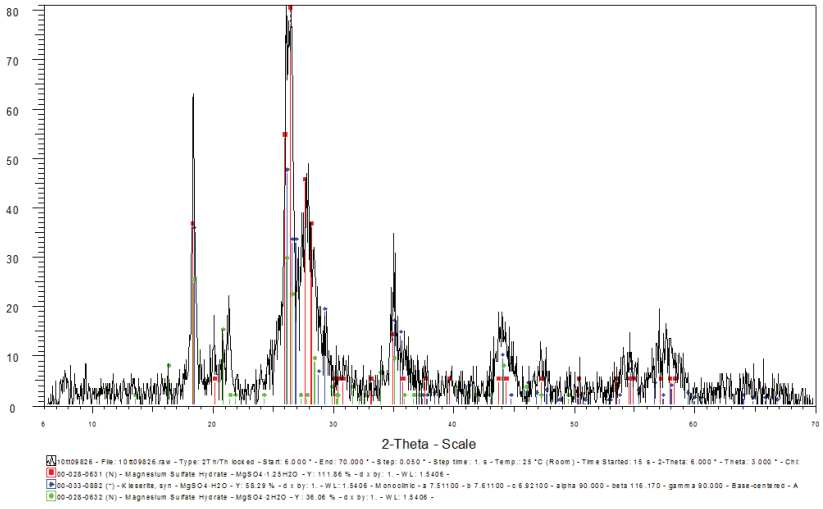

Figure 16. XRD diagram of dried epsomite feed material.

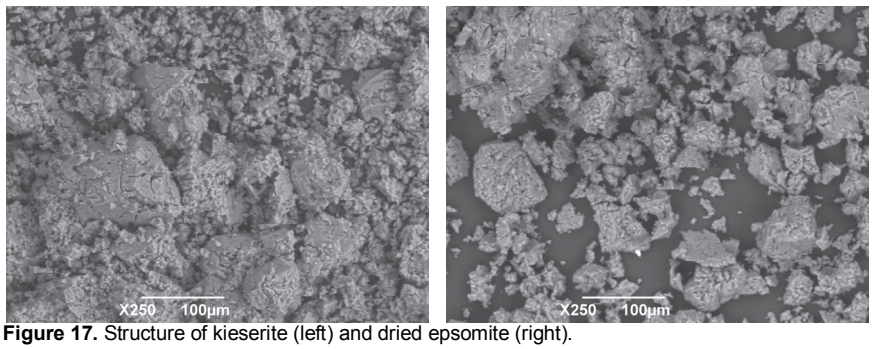

Figure 17. Structure of kieserite (left) and dried epsomite (right).

3.3 Experimental procedure

Based on the literature review it was decided to start the initial fluidization tests at 850-950°C, in order to verify the right decomposition temperature, while still producing reactive magnesium oxide. Magnesium sulfate heptahydrate was chosen as the feed material, as this would be most easily obtained from the waste acid solution under atmospheric conditions, according to the literature. In addition, magnesium sulfate monohydrate was used as well, as this material would be the most ideal for processing in the fluidized bed reactor because of its low crystal water content, which limits possible problems in the off-gas line, such as acid formation and dilution of the off-gas stream. Monohydrate could be obtained from the waste acid solution under elevated temperature and pressure.

3.3.1 Initial reaction tests

Tests were carried during the initial period when the decomposition of magnesium sulfate into magnesium oxide commences. Different types of experiments were carried out: thermogravimetric tests, short chamber furnace experiments, and short fluidized bed experiments.

Short chamber furnace tests

The chamber furnace tests were carried out to determine the structural changes and changes in total sulfur content during the initial part of the decomposition reaction. All particles had the same residence time in this experiment, eliminating the effect of a longer feeding period and therefore differences in their reaction history. The chamber furnace was heated up to the

target temperature and a porcelain boat with magnesium sulfate monohydrate was placed inside the furnace for 1, 2, 5, or 10 minutes. The reductant, in cases where a solid reductant was used, was either mixed with the magnesium sulfate or added after heating of the magnesium sulfate. The boat was placed inside the furnace, close to the feed gas tube. The boat was removed from the furnace and left to cool under a flow of nitrogen outside the furnace. The tests were all carried out with a 100% nitrogen atmosphere, except for the tests with CO, where 10% CO and 90% N_2 was used. The gas flow was started prior to the experiment, to ensure 10% CO in the chamber furnace. An overview of the experiments is shown in Table 4.

Table 4. Overview of chamber furnace experiments, carried out at 900°C.

Sample id	$MgSO_4$ (g)	Solid reductant (g)	Gaseous reductant (partial pressure)	Time (min)	Extra info
Ch_5	1	-		5	
Ch_S_1	2	0.5		1	
Ch_S_2	2	0.5		2	
Ch_S_2.1	1	0.25		2	Sulfur added after 1 min
Ch_S_5	2	0.5		5	
Ch_S_5.1	1	0.25		5	Sulfur added after 1 min
Ch_C_1	2	0.2		1	
Ch_C_2	2	0.2		2	
Ch_C_5	2	0.2		5	
Ch_C_10	1	0.1		10	
Ch_CO_1	2		0.2	1	
Ch_CO_2	2		0.2	2	
Ch_CO_5	2		0.2	5	

Short fluidized bed reactor tests

Fluidization experiments were carried out with only a small amount of magnesium sulfate monohydrate in order to enable a short feeding time, ensuring equal residence times for the particles. The experimental conditions are summarized in Table 5. The fluidized bed tests were carried out with an supporting bed of MgO (50 grams) and five grams of magnesium sulfate monohydrate, which was fed in a feeding time of one minute when the furnace reached the target temperature of 900°C. Samples were taken from the bed after 1, 5, 10, 20, 30, and 60 minutes' residence time in the reactor. The large number of samples relative to the amount of materials may have disturbed the overall system, but in these experiments only the individual particles were

analyzed and not the overall decomposition of a batch of material. Two different experiments were carried out: the first test was carried out with twice the stoichiometric amount of solid sulfur as the reductant in an atmosphere of 100% nitrogen, and the second test was done with a gaseous reductant, in an atmosphere of 10% carbon monoxide and 90% nitrogen.

Table 5. Overview of experimental conditions for short fluidization experiments, gas flow 1.2 L/min, temperature 900°C.

Test	$MgSO_4$ (g)	Solid reductant (g)	Gaseous reductant (partial pressure)	Samples
Fz_S_1.1	5	1.2 g (2x st.)		1, 5, 10, 20, 30, 60 min
Fz_S_1.2	5	1.2 g (2x st.)		1, 5, 10, 20, 30, 60 min
Fz_CO_1	5		0.1	1, 5, 10, 20, 30, 60 min

3.3.2 Fluidized bed reactor tests

Fluidized bed tests were carried out in order to determine the operating window for the successful decomposition of magnesium sulfate. The furnace was preheated under a flow of nitrogen with a 50 g inert MgO bed. Hydrated magnesium sulfate (30 grams) was added manually with a spoon to the furnace during a feeding time of 30 minutes. This relatively long feeding time was required to maintain the target temperature of the furnace. The solid reductants, carbon or elemental sulfur, were mixed with the magnesium sulfate prior to feeding. When carbon monoxide was used as the reductant, the carbon monoxide gas flow was only used during the duration of the experiment, including the feeding period. Before and after the experiment, an atmosphere of 100% nitrogen was used.

Samples were taken with a sample spoon, which was lowered into the bed. The samples taken while the experiment was going on were left to cool in air. The product sample was obtained after the material had slowly cooled under a nitrogen flow inside the furnace. The bed material was separated manually from the products or intermediates prior to XRD and total sulfur analysis, whenever possible. The total sulfur content in the sample was used to calculate the amount of magnesium sulfate that had decomposed. In some experiments it was not possible to distinguish the products/intermediates from the bed material, which is then mentioned in the results chapter. In those experiments,

it was not possible to calculate the amount of magnesium sulfate that had decomposed, because the ratio of bed material and product in these samples is unknown; the total amount of sulfur was therefore reported instead. Off-gas analysis was commenced prior to the start of the experiment and ended when the furnace was switched off. The off-gas composition was measured inside the reactor tube, approximately 15 centimeters from the top of the reactor. As a result, some air leakage may have taken place. This was, however, unavoidable; because the measuring tube would have become blocked too soon when lowered further into the reactor tube.

The conditions for all fluidized bed experiments with a feeding time of 30 minutes are given in Table 6 and the experiment name is used in the results and discussion chapters. The experiment name starts with H or M, which stands for dried magnesium sulfate heptahydrate (dried so that it is composed of $MgSO_4 \cdot H_2O$), or magnesium sulfate monohydrate, respectively. The second letter in the name stands for the reductant used, either solid elemental sulfur (S), solid carbon (C), or carbon monoxide gas (CO). The number in the third part of the name indicates the particle size group (1-4). The following letters were used in the third part of the name:

Pre = Preliminary test
A = Tests with varying amount of reductant
T = Tests with varying temperature
G = Most successful tests for each reductant repeated with gas analysis

Impurities are likely to be present when the magnesium sulfate feed material is obtained from the various waste acid streams of a hydrometallurgical process. Experiments with the addition of a minor amount of iron sulfate, manganese sulfate, and calcium sulfate were therefore carried out, which is indicated in the experimental name by Fe, Ca, or Mn, These impurities were mixed with the feed material as powders. An overview of the amounts of impurities used in the different tests is shown in Table 7.

Table 6. Experimental conditions for all fluidized bed experiments.

Experiment number	Experiment name	$MgSO_4$ hydrate	Amount of reductant	T	Gas flow	Impurity	Particle size	Residence time	Sampling moments
				(°C)	(L/min)		(µm)	(h)	
1	H_Pre_1	Hepta	-	900	1.2-4.5*	-	420-595	-	-
2	H_Pre_2	Hepta	-	900	1.2-4.5*	-	420-595	-	-
3	H_Pre_3	Hepta	-	900	3.5	-	420-595	-	-
4	H_S_1	Hepta (dried)	2x st. S	900	3.5	-	420-595	2	2h, cooled
5	H_CO_1.1	Hepta (dried)	10% CO	900	3.5	-	420-595	3	3h, cooled
6	H_CO_1.2	Hepta (dried)	20% CO	900	3.5	-	420-595	2	feeding, 2h, cooled
7	H_C_1.1	Hepta (dried)	2x st. C	900	3.5	-	420-595	2	2h, cooled
8	H_C_1.2	Hepta (dried)	1x st. C	900	3.5	-	420-595	1	1h cooled
9	H_S_2	Hepta (dried)	2x st. S	900	3.5	-	297-420	2	2h, cooled
10	H_CO_2.1	Hepta (dried)	10% CO	900	3.5	-	297-420	2	2h, cooled
11	H_CO_2.2	Hepta (dried)	20% CO	900	3.5	-	297-420	2	feeding, 2h, cooled
12	H_C_2	Hepta (dried)	2x st. C	900	3.5	-	297-420	2	2h, cooled
13	H_S_3.1	Hepta (dried)	2x st. S	900	1.9	-	105-210	2	2h, cooled
14	H_S_3.2	Hepta (dried)	3x st. S	900	1.9	-	105-210	2	2h, cooled
15	H_CO_3.1	Hepta (dried)	10% CO	900	1.9	-	105-210	2	cooled
16	H_CO_3.2	Hepta (dried)	20% CO	900	1.9	-	105-210	2	2h, cooled
17	H_C_3	Hepta (dried)	2x st. C	900	1.9	-	105-210	2	2h, cooled
18	H_S_4	Hepta (dried)	2x st. S	900	1.2	-	-150	2	2h, cooled
19	H_CO_4	Hepta (dried)	10% CO	900	1.2	-	-150	2	2h, cooling
20	M_Pre_1	Mono	-	900	1.2-4.5*	-	-150	-	2h, cooled
21	M_Pre_2	Mono	-	900	1.2-4.5*		-150	-	-
22	M_4	Mono	-	900	1.2	-	-150	2	feeding, 2h, cooled
23	M_S_3	Mono	2x st. S	900	1.9	-	105-210	2	feeding, 2h, cooled
24	M_S_4	Mono	2x st. S	900	1.2	-	-150	2	feeding, 2h, cooled
25	M_CO_4	Mono	10% CO	900	1.2	-	-150	2	feeding, 2h, cooled
26	M_S_4_A1	Mono	1x st. S	900	1.2	-	-150	4	feeding, 1h, 2h, 3h, 4h, cooled
27	M_S_4_A2	Mono	2x st. S	900	1.2	-	-150	4	feeding, 1h, 2h, 3h, 4h, cooled
28	M_S_4_A3	Mono	4x st. S	900	1.2	-	-150	4	feeding, 1h, 2h, 3h, 4h, cooled
29	M_S_4_T1	Mono	2x st. S	850	1.2	-	-150	4	feeding, 1h, 2h, 3h, 4h, cooled
30	M_S_4_T2	Mono	2x st. S	900	1.2	-	-150	4	feeding, 1h, 2h, 3h, 4h, cooled
31	M_S_4_T3	Mono	2x st. S	950	1.2	-	-150	4	feeding, 1h, 2h, 3h, 4h, cooled
32	M_CO_4_T1	Mono	10% CO	850	1.2	-	-150	1	feeding, 1h, cooled
33	M_CO_4_T2	Mono	10% CO	900	1.2	-	-150	1	feeding, 1h, cooled
34	M_S_4_G	Mono	2x st. S	900	1.2	-	-150	2	feeding, 1h, 2h, cooled
35	M_CO_4_G	Mono	10% CO	900	1.2	-	-150	2	feeding, 1h, 2h, cooled
36	M_C_4_G	Mono	2x st. C	900	1.2	-	-150	2	feeding, 1h, 2h, cooled
37	M_S_3_Fe	Mono	2x st. S	900	1.9	$FeSO_4$	105-210	2	feeding, 2h, cooled
38	M_S_4_Mn	Mono	2x st. S	900	1.2	$MnSO_4$	-150	2	feeding, 2h, cooled
39	M_S_4_Fe	Mono	2x st. S	900	1.2	$FeSO_4$	-150	2	feeding, 2h, cooled
40	M_S_4_Ca	Mono	2x st. S	900	1.2	$CaSO_4$	-150	2	feeding, 2h, cooled
41	M_CO_4_Mn	Mono	10% CO	900	1.2	$MnSO_4$	-150	2	feeding, 2h, cooled
42	M_CO_4_Fe	Mono	10% CO	900	1.2	$FeSO_4$	-150	2	feeding, 2h, cooled
43	M_CO_4_Ca	Mono	10% CO	900	1.2	$CaSO_4$	-150	2	feeding, 2h, cooled

*Gas flow speed was varied during the experiment

Table 7. The type and amount of impurities in experiments 37-43; conditions are given in Table 6.

Test Number	Test Name	Impurity	Amount of impurity	
			wt (%)	mol (%)
37	M_S_3_Fe	$FeSO_4 \cdot 7H_2O$	10.0	5.0
38	M_S_4_Mn	$MnSO_4 \cdot H_2O$	6.0	4.9
39	M_S_4_Fe	$FeSO_4 \cdot 7H_2O$	10.0	5.0
40	M_S_4_Ca	$CaSO_4 \cdot 2H_2O$	6.2	5.0
41	M_CO_4_Mn	$MnSO_4 \cdot H_2O$	6.0	4.9
42	M_CO_4_Fe	$FeSO_4 \cdot 7H_2O$	10.0	5.0
43	M_CO_4_Ca	$CaSO_4 \cdot 2H_2O$	6.2	5.0

4. Results

In this chapter the results of the preliminary TG/DSC tests are given in section 4.1, followed by the results of the initial reaction tests, which were used to determine what happens in the initial stage of the reaction, in section 4.2. The results of the fluidized bed experiments to determine the overall reaction kinetics are given in section 4.3, and the results of the experiments with the preferred conditions are given in section 4.4.

Extensive SEM/EDS analysis was carried out on the samples obtained. For clarity, the different main phases are shown in Figures 18-20. Figure 18 shows coarse magnesium sulfate (left) and fine magnesium sulfate (right). Figure 19 shows magnesium sulfate that decomposed to MgO, with a fine structure (left) and a coarser structure (right). The MgO bed material is shown in Figure 20, which can easily be distinguished from the magnesium oxide decomposition product. The EDS measurements were normalized for clarity and ease of comparison. The total measurement of dense material had to be at least 90% and for material with a high porosity, a minimum total measurement value of 75% was required; results with lower values were not taken into account. The stoichiometric compositions of different compounds are given in Table 8.

The results of the XRD analysis are also described in this chapter. Example XRD diagrams are shown here for clarification of the description. Figure 21 shows partially decomposed magnesium sulfate with clear peaks for both β-$MgSO_4$ and MgO. Figure 22 shows different the types of magnesium sulfate that may be present: β-$MgSO_4$, well crystallized $MgSO_4$ and non-crystalline $MgSO_4$, as well as MgO. Almost fully decomposed magnesium sulfate is shown in Figure 23, with large clear peaks for MgO and minor peaks of β-$MgSO_4$. Fully decomposed magnesium sulfate is shown in Figure 24, with clear MgO peaks only.

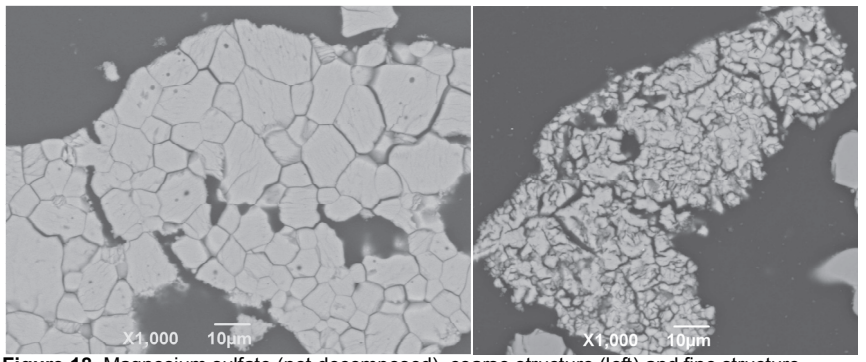

Figure 18. Magnesium sulfate (not decomposed), coarse structure (left) and fine structure (right).

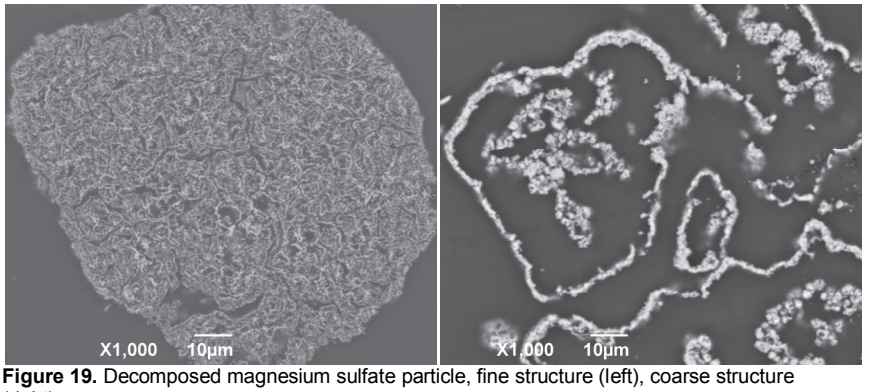

Figure 19. Decomposed magnesium sulfate particle, fine structure (left), coarse structure (right).

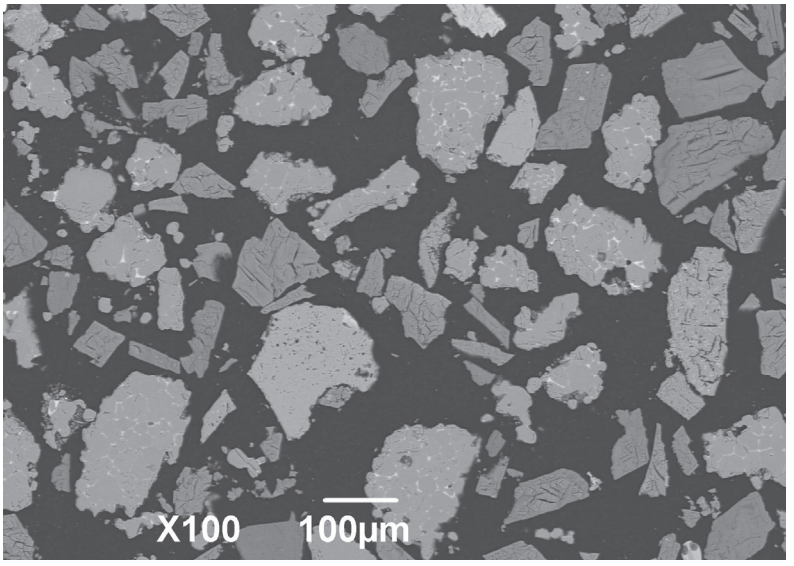

Figure 20. MgO bed material

Table 8. Stoichiometric compositions of various magnesium compounds and their molecular weights.

	MW	Mg %	S%	O %	H %	total
$MgSO_4 \cdot 7H_2O$	246.47	9.86	13.01	71.40	5.73	100
$MgSO_4 \cdot H_2O$	138.38	17.56	23.17	57.81	1.46	100
$MgSO_4$	120.37	20.19	26.64	53.17	-	100
$MgSO_3$	104.37	23.29	30.72	45.99	-	100
$MgSO_2$	88.37	27.50	36.29	36.21	-	100
MgSO	72.37	33.58	44.31	22.11	-	100
MgS	56.37	43.12	56.88	-	-	100
MgO	40.30	60.30	-	39.70	-	100
Mg	24.31	100	-	-	-	100
S	32.07	-	100	-	-	100
O	16.00	-	-	100	-	100
H	1.01				100	100

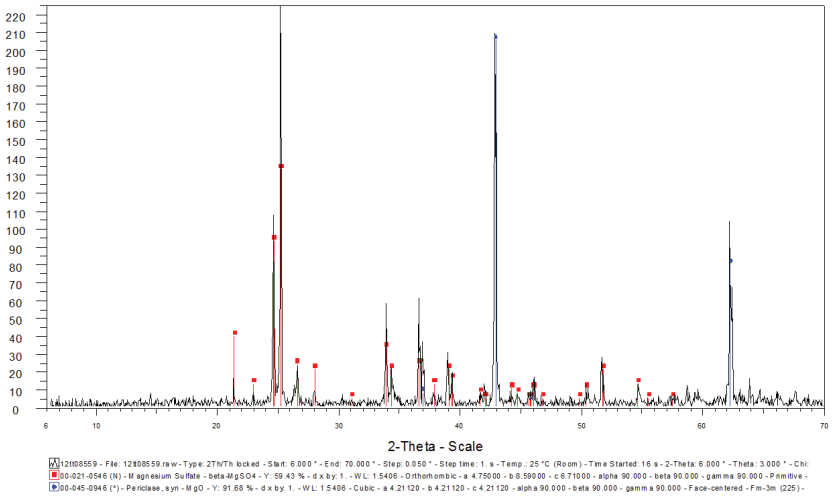

Figure 21. Example of XRD analysis showing mainly β-$MgSO_4$ with peaks for MgO.

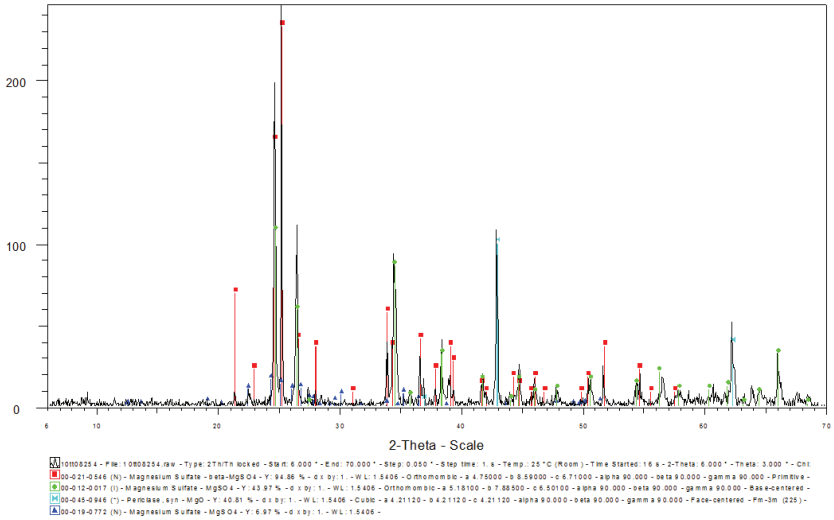

Figure 22. Example of XRD analysis, with mainly β-$MgSO_4$, but also α-$MgSO_4$, MgO, and a minor amount of amorphous $MgSO_4$.

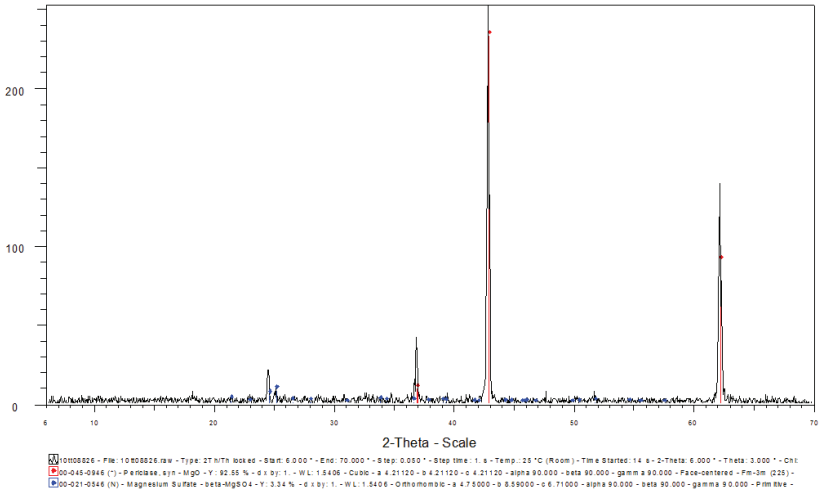

Figure 23. Example of XRD analysis with mainly MgO and a minor amount of β-$MgSO_4$.

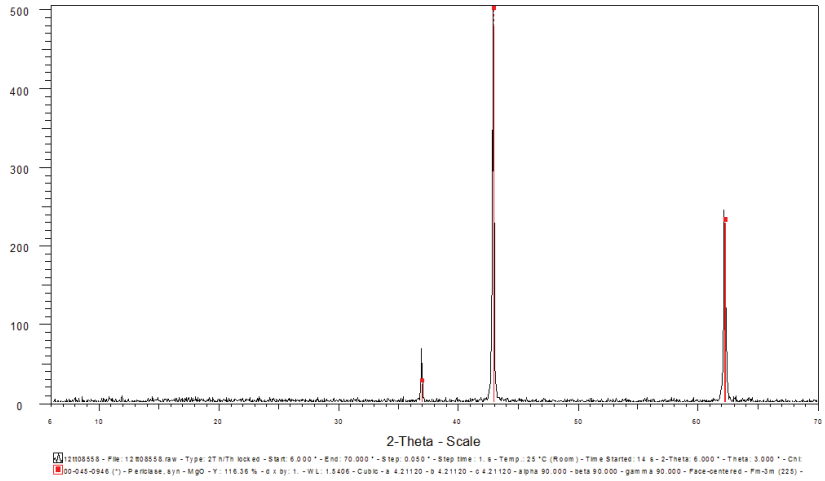

Figure 24. Example of XRD analysis with clear MgO peaks.

4.1 Preliminary TG/DSC tests

Thermogravimetric (TG/DSC) experiments were carried out to determine the decomposition temperature of hydrated magnesium sulfate in the absence of any reductants as well as with carbon monoxide gas. Solid reductants could not be used in these tests, because of their combustion prior to attainment of the decomposition temperature. Both experiments were carried out at a heating rate of 5°C/min and a sample mass of 29.00 mg. One experiment was carried out under a nitrogen atmosphere (Figure 25) and the other experiment was carried out under a nitrogen atmosphere up to 700°C, after which the gas composition was changed to 90% nitrogen and 10% carbon monoxide (Figure 26). The carbon monoxide gas flow was started at elevated temperature in order to prevent deposition of carbon on the surface of the magnesium sulfate.

Both curves show a mass decrease at low temperature (<300°C) due to dehydration, which is in agreement with the results of other researchers [19, 21, 68]. With the change in mass, phase changes also occurred, shown by the peaks of enthalpy contributions in the DSC measurements. The mass remained constant until decomposition of magnesium sulfate commenced at approximately 880°C under both 100% nitrogen and 90% nitrogen with 10% carbon monoxide. The decomposition reaction was completed at different

temperatures: magnesium sulfate was fully decomposed at 1110°C under nitrogen atmosphere and with carbon monoxide as the reductant at 1070°C. The DSC peak at 700°C in Figure 26 was caused by the change in gas composition from 100% to 90% nitrogen and 10% carbon monoxide.

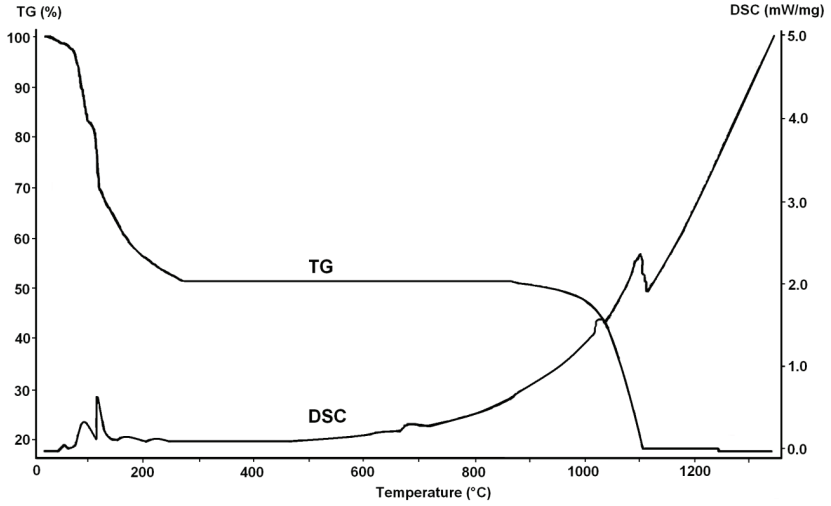

Figure 25. TG-DSC measurements of the decomposition of $MgSO_4 \cdot 7H_2O$ in flowing N_2..

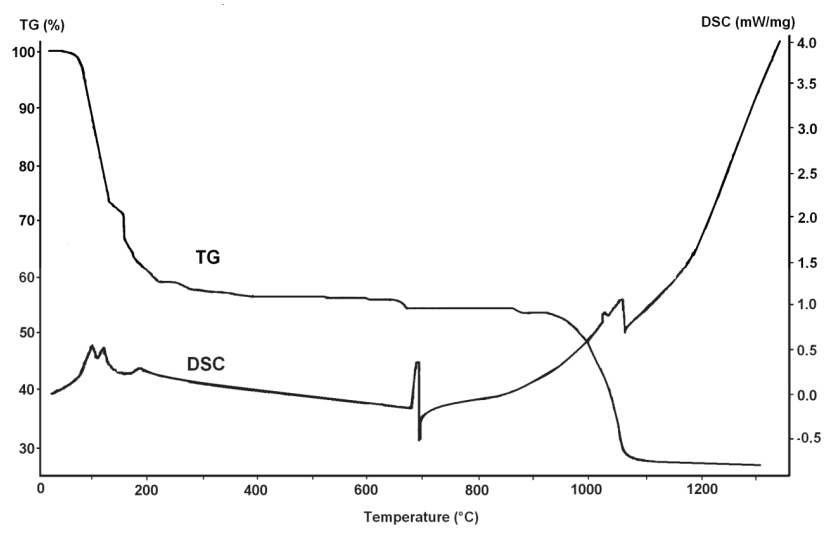

Figure 26. TG-DSC measurements of the decomposition of $MgSO_4 \cdot 7H_2O$, in 100% N_2 from 25-700 °C and in 90% N_2 + 10% CO at 700-1350 °C.

4.2 Initial reaction tests

Different types of tests were carried out to study how the decomposition reactions take place: short chamber furnace tests and short fluidized bed tests with only a small amount of $MgSO_4$, and thus a short feeding time. The aim of these experiments was to find out what happens in the initial stage of the reaction and the effect of the presence of different reductants on the decomposition reaction.

4.2.1 Short chamber furnace experiments

According to stoichiometric composition, magnesium sulfate monohydrate contains 23.17% sulfur and anhydrous magnesium sulfate contains 26.64% sulfur. The sulfur analysis of the experiments in Table 9 shows that little or no decomposition had taken place within 1, 2, 5, or 10 minutes. The samples may have rehydrated slightly due to the hygroscopic character of magnesium sulfate.

Table 9. Total sulfur analysis of the samples from the short chamber furnace experiments.

Sample	S%
Ch_5	25.4
Ch_S_1	25.1
Ch_S_2	24.8
Ch_S_2.1	24.8
Ch_S_5	25.2
Ch_S_5.1	25.3
Ch_C_1	22.9
Ch_C_2	23.7
Ch_C_5	22.1
Ch_C_10	25.8
Ch_CO_1	24.6
Ch_CO_2	24.9
Ch_CO_5	25.2

SEM analysis was carried out on the cross sections as well as on the powder samples obtained after each test. No decomposition was observed in the experiments with sulfur and in the experiments with carbon only some decomposition took place in test Ch_C_10, after a residence time of 10

minutes. This shows that good gas-solid contact is required in order to decompose magnesium sulfate.

The SEM micrographs revealed a difference in structure that was not observed in any of the fluidized bed experiments (Figure 27). The particles showed cavities with the shape of a crystal. This structure was observed after 1, 2, and 5 minutes. This indicates that part of the magnesium sulfate was present in highly soluble form after the experiment and was washed away during the sample-making process, in which water was used. EDS analysis of the magnesium sulfate particles shows that their composition is very close to the stoichiometric assay of magnesium sulfate, regardless of the structural transformations.

In the experiments with CO, no decomposition was observed after 1 or 2 minutes, but approximately 1% of the particles decomposed fully or partially after 5 minutes (Figure 28, left). A clear reaction front is visible for these particles and the magnesium sulfate particles in the sample showed swelling. This can also clearly be seen from the powder sample surfaces (Figure 28, right).

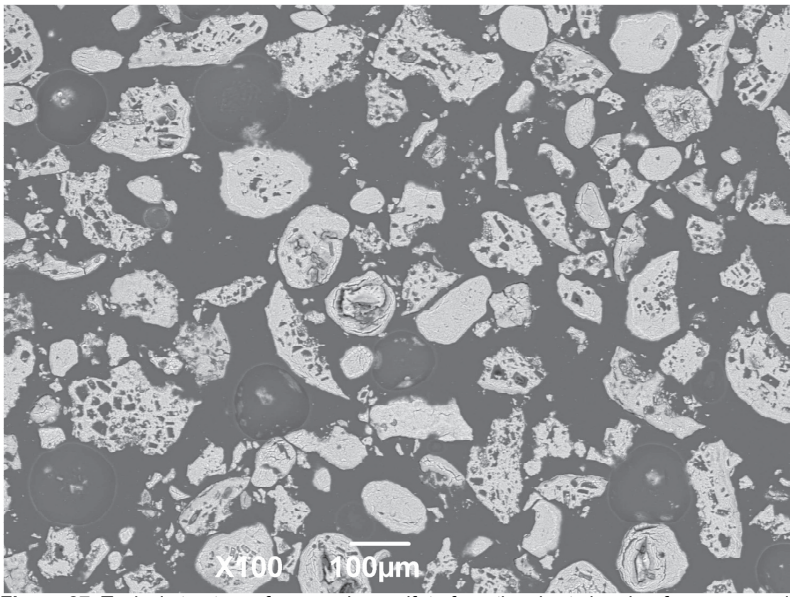

Figure 27. Typical structure of magnesium sulfate from the short chamber furnace experiments.

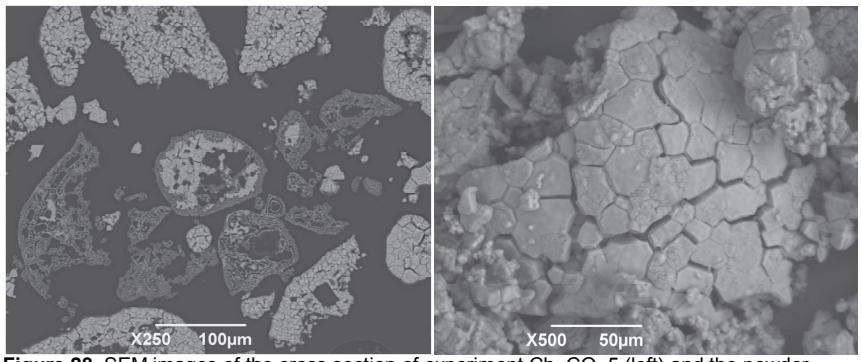

Figure 28. SEM images of the cross section of experiment Ch_CO_5 (left) and the powder sample surface (right).

4.2.2 Short fluidization experiments

Short fluidization tests with sulfur as the reductant

Fluidization problems occurred during test Fz_S_1.1; it was therefore repeated (Fz_S_1.2). The results from the first test show that some decomposition had already occurred at the start of the experiment. During the first 5 minutes, both partially decomposed and unaffected particles were observed (Figure 29, top left). After 10 minutes, particles in different stages of decomposition were observed, from unaffected to decomposed (Figure 29, top right). After 30 minutes, some magnesium sulfate could still be found; only after one hour did full decomposition of most of the particles take place (Figure 29, bottom left and right, respectively). Over time, the overall decomposition of the particles increased, but the particles did not decompose evenly. It took between 30 and 60 minutes until nearly all particles were decomposed, which is longer than expected from the fluidized bed tests with a longer feeding time. After one hour, 95-99% of all magnesium sulfate had decomposed.

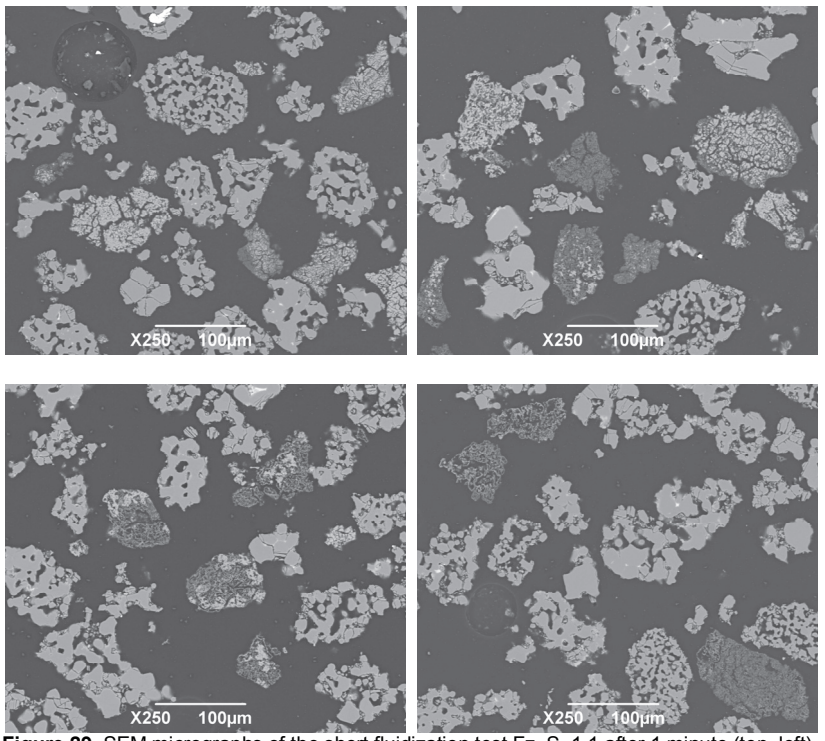

Figure 29. SEM micrographs of the short fluidization test Fz_S_1.1 after 1 minute (top, left), 10 minutes (top, right), 30 minutes (bottom, left), and 60 minutes (bottom, right).

The bed was very well fluidized when the test was repeated (Fz_S_1.2). The SEM micrographs, however, did not show more decomposed particles during the first ten minutes of the experiment. On the contrary, there was more magnesium sulfate in the samples taken after 1 and 10 minutes. During the first 10 minutes, partially decomposed and unaffected particles were observed (Figure 30, top left and right). After 30 minutes, there were still some particles that were only slightly affected, while others were fully decomposed (Figure 30, bottom left). In the samples taken after one hour, there was still some residual magnesium sulfate in the particles, as shown in Figure 30, bottom right. These results show that good fluidization did not improve the reaction kinetics and that the decomposition did not take place evenly from one grain to another.

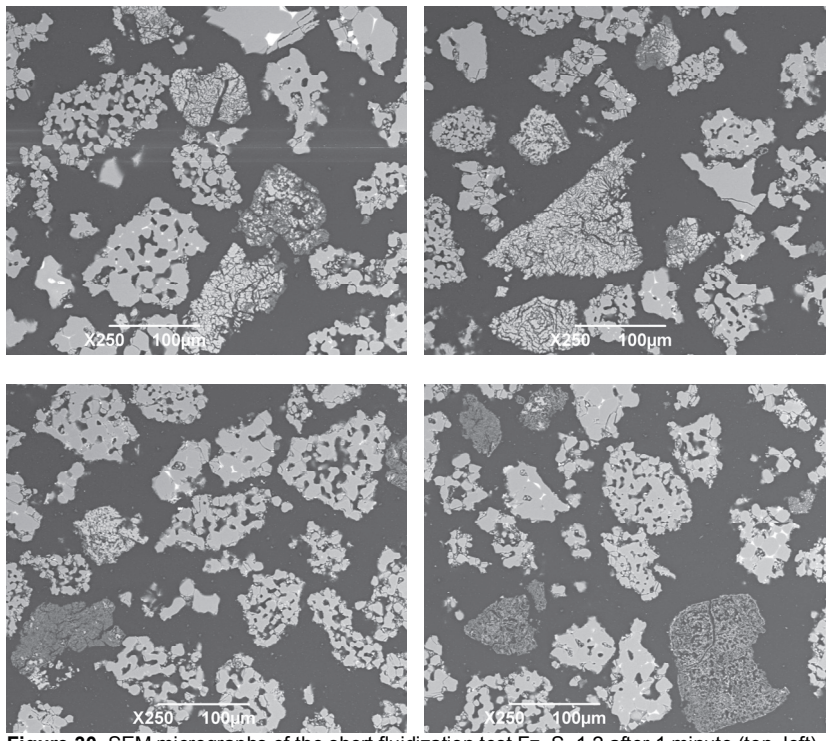

Figure 30. SEM micrographs of the short fluidization test Fz_S_1.2 after 1 minute (top, left), 10 minutes (top, right), 30 minutes (bottom, left), and 60 minutes (bottom, right).

Short fluidization test with carbon monoxide as the reductant

For comparison, a similar test with carbon monoxide as the reductant was carried out, described in section 3.2. The bed was very well fluidized during this test. The amount of fines increased after 30 minutes, which made observation of the fluidizing behavior in the furnace less clear. There was a flame when the 30-minute sample was taken from the reactor, probably due to carbon monoxide gas reacting with oxygen in the upper part of the reactor. This sample may therefore not be reliable.

The SEM micrographs in Figure 31, top left, show that no decomposition took place initially, but that a clear reaction front could be observed after 10 minutes (Figure 31, top right). This was confirmed by EDS analysis. No magnesium sulfate was found in the samples taken after 20, 30, and 60 minutes, as can be seen from Figure 31, bottom left and right for the 30- and 60-minute sample, respectively. This experiment showed that the particles

decomposed more evenly than with sulfur as the reductant. Additionally, no sulfate was left in the cores of the particles.

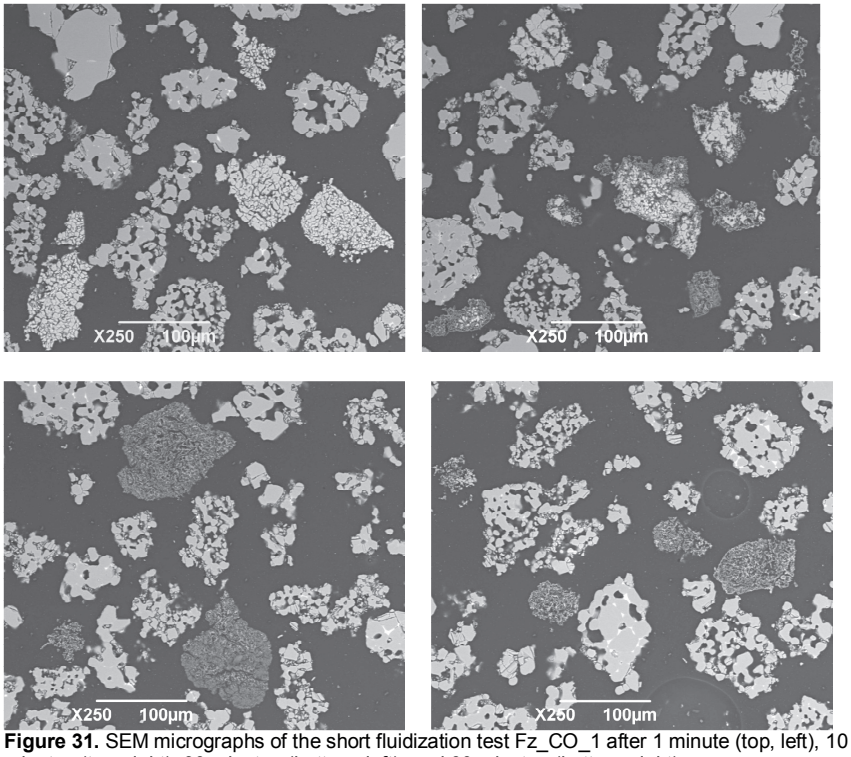

Figure 31. SEM micrographs of the short fluidization test Fz_CO_1 after 1 minute (top, left), 10 minutes (top, right), 30 minutes (bottom, left), and 60 minutes (bottom, right).

4.3 Overall reaction kinetics

The reaction kinetics was studied in different ways: in the fluidized bed experiments with a 30-minute period of feeding and in short experiments where the feeding time was only up to one minute. The reaction kinetics was affected by the type and amount of reductant, temperature, the particle size, and the presence of different impurities.

4.3.1 The use of a reductant

Fluidization tests were carried out in the absence of any reductants, for comparison with the tests where reductants were used. The experiment (M_4) was carried out twice; in both cases there were problems keeping the bed

fluidized. XRD analysis after separation of product and bed material showed that there was mainly primitive orthorhombic β-$MgSO_4$ present with a minor amount of MgO. In one of the experiments, there was a minor amount of base-centered orthorhombic α-$MgSO_4$ as well. The difference between α-$MgSO_4$ and β-$MgSO_4$ is defined in section 2.1.2. Fluidization problems were also experienced during the preliminary tests (H_Pre_1-3 and M_Pre 1-2).

The presence of a reductant will prevent the magnesium sulfate particles from becoming sticky in the bed. A reductant is thus required in the decomposition experiments to keep the bed well fluidized, which is a prerequisite for good gas-solid contact. When the gas-solid contact is poor, decomposition of magnesium sulfate will be minimal at a temperature of 900°C.

SEM analysis of the cross section confirmed that no significant decomposition had taken place, as shown in Figure 32. The majority of the particles have the typical β-$MgSO_4$ structure. Some particles, however, have a morphology that is similar to that of MgO, as shown in Figure 32 (middle part of the image). EDS analysis, however, showed a composition close to that of $MgSO_4$.

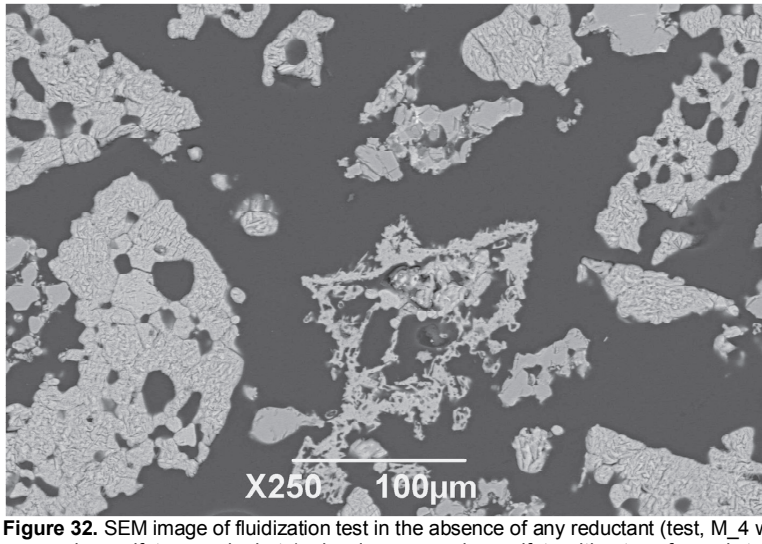

Figure 32. SEM image of fluidization test in the absence of any reductant (test, M_4 with magnesium sulfate monohydrate), showing magnesium sulfate with a transformed structure (middle) and normal magnesium sulfate (other particles).

4.3.2 Raw material

The degree of decomposition and the structure of the products were compared for three different raw materials: magnesium sulfate heptahydrate, dried magnesium sulfate heptahydrate (to monohydrate), and magnesium sulfate monohydrate.

It was not possible to fluidize the magnesium sulfate heptahydrate at 900°C (H_Pre_1), due to the large amount of crystal water that was released when the material was fed to the reactor. The material recrystallized into elongated magnesium sulfate crystals, as shown in Figure 33. XRD analysis showed that the sample was mainly composed of β-$MgSO_4$ as well as minor amounts of α-$MgSO_4$ and $MgSO_4 \cdot 6H_2O$. Predrying is thus required when using magnesium sulfate heptahydrate as the feed material.

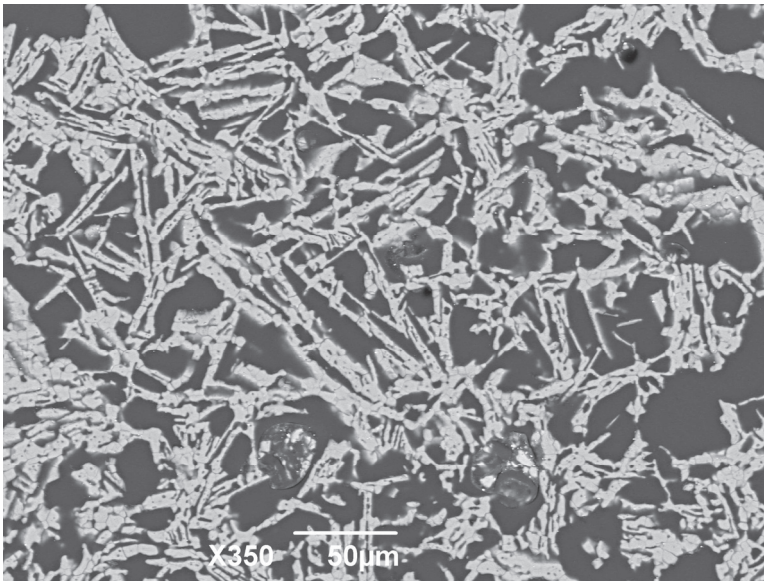

Figure 33. Product of the test with $MgSO_4 \cdot 7H_2O$ as feed material (H_Pre_1).

Experiments using two different feed materials as the raw material were carried out for comparison. The monohydrate in tests M_S_3 and M_S_4 was well fluidized. The bed was fully fluidized, with bubbles visible in the bed region and solids moving downward along the reactor wall. Sulfur particles moved on the grate surface as well as through the bed. The downward movement of the bed was uneven just after feeding was completed, but became smooth as the reaction time proceeded. The interface between bed and

freeboard region was difficult to define in experiment M_S_4, because of some fines that had been deposited on the reactor wall in the freeboard region. In test M_S_3, 51.9% of the magnesium sulfate decomposed and 95.6% for the smaller particle size group in experiment M_S_4. The residual magnesium sulfate was present in the bed as β-$MgSO_4$; no conversion to $MgSO_4$ took place. With dried magnesium sulfate heptahydrate, comparable results were obtained when the bed was well fluidized: 55.3% decomposed in experiment H_S_3 and 88.7% decomposed in test H_S_4. Defluidization of the bed, however, occurred in some of the experiments, which led to poor results (a decomposition yield of only 10% of the magnesium sulfate) and the need to repeat the experiment.

Two similar experiments were carried out with 10% CO as a reductant, with monohydrate or dried heptahydrate as the feed material: M_CO_4 and H_CO_4. A clear difference between the chosen feed materials was observed, as the sulfur content in the product of test M_CO_4 was only 1.7%, whereas it was 15.5% in test H_CO_4. These sulfur percentages represent 93.6% and 41.8% decomposition for monohydrate and dried heptahydrate, respectively. A gas flow with 10% carbon monoxide (1.2 L/min total gas flow) was enough to decompose the monohydrate successfully, but a higher partial pressure of carbon monoxide is required for dried heptahydrate. With the heptahydrate, the bed defluidized multiple times after feeding, which was resolved by briefly increasing the gas flow rate. In one test, the bed defluidized one hour after feeding and it was not possible to refluidize it. This resulted in only 10.6% decomposition of magnesium sulfate. Repeating this experiment resulted in 88.7% decomposition, with no fluidization problems. High conversion of magnesium sulfate to oxide can thus only be achieved when there are no fluidization problems in the fluidized bed, with good mass and heat transfer between the gas and the solids.

These results indicate that a similar degree of decomposition could be achieved with twice the stoichiometric amount of elemental sulfur or 10% CO in the gas (1.2 L/min total gas flow) when using magnesium sulfate monohydrate as the feed material.

The advantage of using monohydrate is therefore that defluidization did not occur whereas it did with dried heptahydrate, which resulted in a smaller degree of decomposition of magnesium sulfate, as can be seen in Figure 34. In

this graph, the results for the tests with sulfur and carbon monoxide as the reductant are given, in order to illustrate the effect of using different raw materials. All tests were done with magnesium sulfate with a particle size of –150 µm. A comparison between the different reductants is made in the discussion chapter.

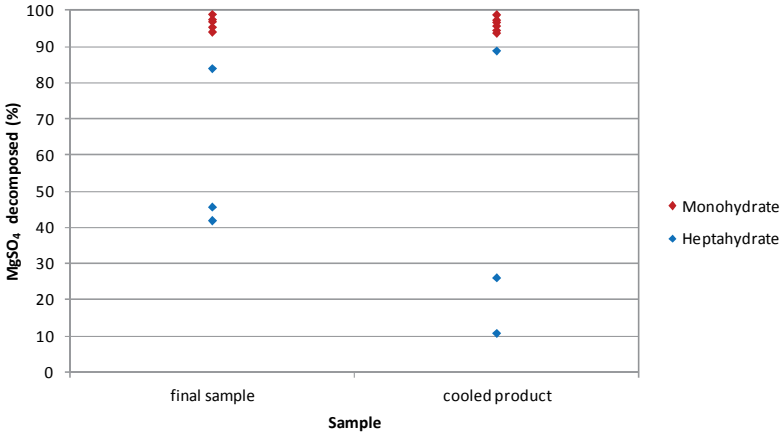

Figure 34. The effect of raw material on the decomposition of magnesium sulfate in the FB.

4.3.3 Temperature

The results of experiments carried out at different temperatures, with magnesium sulfate monohydrate as the raw material and with sulfur as the reductant, are given in Figure 35 (tests M_S_4_T1-3) These results show that the temperature has a clear effect on the reaction rate, as well as on the residual sulfur content in the sample. At 850°C, only some of the magnesium sulfate decomposed and the bed was segregated. A higher sulfur content in the final sample usually indicates segregation of the bed; these samples are more representative than the samples taken during furnace operation. 66% of the magnesium sulfate had decomposed directly after feeding in the experiment at 900°C; for the experiment at 950°C it was as much as 92.1%. The final sulfur content is very similar, even though the reaction kinetics was faster at 950°C.

Not only is the residual amount of sulfur of importance, but also the microstructure of the product. Figure 36 shows the surface structures of the powder product samples. The individual crystals are clearly visible in the

images from the experiments at 850°C and 900°C; diffusion took place at 950°C, which caused a reduction in the specific surface area of the particles.

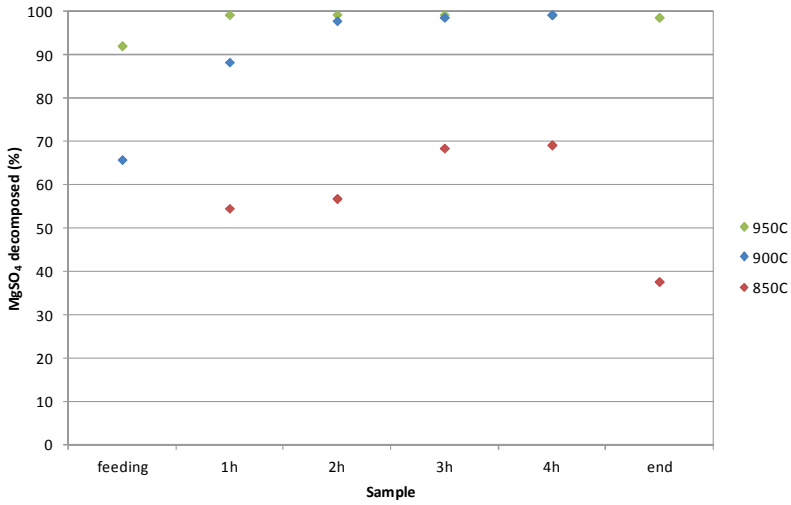

Figure 35. Decomposition of magnesium sulfate as a function of time at 850, 900, and 950°C with twice the stoichiometric amount of sulfur as the reductant, gas flow: 1.2 L/min N_2 (tests M_S_4_T1-3).

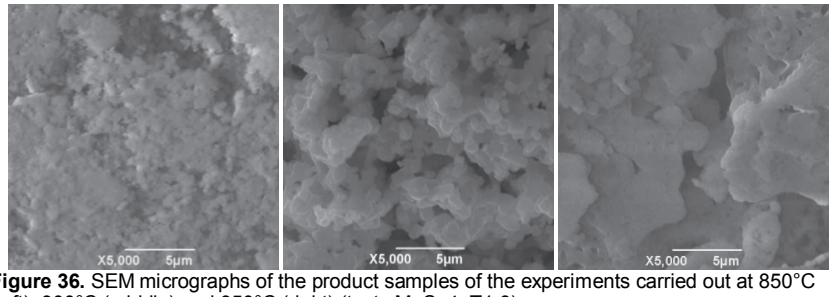

Figure 36. SEM micrographs of the product samples of the experiments carried out at 850°C (left), 900°C (middle) and 950°C (right) (tests M_S_4_T1-3).

The effect of temperature was also tested with carbon monoxide as the reductant, at 850°C and 900°C (tests M_CO_T1-2). The results in Figure 37 show that initially slightly more $MgSO_4$ decomposed at 850°C, but that from 45 minutes onwards, the amounts were equal for the experiments carried out at 850°C and 900°C. The surface structure of the products from both experiments is shown in Figure 38. Both images show a fine structure, with

slightly larger crystals with sharper edges for the experiment carried out at 850°C and finer, more rounded crystals for the test at 900°C.

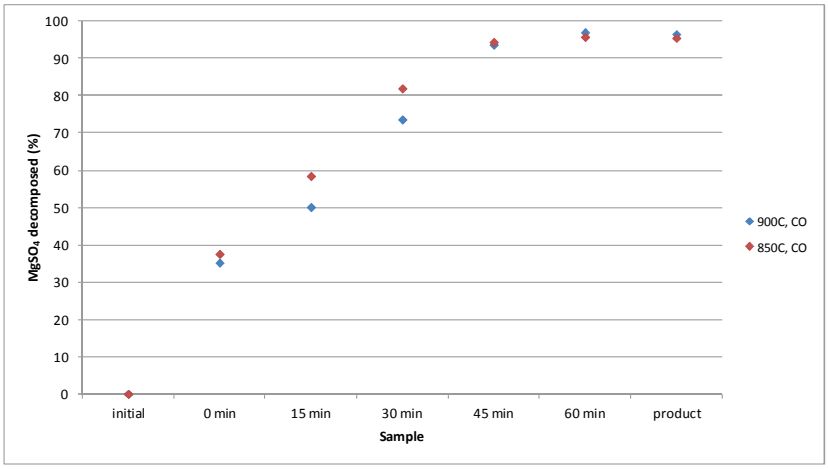

Figure 37. Decomposition of magnesium sulfate as a function of time with 10% CO as the reductant and 90% N_2 (total gas flow 1.2 L/min), carried out at 850°C and 900°C (tests M_CO_T1-2).

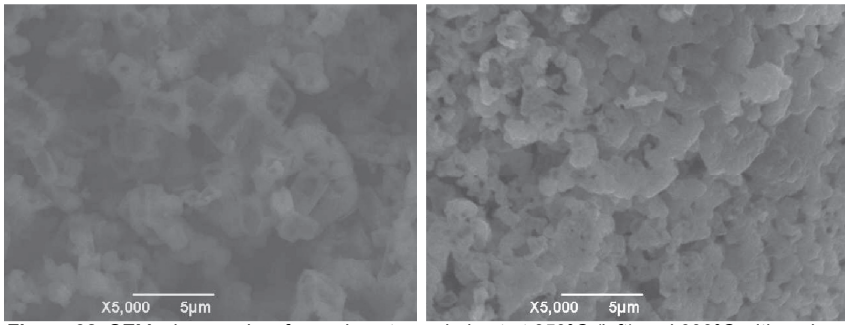

Figure 38. SEM micrographs of experiments carried out at 850°C (left) and 900°C with carbon monoxide as the reductant. (Tests M_CO_T1-2)

4.3.4 Amount of reductant

The effect of the amount of sulfur on the decomposition of magnesium sulfate can be clearly seen directly after feeding (Figure 39). Immediately after feeding, 75, 82, and 91% of magnesium sulfate decomposed using one, two, and four times the stoichiometric amount of sulfur, respectively. The difference in the reaction rate became smaller later on in the experiment. In the final sample, taken after the bed had cooled down, the percentage of

$MgSO_4$ decomposed in experiment M_S_4_A3 was lower than that during the experiment. This can be explained by contamination of the sample by a sulfur-rich material that had deposited on the inside of the reactor wall. In this experiment, a large amount of reductant was used (four times the stoichiometric amount), which caused more deposition of elemental sulfur and magnesium sulfate dust on the upper part inside the reactor tube, as shown in Figure 40. Not only does the amount of reductant have an effect on how much magnesium sulfate is decomposed, it also has an effect on the structure of the magnesium oxide product. SEM surface images of samples from tests M_S_4_A1-3 are shown in Figure 41 for comparison. It can be seen from these images that the surface area is large for the samples from M_S_4_A1 and M_S_4_A2, where one and two times the stoichiometric amount of sulfur was used. The individual crystal grains can be distinguished in the SEM images. With four times the stoichiometric amount of sulfur, however, diffusion has clearly taken place and the specific surface area is therefore smaller than in the other two tests.

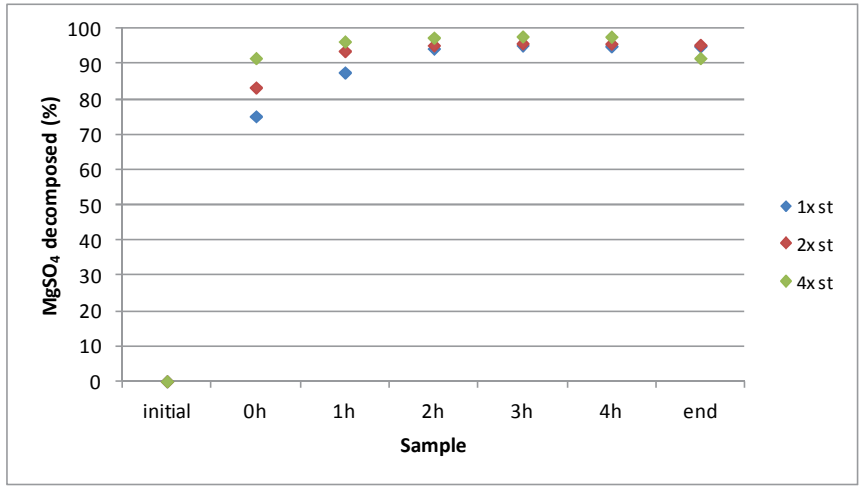

Figure 39. Decomposition of magnesium sulfate monohydrate as a function of time with one, two, and four times the stoichiometric amount of sulfur as reductant. T = 900°C, gas flow 1.2 L/min N_2 (tests M_S_A1-3).

Figure 40. Deposition of sulfur and magnesium sulfate dust inside the top of the reactor tube in experiment M_S_A3, with four times the stoichiometric amount of sulfur.

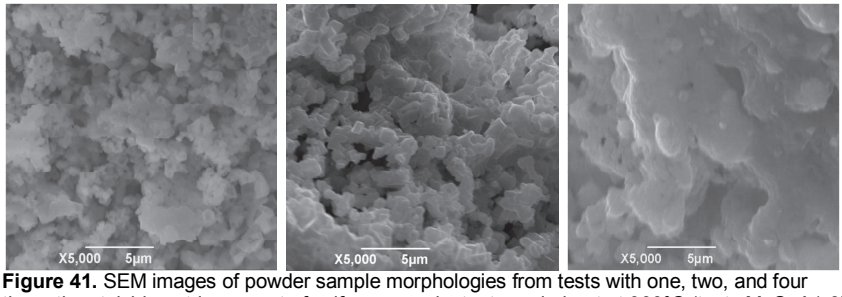

Figure 41. SEM images of powder sample morphologies from tests with one, two, and four times the stoichiometric amount of sulfur as a reductant, carried out at 900°C (tests M_S_A1-3).

Figure 42 shows the effect of the amount of reductant on different particle size groups of dried magnesium sulfate heptahydrate, using carbon monoxide as the reductant. These results show that a CO partial pressure of 0.2 is needed to achieve full decomposition of magnesium sulfate. With a CO partial pressure of 0.1, only 10-50% of the magnesium sulfate decomposed. A large difference between the two-hour sample and the final product indicates segregation in the bed, for example, in particle size group two for both the experiments with a carbon monoxide partial pressure of 0.1 and 0.2. Another explanation for the higher sulfur content in the final sample is contamination

of the sample by some sulfur-rich material from the upper part of the reactor tube. In experiments H_CO_1.1 and H_CO_3.1, in which 10% carbon monoxide was used, some segregation occurred as well. It cannot be determined whether segregation took place in the tests with 20% CO, because the material had fully decomposed.

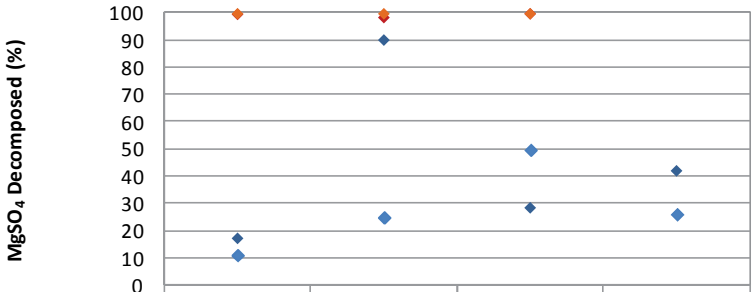

	420-595 µm	297-420 µm	105-210 µm	-150 µm
prod. 10% CO	11.0	24.9	49.7	26.0
prod. 20% CO	99.2	98.2	99.4	
2h 10% CO	17.0	89.9	28.3	41.8
2h 20% CO	99.5	99.5	99.5	

Figure 42. Effect of different CO concentrations on magnesium sulfate decomposition (dried $MgSO_4 \cdot 7H_2O$) for four particle size groups. The experiments were carried out at 900°C (tests H_CO_1.1-1.2, H_CO_2.1-2.2, H_CO_3.1-3.2, H_CO_4).

4.3.5 Particle size

The effect of particle size with sulfur as the reductant

The bed was well fluidized for the two largest particle size classes, 420-595 µm and 297-420 µm, in tests H_S_1 and H_S_2, respectively. The fluidization regime was bubbling during initial feeding, but became more vigorous when feeding was completed. Some fluidization problems occurred in test H_S_3.1 and the experiment had to be repeated several times until no defluidization occurred. In two trials, channeling occurred immediately during feeding and the lower part of the bed was not well fluidized due to sintering of the material. Another experiment was carried out with successful fluidization. The bed slowly expanded upon feeding and the fluidized particles in the freeboard were clearly visible. Bubbles moved upward in the bed, while solids moved downward along the reactor wall. Fluidization problems also occurred in test

H_S_ 4, in which particles of –150 μm were used. In the first trial, the bed was well fluidized until one hour after feeding, when defluidization occurred. It was not possible to refluidize the material by changing the gas flow. However, it was observed that the bed refluidized when the furnace cooled down to 500°C. The test was repeated with successful fluidization. The bed expanded during feeding, with some particles circulating in the freeboard region. The bed height significantly reduced during the reaction time. The FTIR off-gas analysis of this experiment is shown in Figure 43. The measuring tube of the FTIR analyzer is located in the upper part of the reactor tube, and as it is an open system, some oxygen was measured. In experiments of all size classes, sulfur was deposited directly inside the top of the reactor tube due to the lower temperature further away from the reaction zone of furnace. Some insulating material was placed around the reactor tube to prevent solidification of sulfur. Together with the sulfur, some fines were also deposited on the inside of the reactor tube, which were entrained during feeding as well as during the experiment.

The degree of decomposition depended strongly on the particle size, as illustrated by the experimental results in Figure 44. A trend line has been drawn for the experiments in which no fluidizing problems occurred, showing an increase in the degree of decomposition with decreasing particle size. It can also be observed that even though the degree of decomposition increased, problems with fluidization and bed stability occurred, which means problems in the repeatability of the experiments. The conversion of magnesium sulfate to oxide was low when fluidization problems occurred. Samples taken from the reactor after two hours, as well as from the product, were analyzed for sulfur content. Comparing the sulfur content of the sample after two hours with that of the product gives an indication of how well the bed was fluidized; a higher degree of decomposition after two hours compared with the product indicates segregation of the bed. Severe segregation occurred in experiments where the bed was not well fluidized.

The SEM analysis in Figure 45 shows the hollow structure of magnesium sulfate that is formed due to drying of magnesium sulfate heptahydrate from experiment H_S_1. This hollow structure was mainly found for particles in particle size group 420-595 μm and 297-420 μm. Figure 46 (left) shows fully and partly decomposed particles from test H_S_4. The overview micrograph

in Figure 46 (right) shows sintering and agglomeration that took place due to defluidization of the bed.

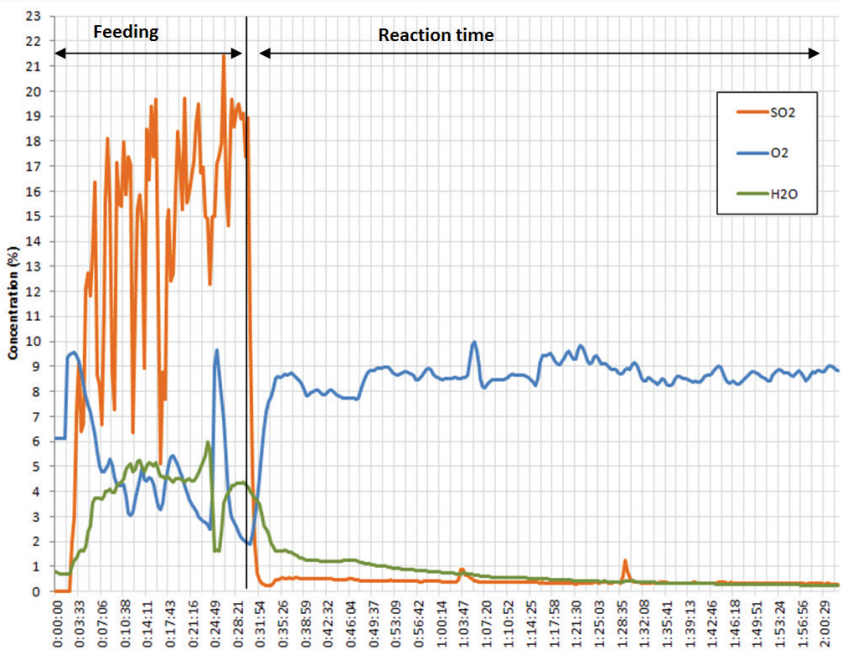

Figure 43. Gas analysis of experiment H_S_4 with sulfur as the reductant.

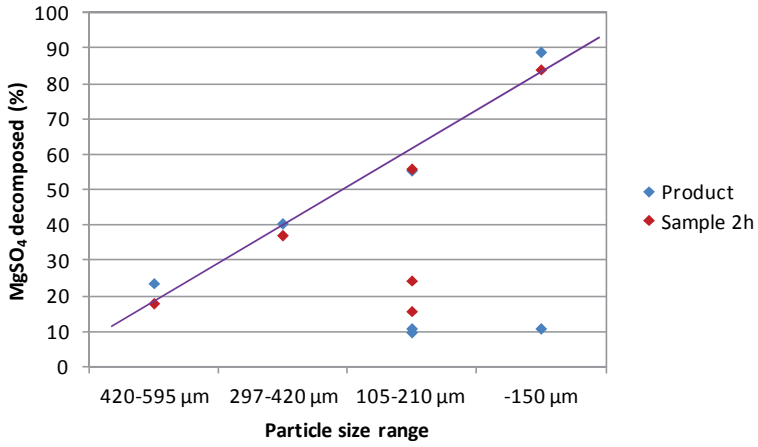

Figure 44. The effect of particle size class on the degree of decomposition of $MgSO_4$ with sulfur as the reductant, T = 900°C.

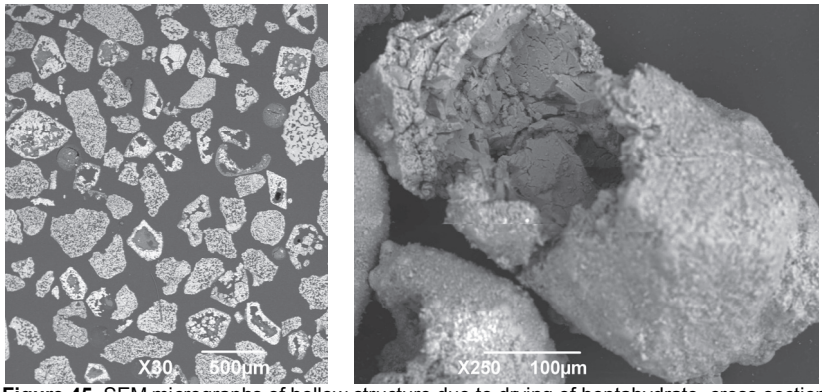

Figure 45. SEM micrographs of hollow structure due to drying of heptahydrate, cross section overview (left), hollow particle (right), from experiment H_S_1, carried out at 900°C.

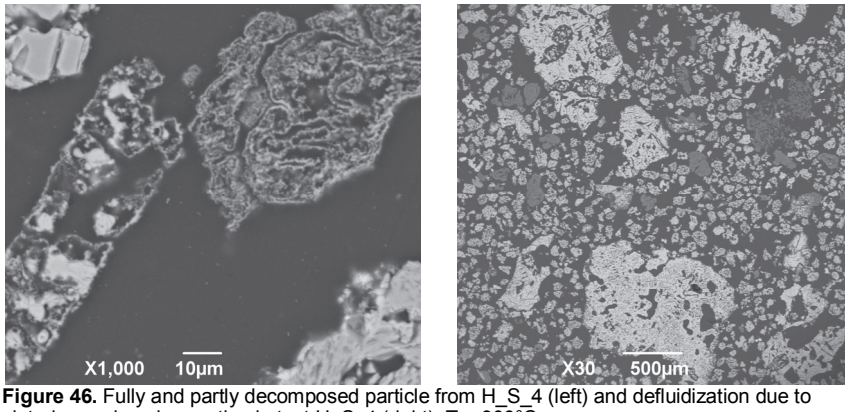

Figure 46. Fully and partly decomposed particle from H_S_4 (left) and defluidization due to sintering and agglomeration in test H_S_4 (right). T = 900°C.

The effect of particle size with carbon monoxide as the reductant

In section 4.3.4 the amount of reductant was discussed, which showed that a carbon monoxide partial pressure of 0.2 is required to decompose magnesium sulfate. Therefore, only the tests with different particle sizes and a carbon monoxide partial pressure of 0.2 are compared in this section. The bed was quite well fluidized in test H_CO_1.2 (420-595 µm), but the bed surface was difficult to distinguish, due to a large amount of fines in the freeboard which also deposited on the inside of the reactor tube. The samples that were taken during the experiment show that sintering and agglomeration had taken place. The behavior of the bed during test H_CO_2.2 (297-420 µm) and H_CO_3.2 (105-210 µm) was similar to that of test H_CO_1.2. The deposition of sulfur on the inside of the reactor wall in Figure 47 shows that decomposition already

took place during feeding. The sulfur originated from the gaseous decomposition product, which was reduced to sulfur gas by carbon monoxide. Sulfur solidified on the inside of the reactor tube as the top of the reactor tube was not insulated in these experiments. In all experiments with a carbon monoxide at a partial pressure of 0.2 as the reducing gas, >98% decomposition of sulfate took place, both after two hours and in the final product, as shown in Figure 48. The XRD curves show only peaks for MgO. In test H_CO_1.2 and H_CO_3.2 there was no segregation of the bed, because the sulfur content of the sample taken after two hours was very similar to that of the product. The sulfur content in the product of test H_CO_2.2 was higher than in the sample taken after two hours. This could be due to segregation, but it is more likely that the sample was contaminated with some sulfur from the inside of the reactor tube.

Figure 47. Sulfur deposited on the inside of the reactor wall during test H_CO_3.2, picture taken directly after feeding.

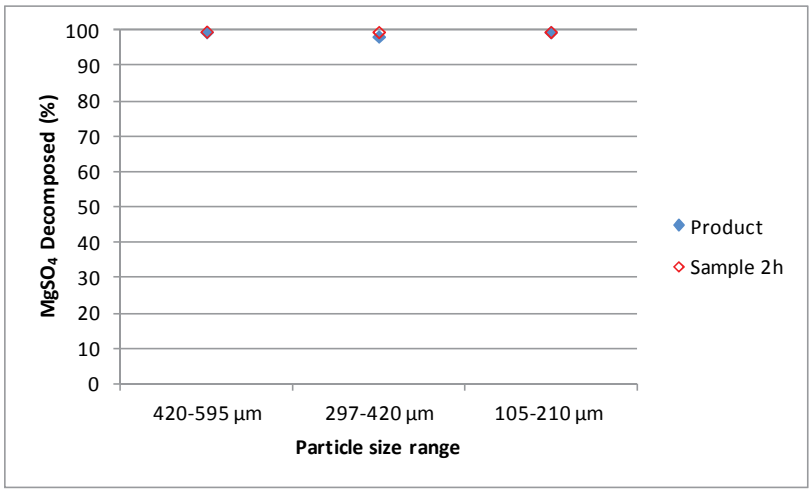

Figure 48. The effect of particle size class on the degree of decomposition of $MgSO_4$ (dried magnesium sulfate heptahydrate), carried out at 900°C in an atmosphere of 20% CO and 80% N_2 (tests H_CO_1.2, H_CO_2.2, and H_CO_3.2)

The effect of particle size with carbon as the reductant

The bed was quite well fluidized during test H_C_1.1 (420-595 µm), but the solids density in the dense phase was high. The solid density in the dense phase of test H_C_2 (297-420 µm) was also high. Some agglomeration took place on the bottom and some material build-ups were formed on the temperature element. Channeling occurred in test H_C_3 (105-210 µm), and the bed even defluidized once during feeding, but this was resolved by stirring the bed using the temperature measurement element. In these experiments >93% of the magnesium sulfate decomposed. Some segregation or contamination of the sample with sulfur from the reactor tube took place during each experiment, as can be seen from the results in Figure 49. The XRD analysis shows clear peaks for MgO and no other species are present, which suggests that the slightly higher sulfur content in the final sample was due to contamination of the final product sample by sulfur-rich material that was deposited on the upper part of the reactor tube.

The off-gas composition was also analyzed during these experiments, which is shown in Figure 50, Figure 51, and Figure 52 for tests H_C_1.1, H_C_2, and H_C_3, respectively. The curves show that the decomposition of magnesium sulfate started during the feeding period. The sulfur dioxide concentration in test H_C_1.1 increased after feeding had been completed (after 30 minutes),

probably due to the high solids density during the feeding period. Complete decomposition was achieved after 30 minutes of feeding time, followed by 43 minutes of reaction time. The peak in oxygen concentration after one hour and forty minutes was caused by removal of the FTIR measuring tube for a short moment, so that it was actually measuring the air outside the furnace. The gas analysis curves for H_C_2 and H_C_3 are quite similar; the sulfur dioxide concentration increased strongly after 7 minutes of feeding time. The decomposition of magnesium sulfate at a high reaction was completed after a 30-minute feeding period, followed by 11 minutes of reaction time.

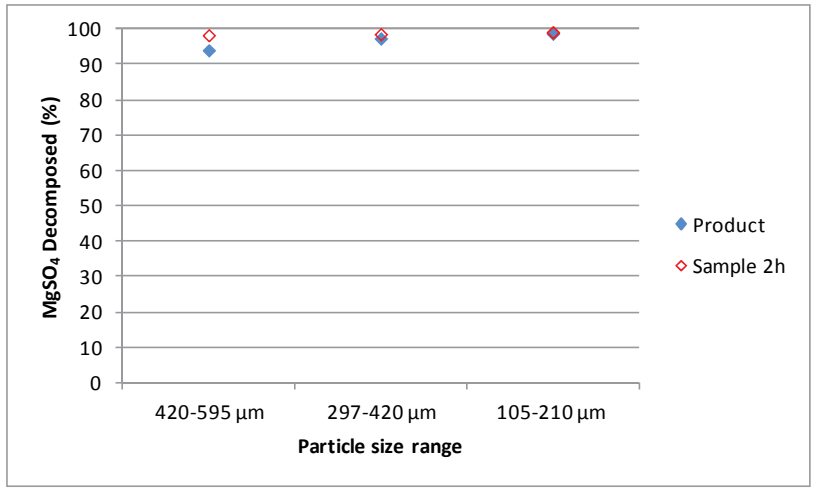

Figure 49. The effect of particle size class on the degree of decomposition of $MgSO_4$ (dried magnesium sulfate heptahydrate) with carbon as the reductant, T = 900°C, 100% N_2.

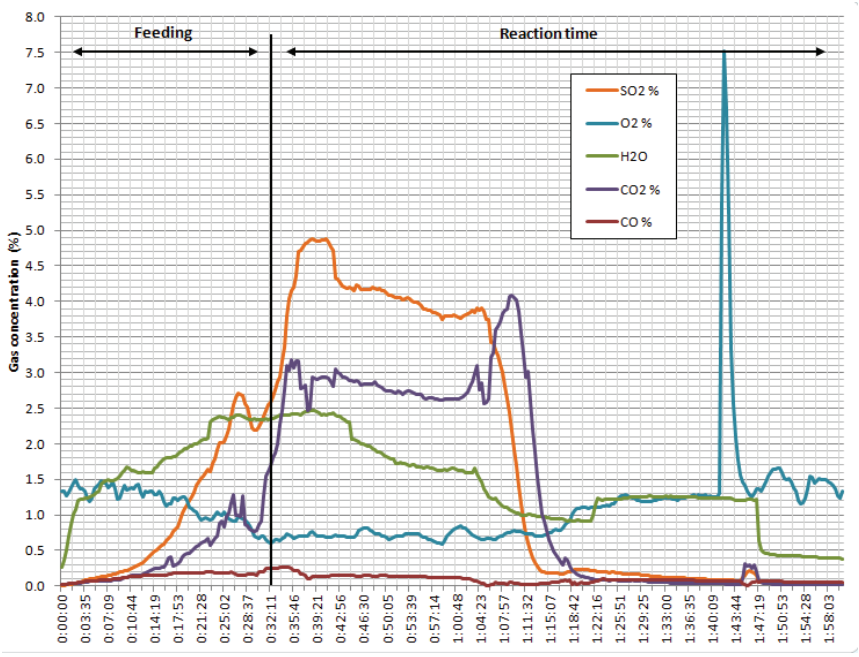

Figure 50. Gas analysis of experiment H_C_1.1, with carbon as the reductant.

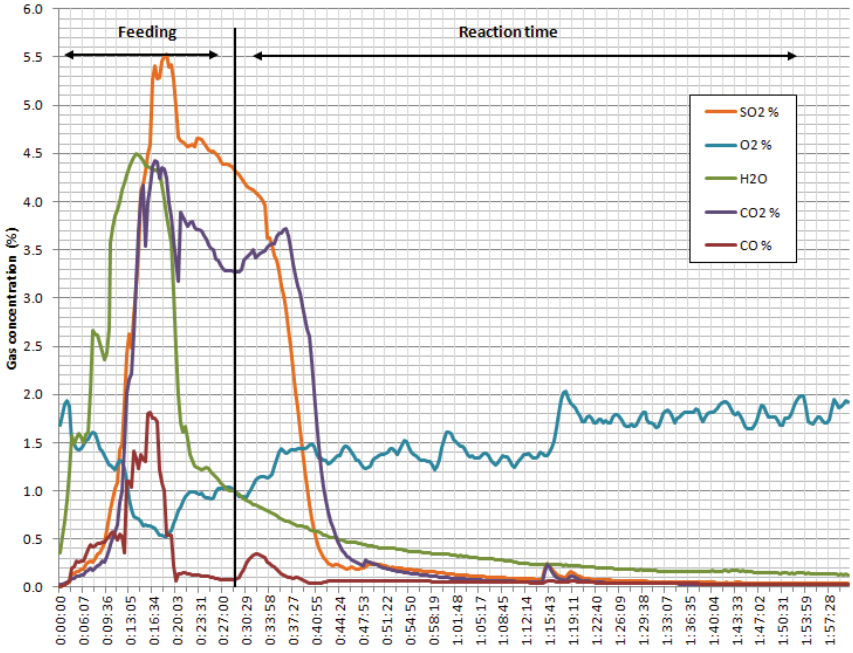

Figure 51. Gas analysis of experiment H_C_2, with carbon as the reductant.

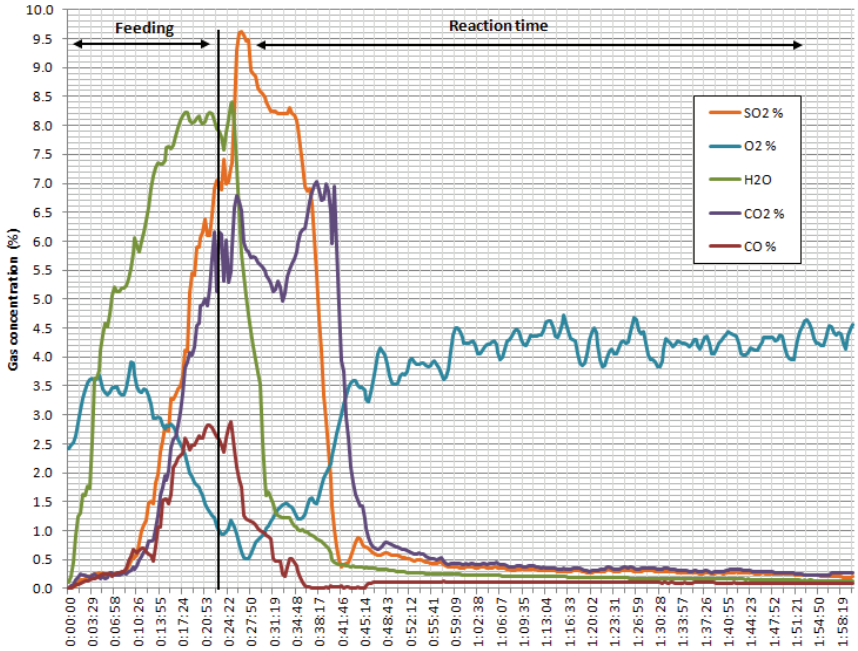

Figure 52. Gas analysis of experiment H_C_3, with carbon as the reductant.

4.3.6 Impurities

Experiments with manganese sulfate, calcium sulfate, or iron sulfate as an impurity were carried out in order to evaluate the effect of the presence of a minor amount of impurity on the decomposition of magnesium sulfate. The sulfur concentrations of the samples from the tests are summarized in Table 10. The results are described in detail for each impurity in the following sections. In these experiments, it was not possible to separate the bed material from the products or intermediates for total sulfur analysis and as a result, the amount of magnesium sulfate decomposed could not be calculated. In the graphs in this section, therefore, only the sulfur concentration in the bulk material is given.

Table 10. Residual sulfur content in the experiments with impurities.

	Sulfur (%)		
Test	**feeding**	**2h**	**product**
M_S_4_Mn	1.4	0.31	0.23
M_CO_4_Mn	8.8	0.45	0.70
M_S_4_Ca	5.0	3.4	5.7
M_CO_4_Ca	12.7	0.85	1.0
M_S_4_Fe	0.25	0.17	0.61
M_CO_4_Fe	6.7	0.34	0.34
M_S_3_Fe	0.61	0.34	0.82

Manganese sulfate as the impurity with sulfur as the reductant

A comparison of M_S_4_Mn with experiments carried out under the same conditions, except for the presence of manganese sulfate as the impurity (M_S_4 and M_S_4_G), shows the effect of the presence of manganese sulfate on various aspects of the experiment. The fluidization behavior was similar, with a bed region where bubbles and sulfur particles were clearly visible. The bed behavior changed from bubbling to more vigorous as feeding proceeded. The entire bed was well fluidized throughout the experiment. In experiment M_S_4_Mn, however, no fines became stuck to the reactor wall in the freeboard region as they did in the experiments without manganese sulfate.

The SEM micrographs of the product in Figure 53 showed that the manganese particles retained their round shape, which indicates that the manganese particles did not melt in the experiment. The manganese sulfate particles formed an intermediate manganese sulfide compound directly after feeding, before the formation of manganese oxide, according to EDS analysis.

Some magnesium sulfate was still present directly after feeding, but after two hours and upon cooling, only MgO was detected, corresponding to an overall sulfur content of <0.31 wt%. The sulfur content of the samples is shown in Table 10. The sulfur content of the samples of M_S_4_Mn and similar experiments without manganese sulfate as the impurity (including M_S_4) is also shown in Figure 54. These results show that in presence of manganese sulfate a slightly lower final sulfur content was achieved than without manganese sulfate as the impurity. The presence of small amounts (6 wt%) of

manganese sulfate does not therefore have a detrimental effect on the decomposition of magnesium sulfate.

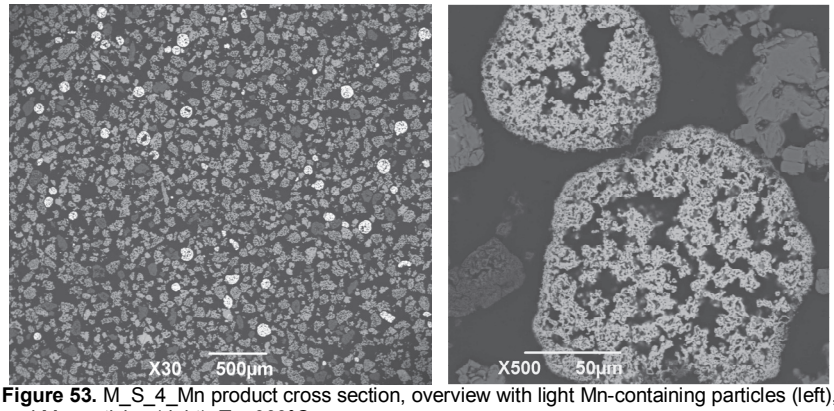

Figure 53. M_S_4_Mn product cross section, overview with light Mn-containing particles (left), and Mn particles (right), T = 900°C.

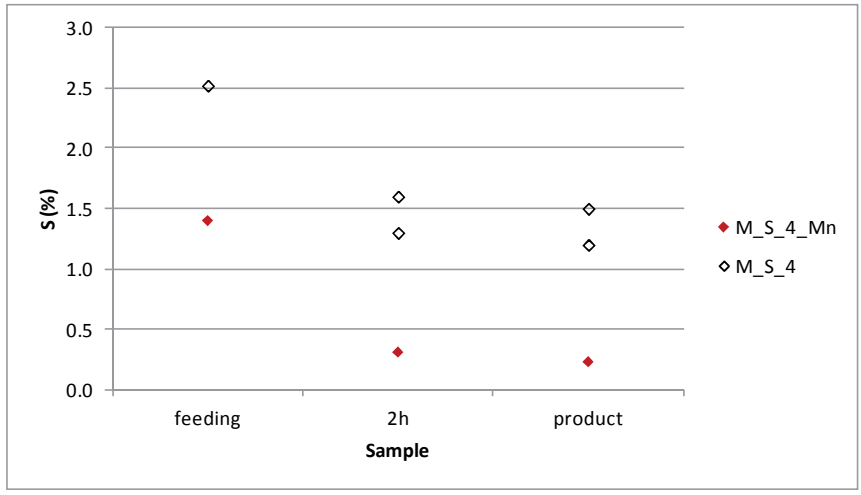

Figure 54. Results of tests with magnesium sulfate (-150 µm) with 6% manganese sulfate as the impurity, T = 900°C, twice the stoichiometric amount of sulfur.

Manganese sulfate as the impurity with carbon monoxide as the reductant

Comparison of experiment M_CO_4_Mn with similar experiments without impurities shows the effect of the impurity on various aspects of the experiment. In all experiments fluidization problems occurred. In test M_CO_4_Mn, channeling took place when feeding was started. The bed was not very stable initially, but fluidization improved one hour after feeding. In

the experiments without manganese sulfate (M_CO_4 and M_CO_4_G and M_CO_4_T2) the bed was not well fluidized and needed to be stirred with a stick to make it fluidize again.

The SEM micrographs in Figure 55 show that the manganese sulfate particles did not melt under these conditions either. The manganese particles have a darker layer around them, which contains MgO. Some smaller particles containing both manganese and magnesium together with sulfur and oxygen were found, which indicates that the starting materials reacted with each other during decomposition in 90% N_2 (g) and 10% CO (g). This did not occur in test M_S_4_Mn. More fines were formed during this test than in M_S_4_Mn.

The XRD analysis shows clear peaks for MgO for all three samples. Immediately after feeding, there are still clear peaks for β-$MgSO_4$; much more than in a comparable test with sulfur as the reductant. Sulfur analysis shows that there is 8.8% sulfur in the sample. In the final sample there were very small peaks of MnS (alabandite, well crystallized) visible, but they were so low that the actual presence of MnS may be debatable. The sulfur content in the sample taken after two hours was 0.45% and after cooling the sulfur content was 0.70%.

The results of the sulfur analysis for M_CO_4_Mn and similar experiments without manganese sulfate as the impurity are shown in Figure 56. This shows that manganese sulfate has no clear effect on the sulfur content in the samples and thus on the decomposition rate.

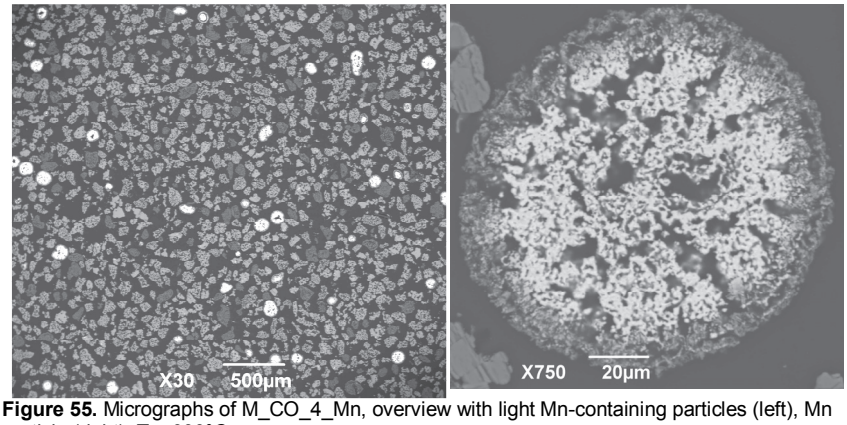

Figure 55. Micrographs of M_CO_4_Mn, overview with light Mn-containing particles (left), Mn particle (right), T = 900°C.

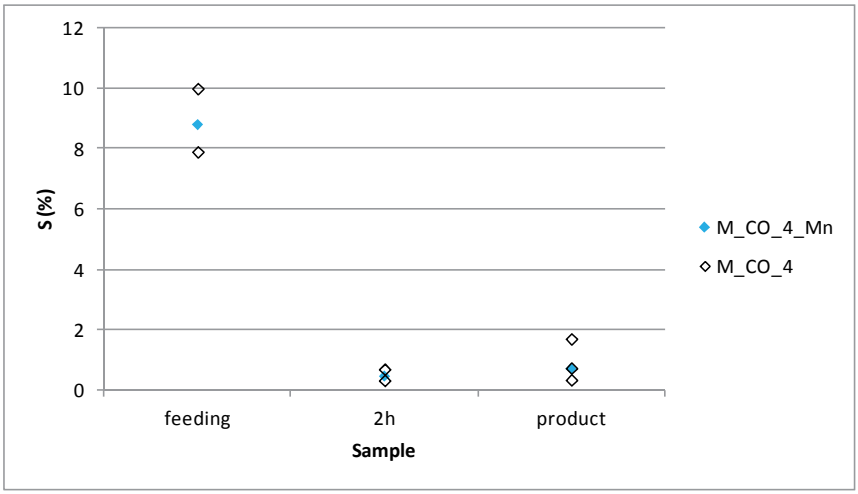

Figure 56. Results of tests with magnesium sulfate (-150 µm) and manganese sulfate as the impurity. T = 900°C, CO partial pressure: 0.1.

Calcium sulfate as the impurity with sulfur as the reductant

Comparing M_S_4_Ca with similar experiments without impurities ((M_S_4 and M_S_4_G) shows the effect of the presence of calcium sulfate on various aspects of the experiment.

The XRD analysis of test M_S_4_Ca shows peaks for β-$MgSO_4$ and $CaSO_4$ in addition to MgO in all samples. In the sample taken after two hours and in the product, the compound $CaMg_3(SO_4)_4$ was also detected, which indicates a reaction between calcium and magnesium particles. The formation of such a compound was confirmed by SEM/EDS analysis, shown in Figure 57 and Table 11.

The bed was well fluidized in all experiments, with some dust deposited on the reactor wall in the freeboard region. A sharp decrease in bed height took place for test M_S_4_Ca during the first twenty minutes upon completion of feeding. A significant amount of sulfur was detected in the samples: 5.0% directly after feeding, 3.4% after two hours, and 5.7% in the product, compared to values of 1.16% and 1.26% for the samples after two hours and the product in test M_S_4 and 2.52% after feeding, 1.6% after two hours, and 1.5% in the product of test M_S_4_G, as shown in Figure 58. The fact that the values of the sulfur analysis may not be so reliable needs to be taken into account, because only the bulk material was analyzed; separation of the product and

bed material could not be made. Nevertheless, it shows that there is more residual sulfur when calcium sulfate is the impurity than in the test without any impurities or in the test with manganese sulfate as the impurity, for example.

The results of this test show that a minor amount of calcium sulfate, as little as 6.0 wt%, results in higher final sulfur content. Some of the magnesium sulfate will react with $CaSO_4$ to form $CaMg_3(SO_4)_4$ and this part of the magnesium sulfate will not decompose. The presence of calcium sulfate should therefore be avoided.

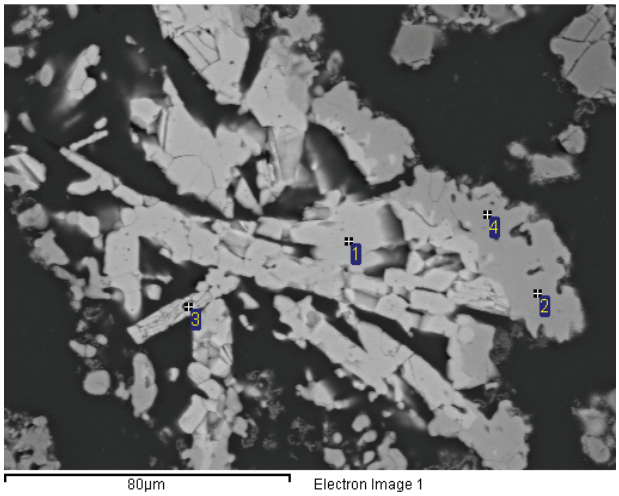

Figure 57. SEM image of a calcium sulfate particle that also contains magnesium after two hours' reaction time from M_S_4_Ca, T= 900°C

Table 11. EDS analysis points relating to the SEM image in Figure 57.

Spectrum	O	Mg	S	Ca	Total
1	43.8		23.4	32.8	100
2	40.8	15.27	29.82	14.12	100
3	49.72	0.44	20.87	28.96	100
4	41.83	17.7	27.93	12.54	100

Processing option : All elements analyzed (Normalized)

All results in weight%

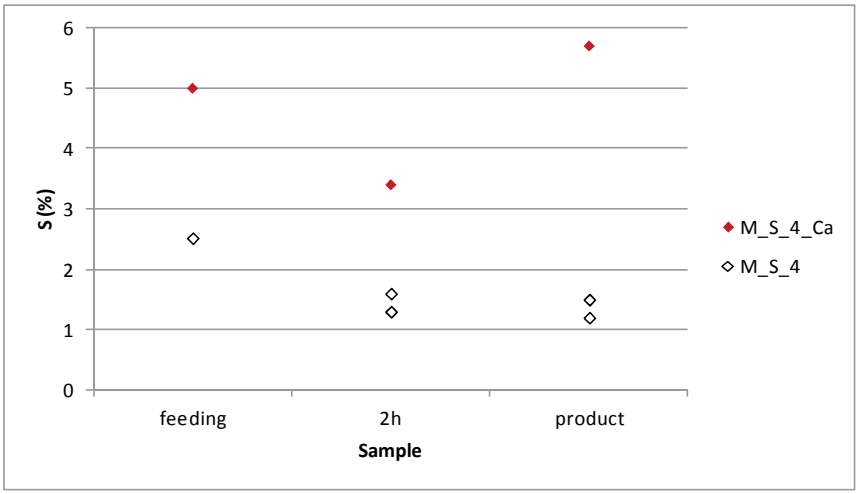

Figure 58. Results of the tests with magnesium sulfate (-150 µm) and calcium sulfate as the impurity at 900°C, twice the stoichiometric amount of sulfur.

Calcium sulfate as the impurity with carbon monoxide as the reductant

In all the tests, fluidization problems occurred. In tests M_CO_4 and M_CO_4_G, the bed defluidized multiple times and stirring was needed to refluidize the bed. In test M_CO_4_Ca, channeling occurred and the bed also needed to be stirred in order to avoid defluidization during the first 30 minutes after feeding. After this, the bed was very well fluidized. Observation of the bed was difficult during the experiment due to fines that deposited inside the reactor tube walls.

The SEM/EDS analysis (Figure 59 and Table 12) showed that a compound composed of Mg-Ca-O-S was formed, as analyzed in spectra 1-5, 9, and 10. The calcium content in the particles varied from 6.5 to 40% and the sulfur content related to the presence of calcium. The particle structure of this compound was similar to that of MgO, but there was still a high sulfur content present.

A comparison between M_CO_4_Ca and similar tests without impurities (M_CO_4, M_CO_4_G, M_CO_4_T2) is shown in Figure 60. These results show that the effect of calcium on the sulfur content of the decomposition product was minimal in the two-hour sample and the end product. There was more sulfur in the sample of M_CO_4_Ca directly after feeding than in a comparable test without calcium sulfate as the impurity. This difference

directly after feeding may be a result of the fluidization and bed stability problems that occurred in each test.

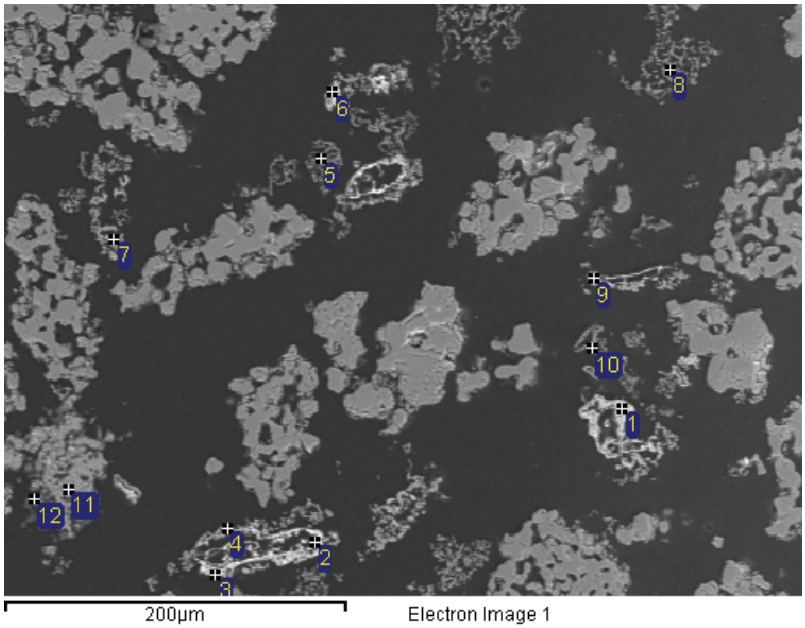

Figure 59. SEM image of the product of M_CO_4_Ca, T = 900°C.

Table 12. EDS analysis points relating to the SEM image in Figure 59.

Spectrum	O	Mg	S	Ca	Total
1	18.13	18.28	23.79	39.79	100
2	15.9	14.69	29.88	39.53	100
3	35.69	35.7	13.08	15.52	100
4	37.44	40.05	10.2	12.3	100
5	31.19	57.29	4.96	6.56	100
6	25.16	11.97	27.01	35.87	100
7	35.83	47.35	7.69	9.13	100
8	35.79	64.21			100
9	38.67	45.83	7.11	8.39	100
10	35.41	41.08	10.36	13.16	100
11	53.8	23.45	22.74		100
12	38.91	56.81	4.27		100

Processing option : All elements analyzed (Normalized)
All results in weight%

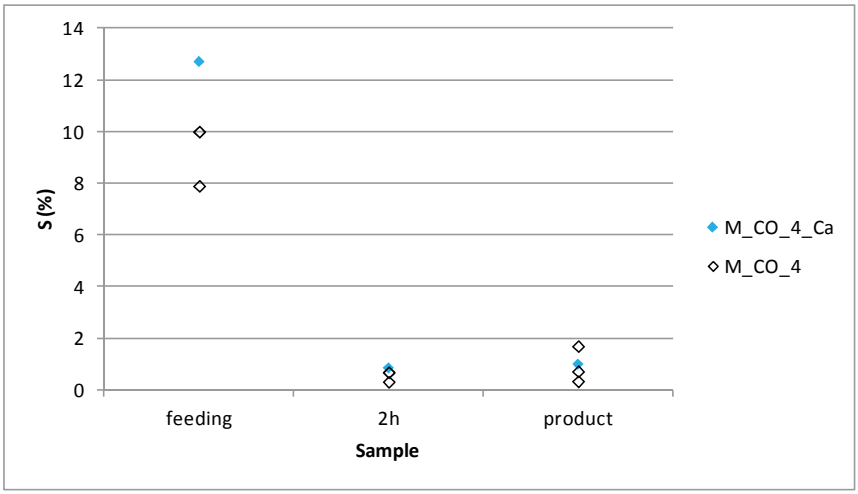

Figure 60. Decomposition results of the tests with magnesium sulfate (-150 µm) and calcium sulfate as the impurity, T = 900°C, CO partial pressure: 0.1.

Iron sulfate as the impurity with sulfur as the reductant

Comparing M_S_4_Fe with M_S_4 and M_S_4_G and comparing M_S_3_Fe with M_S_3 shows the effect of the presence of iron sulfate on various aspects of the experiment. Fluidization was better with particle size group 105-210 µm than with particle size group -150 µm, both in the presence and absence of iron sulfate as an impurity. In the presence of iron sulfate, some black fines deposited inside the top of the reactor tube, in addition to the sulfur and magnesium oxide and magnesium sulfate fines that were normally deposited. A clear freeboard region was visible for M_S_3_Fe, but for M_S_4_Fe the bed-freeboard interface was more difficult to distinguish due to dust deposition on the reactor wall.

The sulfur analysis of M_S_4_Fe shows the low sulfur percentages of the bulk: 0.25% directly after feeding, 0.17% and 0.61% after two hours and in the product, respectively. For the tests without any impurities, the sulfur content of the two-hour sample was 1.16%, 1.26% for the samples after two hours and the product in test M_S_4, and 2.52% after feeding, 1.6% after two hours, and 1.5% in the product of test M_S_4_G, as shown in Figure 61.

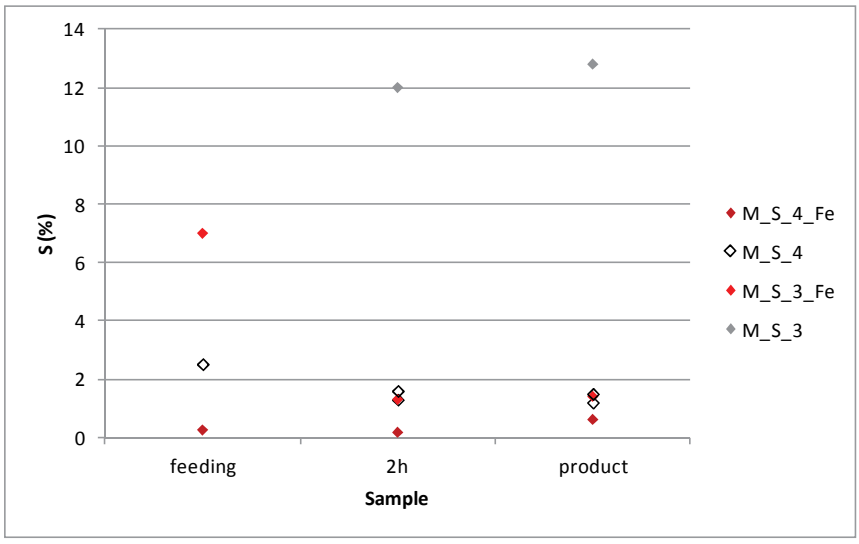

Figure 61. Effect of the presence of iron sulfate on the decomposition of magnesium sulfate in particle size class three and four, T = 900°C, twice the stoichiometric amount of sulfur. M_S_4 includes experiment M_S_4 and M_S_4_G.

MgO is the only magnesium-containing compound detected in M_S_4_Fe according to the XRD analysis. In similar tests without iron sulfate as the impurity, there was a minor amount of β-$MgSO_4$ in addition to MgO. SEM/EDS analysis showed that the remaining sulfur is associated with the iron particles, as can be seen from Figure 62 and Table 13. The composition of spectrum 2 and 6 is close to that of FeS, which has a theoretical composition of 63.53% Fe and 36.47% S. Iron was also present as iron oxide, as shown in spectrum 1. EDS analysis shows that diffusion of magnesium into the iron oxide particles had taken place, as a decreasing concentration of magnesium is detected from the center of the particle towards its edge.

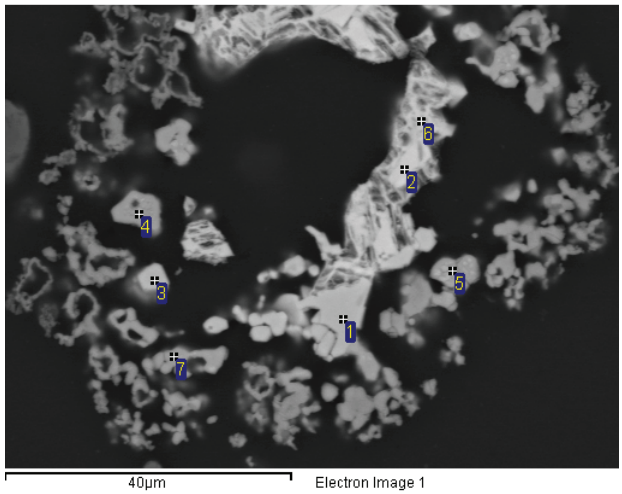

Figure 62. SEM image of an iron particle that contains magnesium from M_S_4_Fe product, T= 900°C.

Table 13. EDS analysis points relating to the SEM image in Figure 62.

Spectrum	O	Mg	S	Fe	Cu	Total
1	23.37	2.09		74.54		100
2			33.29	66.71		100
3	23.87	3.24		72.89		100
4	25.74	23.28		50.98		100
5	25.52	18.6		55.88		100
6	10.66		29.43	56.95	2.97	100
7	26.67	20.95		52.38		100

Processing option : All elements analyzed (Normalized)
All results in weight%

The bulk sulfur percentages of M_S_3_Fe were 7%, 1.3%, and 1.4% for the samples taken directly after feeding, after two hours, and the product, respectively. This indicates that there was still a significant amount of magnesium sulfate present in the sample, which is in accordance with the XRD analysis, where clear peaks for β-$MgSO_4$ were detected in addition to MgO directly after feeding. MgO was mainly detected, together with minor peaks for β-$MgSO_4$after two hours and in the product. The samples of M_S_3 contained 12.0% and 12.8% sulfur after two hours and in the final product, respectively, and XRD analysis also showed significant amounts of β-$MgSO_4$ in addition to MgO in both samples.

SEM/EDS analysis of the sample taken directly after feeding, shown in Figure 63 and Table 14, indicates that spectra 1-3, 5 and 6 are close to the composition of FeS, which has a theoretical composition of 63.53% Fe and 36.47% S. Spectra 7-13 are composed of an iron-magnesium oxide, with varying amounts of these three compounds. It can be seen from the SEM image that there is a clear reaction front. The core of the particle is composed of iron sulfide and the outer layer is composed of iron-magnesium oxides. SEM/EDS analysis of the sample taken after two hours and of the product shows that nearly all the iron is present in oxide form.

These results show that a higher degree of magnesium sulfate decomposition was achieved after two hours' reaction time in the presence of small amounts of iron sulfate. The effect was not so clear when particles in size group -150 µm were used and could be merely the result of uncertainties introduced during sampling. The effect is, however, significant for particle size group 105-210 µm. The difference in sulfur percentage in the product cannot be explained simply by errors introduced during sampling; significantly, more magnesium sulfate had decomposed in the presence of iron sulfate. This means that the presence of iron sulfate enables the use of larger magnesium sulfate particle sizes. The presence of iron sulfate is therefore beneficial to the decomposition of magnesium sulfate.

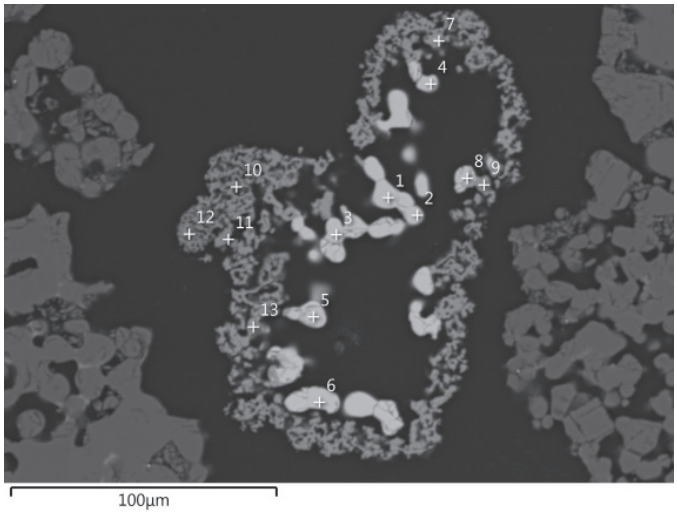

Figure 63. SEM image of an iron particle that contains magnesium from the sample taken directly after feeding from test M_S_3_Fe, T = 900°C.

Table 14. EDS analysis points relating to the SEM image in Figure 63.

Spectrum	O	Mg	Si	S	Fe	Total
1				36.5	63.5	100
2				36.59	63.41	100
3				36.54	63.46	100
4	0.95			36.31	62.75	100
5				36.69	63.31	100
6				36.62	63.38	100
7	24.02	21.67	0.26	3.04	51.01	100
8	2.89	0.51	1.05	31.51	64.04	100
9	26.27	23.34			50.39	100
10	21.07	27.81	0.21		50.91	100
11	23.77	26.65			49.58	100
12	29.36	33.89			36.74	100
13	23.95	21.58			54.46	100

Processing option : All elements analyzed (Normalized)

All results in weight%

Iron sulfate as the impurity with carbon monoxide as the reductant

In both tests fluidization problems occurred. In tests M_CO_4 and M_CO_4_G, the bed defluidized multiple times and stirring was needed to refluidize the bed. In test M_CO_4_Fe the bed was not at all well fluidized, but this improved during feeding. Dust was deposited on the reactor wall, which made observation of the fluidizing behavior more difficult. The lower part of the bed, however, was not well fluidized after feeding. The SEM/EDS analysis shows that an Mg-Fe-S-O compound was formed, with local variations in the composition. In addition to this, a compound mainly composed of iron (>94%) with minor amounts of magnesium and/or sulfur was found (Figure 64 and Table 15).

The analysis of the experiments carried out without iron (M_CO_4, M_CO_4_G and M_CO_4_T2 in Figure 65) was performed after separating out the bed material. It also needs to be noted that in the bulk analysis for the tests with iron sulfate, the iron particles were also included in the bulk. The results show that the sulfur content in the sample was lower directly after feeding when iron sulfate is present as the impurity. There was little to no difference after two hours and in the product sample, as can be seen in Figure 65.

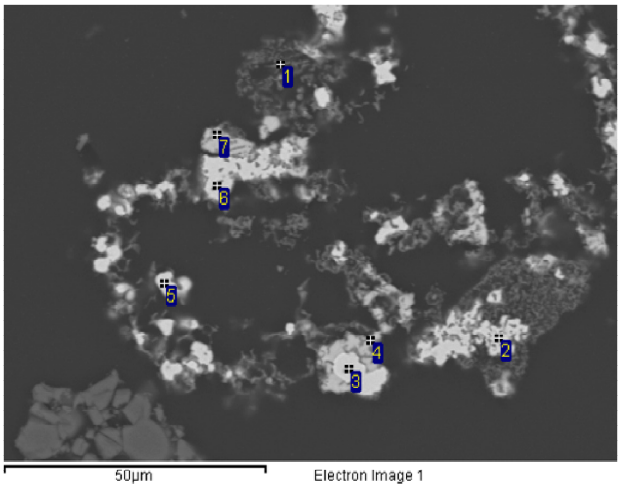

Figure 64. SEM image of the product of M_CO_4_Fe, T= 900°C.

Table 15. EDS analysis points relating to the SEM image in Figure 64.

Spectrum	O	Mg	S	Fe	Total
1	33.5	54.25		12.25	100
2	7.52	15.79		76.69	100
3		0.73	0.76	98.51	100
4	7.26	12.58	25.64	54.52	100
5				100	100
6		5.35		94.65	100
7	4.93	5.69	28.78	60.60	100

Processing option : All elements analyzed (Normalized)
All results in weight%

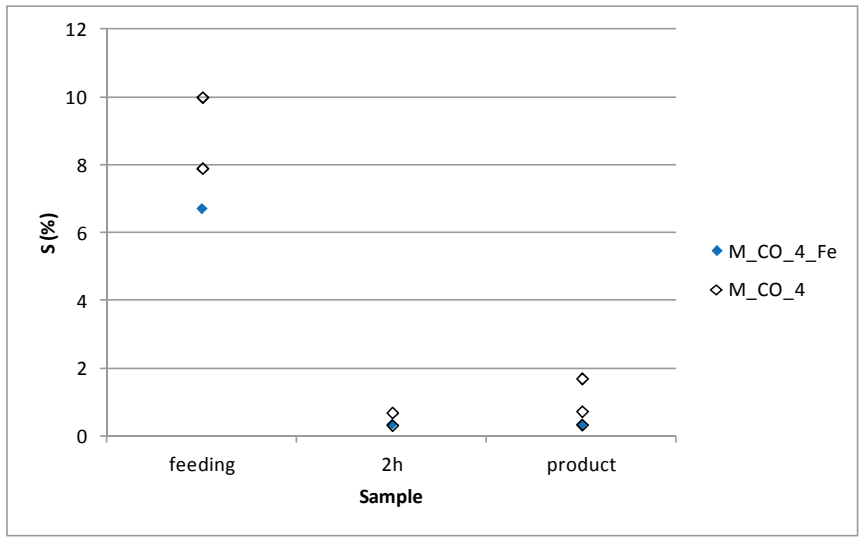

Figure 65. Effect of the presence of iron sulfate on the decomposition of magnesium sulfate, T = 900°C.

4.4 Repeated experiments with preferred conditions

The experiment with the preferred conditions for decomposition of magnesium sulfate in the presence of sulfur as the reductant was repeated and the off-gas composition was analyzed. Experiments with the same conditions but with carbon and carbon monoxide as the reductant were also carried out for comparison. The gas analysis from the fluidized bed tests shows a difference in the decomposition reaction, depending on the choice of reductant, as can be seen when comparing Figure 66, Figure 67, and Figure 68.

The off-gas analysis of the experiment with sulfur as the reductant (Figure 66) shows that the majority of the decomposition reaction took place during feeding; the SO_2 concentration decreased significantly when feeding was completed. This also shows that the sulfur used as reductant burned when it entered the bed. The SO_2 concentration dropped down to 0.4% after the feeding period and slowly decreased further to 0.2% during the remainder of the experiment. Crystal water was liberated during the entire experiment, which indicates, that on a macro scale, dehydration and decomposition took place simultaneously. The bed was well fluidized throughout the experiment. The strong fluctuations in the concentration of sulfur dioxide and also of water

vapor and oxygen was due to the blockage of the sampling tube for the off-gas analysis.

In the gas analysis graph (Figure 67) of the experiment with carbon as the reductant, there was first a peak in water vapor concentration in the off-gas. During this peak, fluidization problems occurred, and the sulfur dioxide concentration in the off-gas was low. The sulfur dioxide concentration increased after the water vapor concentration decreased, indicating that decomposition of magnesium sulfate commenced. Magnesium sulfate is the only sulfur-containing component in the system and can therefore easily be linked to the concentration of sulfur dioxide in the off-gas.

Decomposition also commenced when feeding was started in the experiment with carbon monoxide as the reductant. The off-gas analysis in Figure 68 shows that there was free carbon monoxide in the off-gas throughout the entire experiment. The SO_2 concentration decreased when fluidization problems took place. The water vapor concentration increased during feeding and as a result of this, the particles may have become sticky. The sulfur dioxide concentration and thus the decomposition continued at a higher rate when the bed was well fluidized again, once feeding had been completed.

The total sulfur analysis of the different samples taken during the tests is shown in Figure 69. From these results, it can clearly be seen that the sulfur content was lowest directly after feeding with sulfur as the reductant, which means that the decomposition reaction with sulfur as the reductant was the fastest. Lower residual sulfur values, however, could be achieved when using carbon or carbon monoxide.

The SEM micrographs of the samples taken directly after feeding are shown in Figure 70, Figure 71, and Figure 72. These samples also contain MgO bed material. The sample taken directly after feeding in the test with sulfur shows particles with various degrees of decomposition, ranging from unaffected to fully decomposed, independent of the particle size. The sample of the test with carbon shows only unaffected particles directly after feeding. The magnesium sulfate particles, however, were cracked during the process, as shown in Figure 73. The sample of the test with CO as the reductant (Figure 72) shows mainly unaffected particles and some particles with decomposition on the outer

surface. The cross sections of the partially decomposed particles show a clear reaction front.

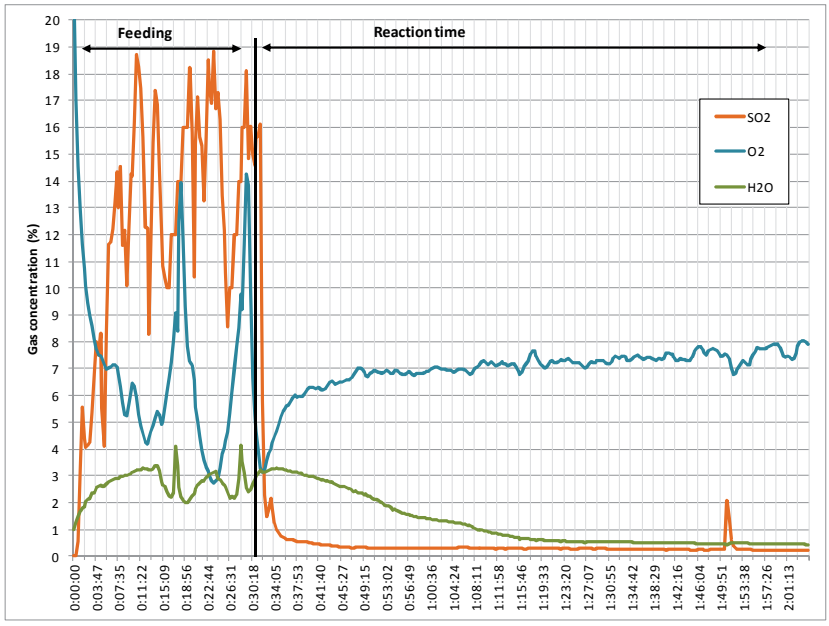

Figure 66. Gas analysis of experiment M_S_4_G with sulfur as the reductant.

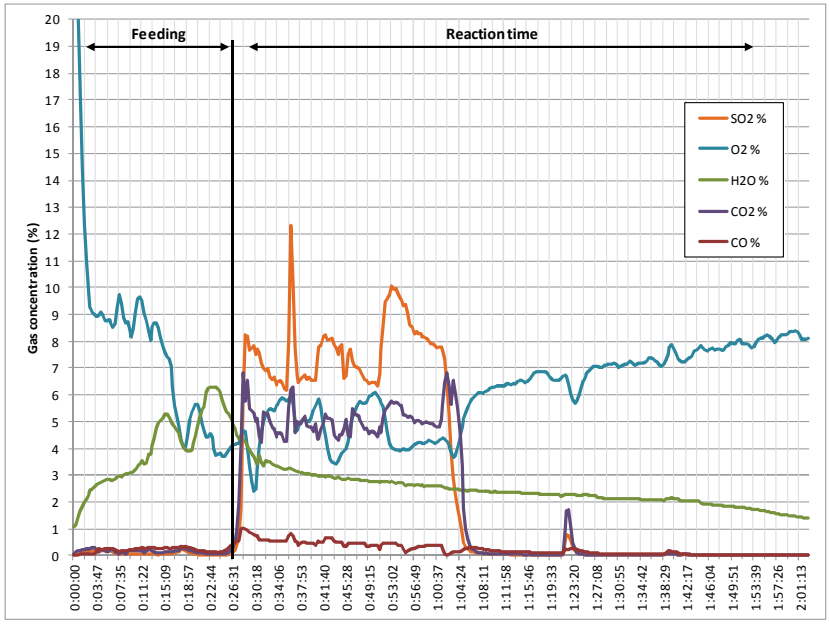

Figure 67. Gas analysis of experiment M_C_4_G with solid carbon as the reductant.

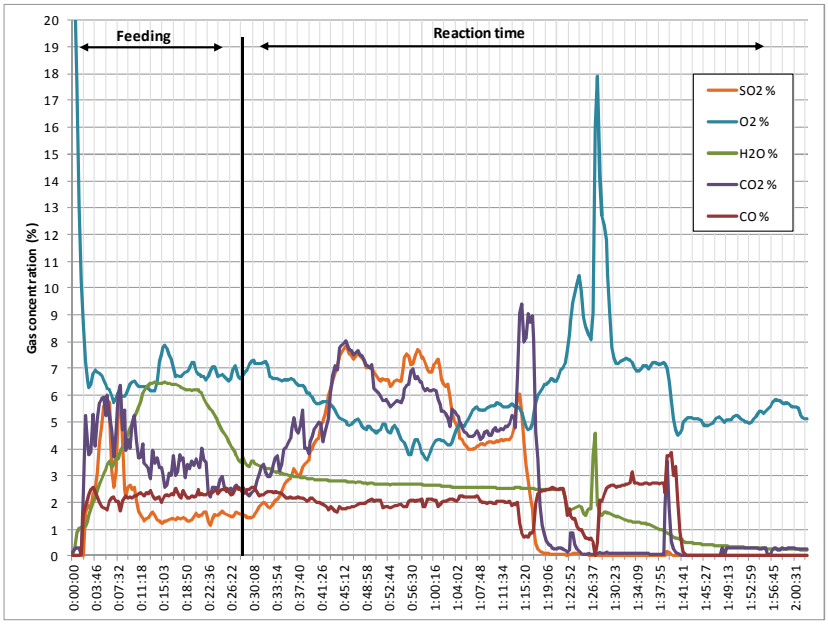

Figure 68. Gas analysis of experiment M_CO_4_G with carbon monoxide as the reductant.

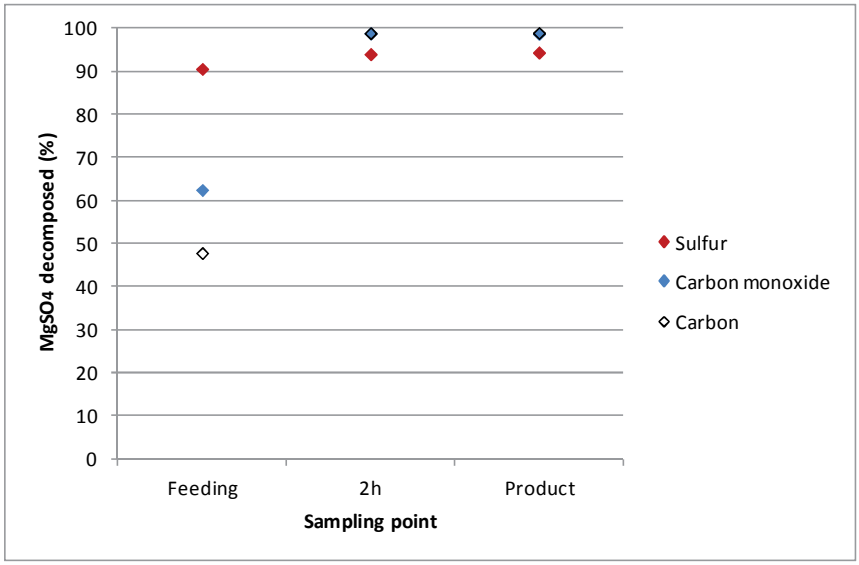

Figure 69. Comparison of the different reductants in fluidized bed decomposition, T=900°C.

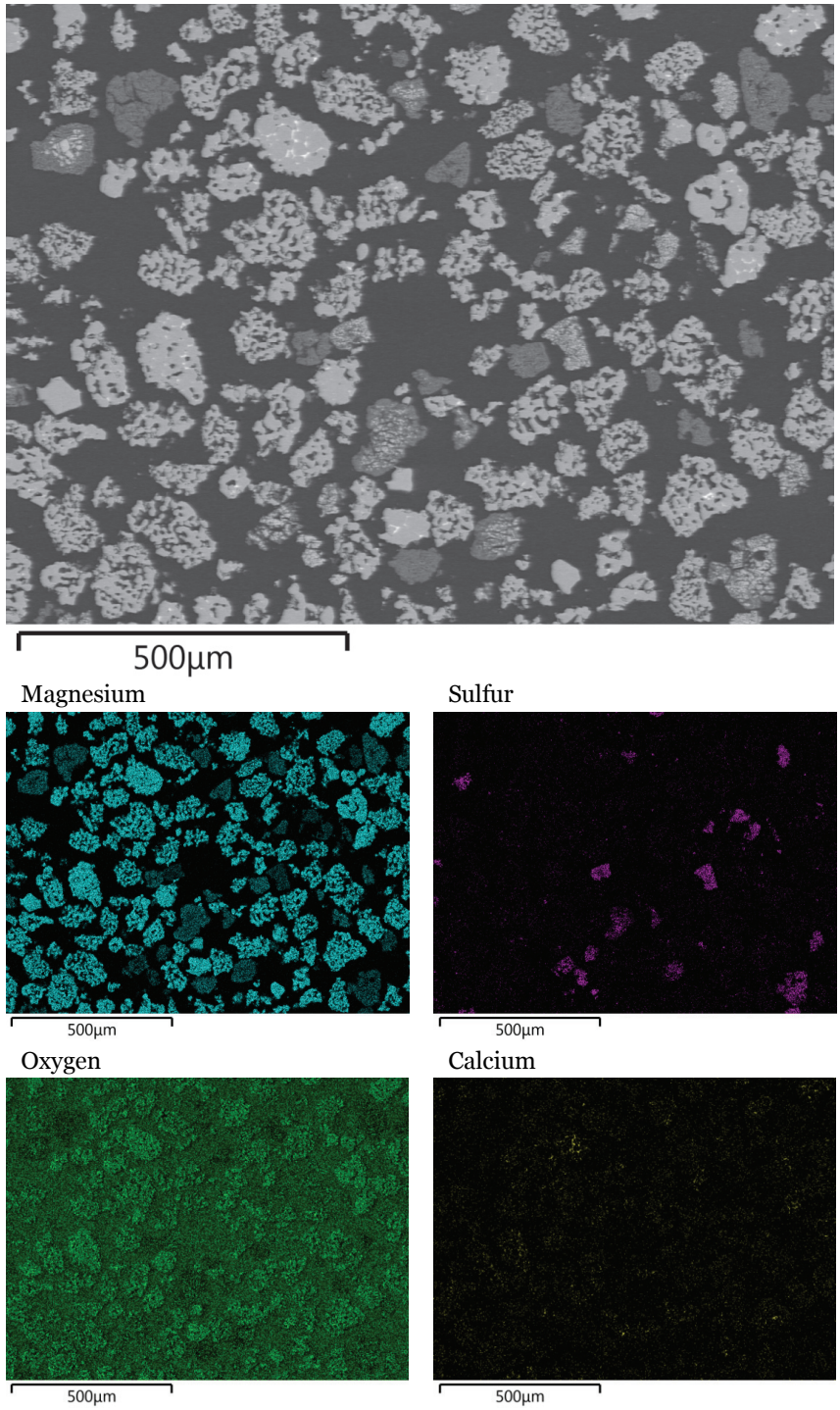

Figure 70. SEM image with element maps from the sample taken directly after feeding of the FB test with sulfur as the reductant.

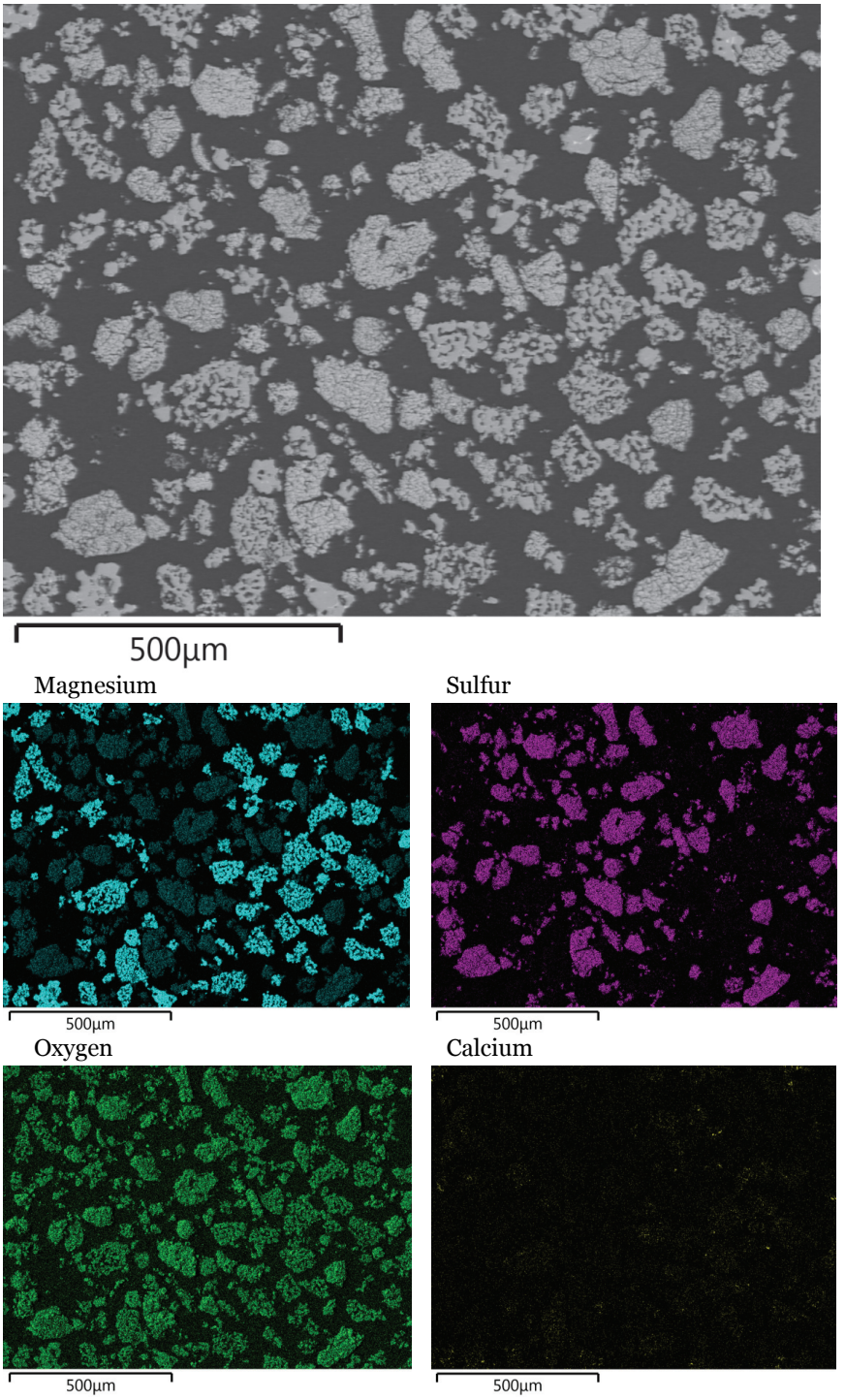

Figure 71. SEM image with element maps from the sample taken directly after feeding of the FB test with carbon as the reductant.

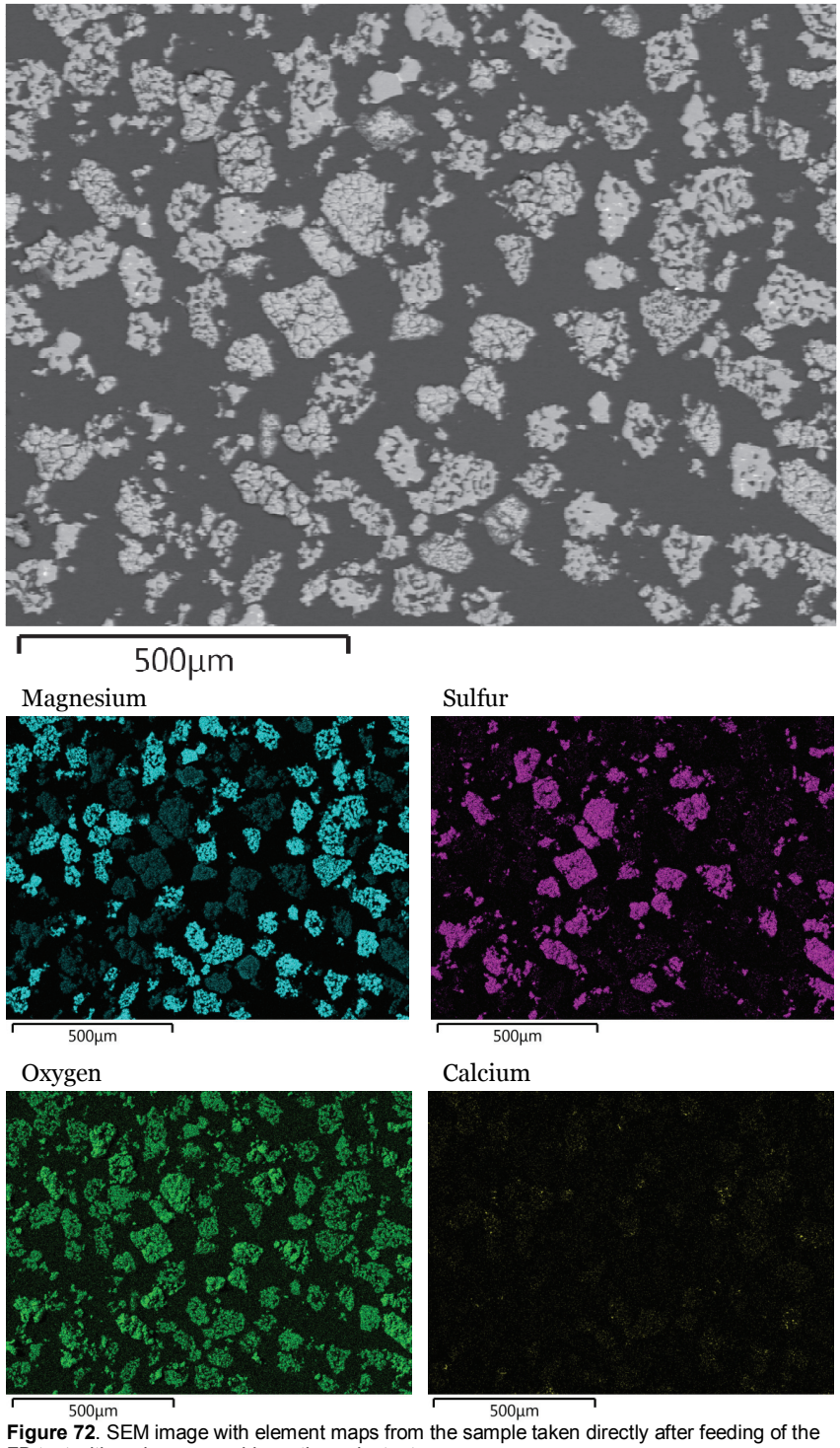

Figure 72. SEM image with element maps from the sample taken directly after feeding of the FB test with carbon monoxide as the reductant.

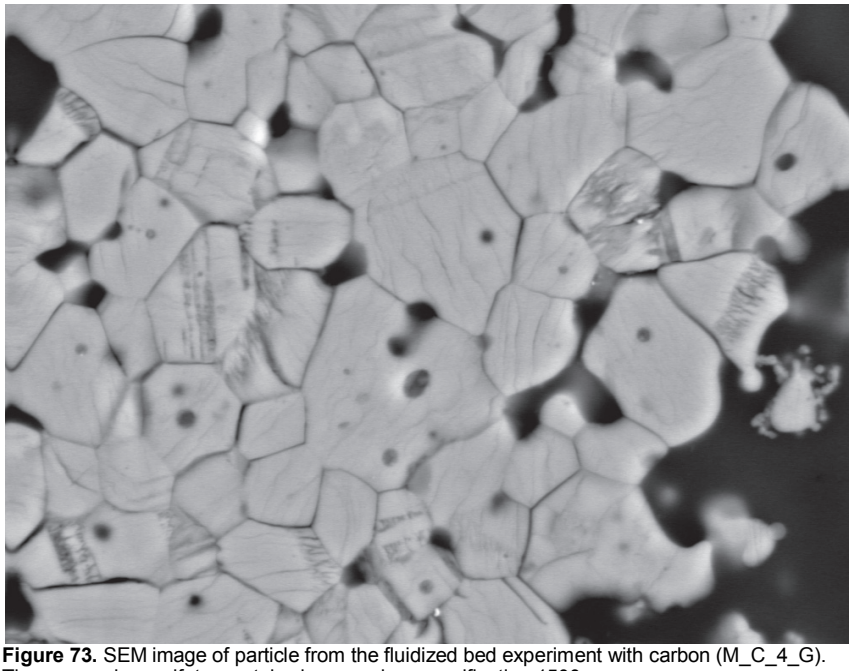

Figure 73. SEM image of particle from the fluidized bed experiment with carbon (M_C_4_G). The magnesium sulfate crystals show cracks, magnification 1500x.

4.5 Summary

The chamber furnace experiments showed minimal decomposition of magnesium sulfate in the presence of reductants. Short fluidization tests showed that magnesium sulfate does not decompose evenly in the presence of reductants; particles with various stages of decomposition were found in the samples.

The main results from the fluidized bed reactor tests in section 4.3 are summarized in Table 16. The experimental conditions for these tests are presented in Table 6.

Table 16. The main results of all fluidization tests in section 4.3.

Experiment number	Experiment name	S(%)	XRD			Fluidization behavior
			Main	Minor	Other	
1	H_Pre_1	23.1	β-$MgSO_4$	α-$MgSO_4$	hexahydrate	Liquid/molten material
2	H_Pre_2	n/a	β-$MgSO_4$	α-$MgSO_4$		Liquid/molten material
3	H_Pre_3	20.9	β-$MgSO_4$	α-$MgSO_4$	amorphous	Bed defluidized
4	H_S_1	20.4	β-$MgSO_4$	α-$MgSO_4$		
5	H_CO_1.1	18.5	β-$MgSO_4$	α-$MgSO_4$	amorphous	
6	H_CO_1.2	0.14	MgO			
7	H_C_1.1	1.60	MgO			
8	H_C_1.2	18.5	β-$MgSO_4$	α-$MgSO_4$	amorphous	
9	H_S_2	15.9	β-$MgSO_4$	α-$MgSO_4$		
10	H_CO_2.1	20.0	β-$MgSO_4$	α-$MgSO_4$	amorphous	
11	H_CO_2.2	3.60	MgO			
12	H_C_2	0.35	MgO			
13	H_S_3.1a	24.1	β-$MgSO_4$	α-$MgSO_4$		Bed defluidized
13	H_S_3.1b	23.8	β-$MgSO_4$	α-$MgSO_4$		Bed defluidized
13	H_S_3.1c	11.9	β-$MgSO_4$			
14	H_S_3.2	23.4	β-$MgSO_4$	α-$MgSO_4$		
15	H_CO_3.1	22.9	β-$MgSO_4$	α-$MgSO_4$		
16	H_CO_3.2	0.15	MgO			
17	H_C_3	0.70	MgO			Channeling at the beginning
18	H_S_4	23.8	β-$MgSO_4$	α-$MgSO_4$		Bed defluidized
19	H_CO_4	19.7	α-$MgSO_4$	β-$MgSO_4$	$MgSO_4 \cdot 1.5H_2O$ $2MgSO_4 \cdot H_2O$	
20	M_Pre_1	n/a	n/a			Bed defluidized
21	M_Pre_2	n/a	n/a			Bed defluidized
22	M_4	17.9	β-$MgSO_4$	α-$MgSO_4$	amorphous	Bed defluidized
23	M_S_3	12.8	β-$MgSO_4$			
24	M_S_4	1.16	β-$MgSO_4$			
25	M_CO_4	1.70	β-$MgSO_4$	α-$MgSO_4$		Bed defluidized at the beginning
26	M_S_4_A1	0.79	n/a			
27	M_S_4_A2	0.74	n/a			
28	M_S_4_A3	1.30	n/a			
29	M_S_4_T1	16.6	β-$MgSO_4$	α-$MgSO_4$		
30	M_S_4_T2	0.19	n/a			
31	M_S_4_T3	0.35	n/a			
32	M_CO_4_T1	0.73	n/a			
33	M_CO_4_T2	0.56	n/a			
34	M_S_4_G	1.50	α-$MgSO_4$			
35	M_CO_4_G	0.34	MgO			Bed defluidized at the beginning
36	M_C_4_G	0.30	MgO			Bed defluidized at the beginning
37	M_S_3_Fe	1.40	MgO		β-$MgSO_4$	
38	M_S_4_Mn	0.31	MgO			
39	M_S_4_Fe	0.61	MgO			
40	M_S_4_Ca	5.70	β-$MgSO_4$			
41	M_CO_4_Mn	0.70	MgO		MnS	Bed defluidized at the beginning
42	M_CO_4_Fe	0.34	MgO			Bed defluidized at the beginning
43	M_CO_4_Ca	1.00	MgO	CaS		Bed defluidized at the beginning

5. Discussion

In this chapter, the decomposition reaction mechanism of magnesium sulfate and the effect of the choice of reductant on the reaction mechanism will be discussed first in section 5.1. This will be followed by a discussion on the operating window with sulfur as the reductant in section 5.2.1. In section 5.2.2, the operating window with carbon and carbon monoxide as the reductant is discussed and compared with sulfur as the reductant.

5.1 The mechanism of magnesium sulfate decomposition

5.1.1 The effect of the gas-solid contact on the decomposition of magnesium sulfate

In order to decompose magnesium sulfate with sulfur as the reductant, good gas-solid contact and mixing is required, which is shown by comparing experiments in the chamber furnace against experiments in the fluidized bed reactor, of which the results are given in section 4.2.1 and 4.2.2, respectively. The conditions for both types of experiments were the same: a temperature of 900°C, twice the stoichiometric amount of sulfur, and two grams of magnesium sulfate monohydrate as the feed material. The chamber furnace tests (the results are described in more detail in section 4.2.1) were unsuccessful; SEM micrographs did not show any signs of decomposition and the overall sulfur content was comparable to the initial sulfur content. Additionally, the addition of sulfur after the magnesium sulfate particles had heated up was tested, in order to let the crystal water evaporate prior to adding the reductant. Unfortunately, these tests were not successful either. Short experiments in the fluidized bed reactor using the same conditions as in the chamber furnace showed that some decomposition took place during the first minute.

These results are in agreement with the theory part (section 2.2.1), where it was described that a stagnant sulfur trioxide gas film around the magnesium sulfate particles would be present. High sulfur trioxide concentrations increase the temperature at which magnesium sulfate becomes instable. Good gas solid contact and mixing ensure that the gaseous decomposition product (SO_3(g)) in the stagnant gas film around the particles is replaced efficiently. It was also mentioned by Ducarroir et al. [69] that the conversion time of magnesium sulfate is highly influenced by mass transfer.

The decomposition of magnesium sulfates results in a strong decrease in temperature of the solids as well as that of the surrounding gas, because the decomposition reaction is strongly endothermic. Fluidizing conditions ensure efficient heat transfer from the particle surface and the surrounding gas film to the bulk gas, so that the temperature at the particle surface as well as in the surrounding gas film increases rapidly, eliminating the retardation of the decomposition reaction at the reaction interface. It was estimated that heating a magnesium sulfate spherical particle 150 microns in diameter would regain the same temperature as the surroundings within approximately 0.02 seconds after being cooled down to below 0°C. This estimation was done using the method from Kunii and Levenspiel [55].

5.1.2 Fluidizing behavior – the effect of a reductant

The fluidizing behavior of magnesium sulfate was affected by the presence of a reductant and by the type of reductant that was used. It was not possible to keep the bed fluidized when feeding of $MgSO_4$ was started without any reductants present and it was therefore concluded at an early stage of the experimental work that a reductant was required in order to be able to carry out the testwork. The fluidizing behavior in the initial stage of the experiment differed depending on the type of reductant that was used.

The differences in fluidizing behavior can be explained by the kinetics of the decomposition reaction between magnesium sulfate and the reductant; the bed was well fluidized in cases where part of the magnesium sulfate decomposed immediately on entering the bed. Problems occurred when the magnesium sulfate did not react initially. The magnesium oxide on the outer layer of the particles keeps the bed well fluidized, because of its high melting

point (2800°C [22]) and consequently higher softening point than that of magnesium sulfate, which melts in the range of 1120-1185°C [22, 40]. In cases where no decomposition of magnesium sulfate takes place initially, the individual particles will stick together and thus cause fluidization problems.

Part of the magnesium sulfate reacted in the initial stage of the experiment when sulfur was used as the reductant, because the sulfur burned immediately on entering the bed, causing a short period of high sulfur gas partial pressure. This is shown by both the gas analysis (section 4.4, Figure 66) and, for example, the SEM element maps (section 4.4, Figure 70) from experiment M_S_4_G. The gas analysis shows that the sulfur dioxide concentration in the off-gas strongly increased when the experiment started and strongly decreased once feeding of the magnesium sulfate monohydrate and sulfur had been completed. This indicates that both the elemental sulfur burned during the feeding period and that most of the magnesium sulfate decomposed during feeding. The SEM element maps show that the sulfur content in the particles decreased significantly after feeding had been completed. No defluidization occurred during this experiment as this was prevented by the formation of magnesium oxide.

The short fluidization tests with sulfur showed that even though the sulfur partial pressure was low after the initial stage of the experiment, decomposition of magnesium sulfate continued, although at a much lower rate than in the presence of sulfur. This indicates that decomposition of magnesium sulfate can actually take place in a nitrogen atmosphere in the absence of a reductant, but that the reductant is required to improve the surface properties of the magnesium sulfate particles so that fluidization is possible. Sulfur is therefore not only a reducing agent; it also improves the fluidizing behavior of the magnesium sulfate particles.

In the presence of carbon or carbon monoxide as the reductant, fluidization problems were observed in the bed. These reductants react slower than sulfur, as can be seen from the gas analysis graphs in section 4.4, Figure 67 and Figure 68, respectively. The magnesium sulfate started decomposing in the presence of carbon after feeding had been completed and the bed was well fluidized again after experiencing fluidizing problems during the feeding period. In the presence of carbon monoxide, magnesium sulfate started decomposing when feeding started, after which the sulfur dioxide

concentration decreased due to fluidization problems, until feeding was completed and the sulfur dioxide concentration increased again. The SEM element maps from the samples taken once feeding had been completed (section 4.4, Figure 71 and Figure 72) show that the amount of sulfur in the material was significantly higher than in the experiment with sulfur as the reductant (section 4.4, Figure 70). The magnesium sulfate softened and, as little or no decomposition took place during the initial stage of the reaction, there was no protective magnesium oxide layer around the particles to prevent the particles from sticking together.

It needs to be noted, that in addition to the phenomena described above, the particle size of the material has an effect on the fluidizing behavior and that the cohesion between these very fine particles may cause fluidization problems. The typical properties of different particle sizes are described in more detail in the theory part, in section 2.2.3. In the experimental work, cohesion between particles was a cause of fluidization problems for the experiments with particles smaller than 150 microns and especially for the experiments where dried magnesium sulfate heptahydrate was used as the feed material. This was a general problem, regardless of the reductant used.

5.1.3 Uneven decomposition of the particles

Most $MgSO_4$ had already decomposed straight after the feeding period in the fluidized bed experiments with a feeding time of 30 minutes and sulfur as the reductant. This feeding time was required in order to avoid an excessive temperature drop due to the addition of cold materials, dehydration of magnesium sulfate, and decomposition of magnesium sulfate, as well as fluidization problems in the experiments where the operating window was determined. The samples taken directly after feeding contained particles in different stages of decomposition, from hardly affected to fully decomposed. Initially, this was suspected to be due to the long feeding time, which resulted in different residence times for the particles. FTIR gas analysis from these tests (an example is given in section 4.4, Figure 66) showed that there was a high sulfur dioxide concentration during feeding of the material, which rapidly decreased down to 0.2-0.3 vol.% once feeding had been completed. This showed that the sulfur burnt rapidly and that the reaction mainly took place during feeding of the material.

Tests with a relatively small amount of magnesium sulfate, enabling a feeding time of only one minute were carried out as well, in order to avoid the wide range of residence times of the particles. In the sample taken one minute after feeding, however, particles with different degrees of decomposition were found, comparable to the other fluidized bed tests with a longer feeding time. Some particles showed one-sided decomposition, as shown in the SEM image (Figure 74) and EDS analysis (Table 17). This indicates that magnesium sulfate only decomposed when close to a sulfur (gas-releasing) particle. Decomposition of the particles continued throughout the experiments and most $MgSO_4$ had decomposed after one hour, even though all the sulfur (reductant) had left the system in the initial stage of the experiment.

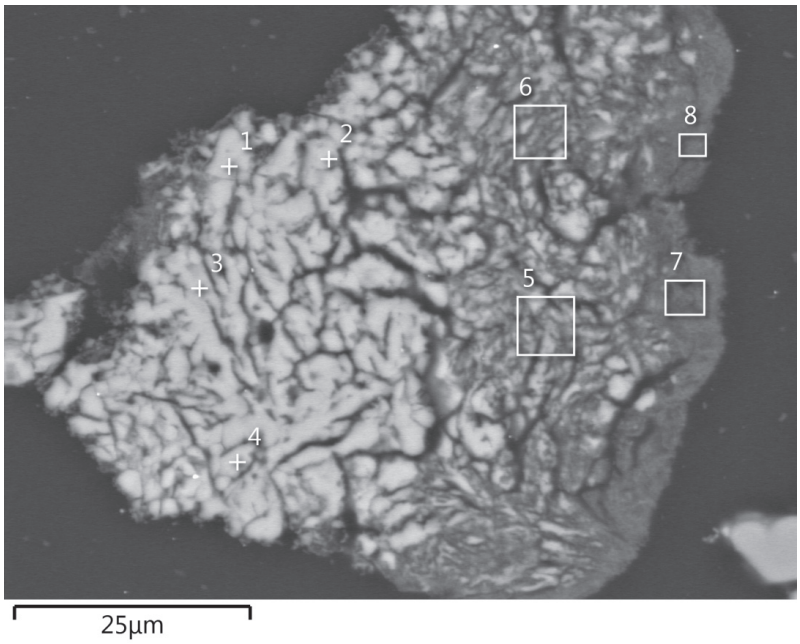

Figure 74. SEM image of a particle with one-sided decomposition.

Table 17. EDS analysis points relating to the SEM image in Figure 74.

Spectrum	O	Mg	S	Total
1	52.4	22.47	25.13	100
2	53.26	19.92	26.82	100
3	53.63	18.81	27.56	100
4	53.58	18.96	27.46	100
5	50.44	28.3	21.26	100
6	49.05	32.44	18.51	100
7	40.82	56.93	2.24	100
8	39.69	60.31		100

Processing option : All elements analyzed (Normalized)
All results in weight%

These results show that the overall sulfur content in the bed decreases over time, but that individual particles are not in the same stage of decomposition at the different sampling points. A constant feed of elemental sulfur in the experiments with a feeding time of 30 minutes improved the reaction kinetics due to the constant sulfur gas pressure during the feeding period. In the experiment with a short feeding time, the sulfur gas partial pressure was only briefly elevated and the reaction rate was therefore lower.

5.1.4 Structural changes

Structural changes of unreacted magnesium sulfate

The epsomite raw material was composed of $MgSO_4 \cdot 6H_2O$ and $MgSO_4 \cdot 7H_2O$, as described in 3.2. The hexahydrate has a monoclinic crystal structure and the heptahydrate is orthorhombic. In most experiments, the unreacted magnesium sulfate was dehydrated and mainly present in the form of primitive orthorhombic β-$MgSO_4$, with the following crystal axis lengths: a = 4.750, b = 8.590, c = 6.710. Sometimes minor amounts of base- centered $MgSO_4$, with axis lengths a = 5.181, b = 7.885, c = 6.501 were also detected. It was observed that the primitive orthorhombic β-$MgSO_4$ was converted to base-centered $MgSO_4$ upon cooling in a nitrogen atmosphere. It was especially clear in the experiments where the conversion to MgO was low. In the experiments with sulfur as the reductant, this mainly occurred in experiments with dried heptahydrate as the raw material. In experiments with carbon and carbon monoxide, this was observed when too little reductant was used: i.e. in the

experiments with dried heptahydrate and a carbon monoxide partial pressure of 0.1 and in the experiment with dried heptahydrate at one time the stoichiometric amount of carbon. An overview of the crystal structures and the lengths of the crystallographic axis for both the feed materials as well as the products are shown in Table 18, which was obtained from XRD analysis [30].

Table 18. Overview of the crystal structure and lengths of the crystallographic axis of feed material and products. [30]

	Mineral	Crystal structure	Length of crystallographic axis		
			a	b	c
Feed material					
Epsomite	$MgSO_4 \cdot 7H_2O$	orthorhombic	11.86900	11.98400	6.84700
Epsomite	$MgSO_4 \cdot 6H_2O$	monoclinic	24.44200	7.21600	10.11900
Kieserite	$MgSO_4 \cdot H_2O$	base-centered monoclinic	7.51100	7.61100	6.92100
Dried Epsomite	α-$MgSO_4 \cdot 2H_2O$	not well crystallized	-	-	-
Dried Epsomite	$MgSO_4 \cdot 1.25H_2O$	not well crystallized	-	-	-
Dried Epsomite	β-$MgSO_4 \cdot 2H_2O$	not well crystallized	-	-	-
Dried Epsomite	$MgSO_4 \cdot H_2O$	base-centered monoclinic	6.90000	7.71000	7.54000
Products					
Unreacted magnesium sulfate	β-$MgSO_4$	primitive orthorhombic	4.75000	8.59000	6.71000
Unreacted magnesium sulfate	$MgSO_4$	base-centered orthorhombic	5.18100	7.88500	6.50100
Unreacted magnesium sulfate	$MgSO_4$	not well crystallized	-	-	-
Magnesium oxide (from $MgsO_4$)	MgO	face-centered cubic	4.21120	4.21120	4.21120

Not only did a change of crystal structure take place when monoclinic kieserite dehydrated to orthorhombic anhydrous magnesium sulfate; crystal growth also occurred when the material was heated. The kieserite feed material was composed of larger grains containing small crystals, as shown in Figure 75 (left). An example of unreacted magnesium sulfate after heating is shown in Figure 75 (right). Comparison of these two images clearly shows that individual crystal growth had occurred. The number of crystals is reduced when comparing the raw material with the heated material. This is due to the growth of crystal grains with more than six sides (in cross section) and the shrinkage of grains with fewer than six sides, which eventually disappear [70].

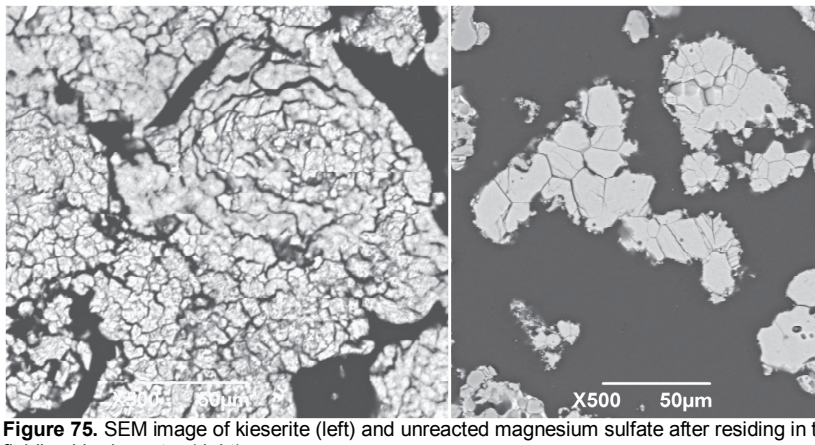

Figure 75. SEM image of kieserite (left) and unreacted magnesium sulfate after residing in the fluidized bed reactor (right).

Structural changes related to decomposition - intermediate phase formed prior to decomposition

An intermediate phase between $MgSO_4$ and MgO was observed in the SEM micrographs. The material has a structure similar to that of MgO, but a composition that is closer to $MgSO_4$. An example of this structure change is shown in the SEM image and element maps in Figure 76, taken from test M_C_4_G. The normal magnesium sulfate structure can be seen from the left-hand side of the image. The material on the right-hand side of the image appears to have the structure of magnesium oxide, but the element maps show that sulfur is still detected, on the right-hand side of the image. This structure was not only detected in the experiments with carbon as the reductant; similar behavior was found with the other reductants, for example in the short fluidization tests with sulfur as the reductant. SEM/EDS analysis from this experiment is shown in Figure 77 and Table 19. The sulfur content in spectra 1-4 is in accordance with the theoretical composition of magnesium sulfate (slightly higher). In spectra 5-8, the sulfur content is slightly decreased, as well as the oxygen content, indicating that some of the sulfur and oxygen had left the magnesium sulfate crystal structure. In spectra 9-10, the sulfur and oxygen content decreased even further.

The intermediate phase can be explained by the fact that some local spots within the solid magnesium sulfate particle start to decompose, which causes the structural change that is visible in Figure 77.

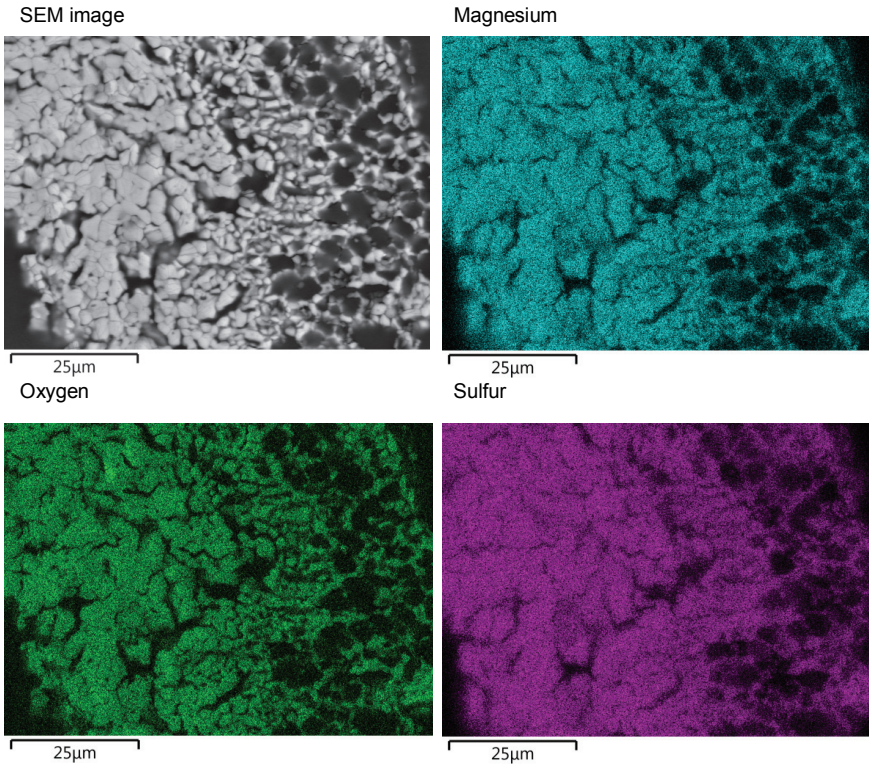

Figure 76. SEM image and element maps of M_C_4_G, showing a particle in which a structural change took place within the magnesium sulfate particle prior to decomposition.

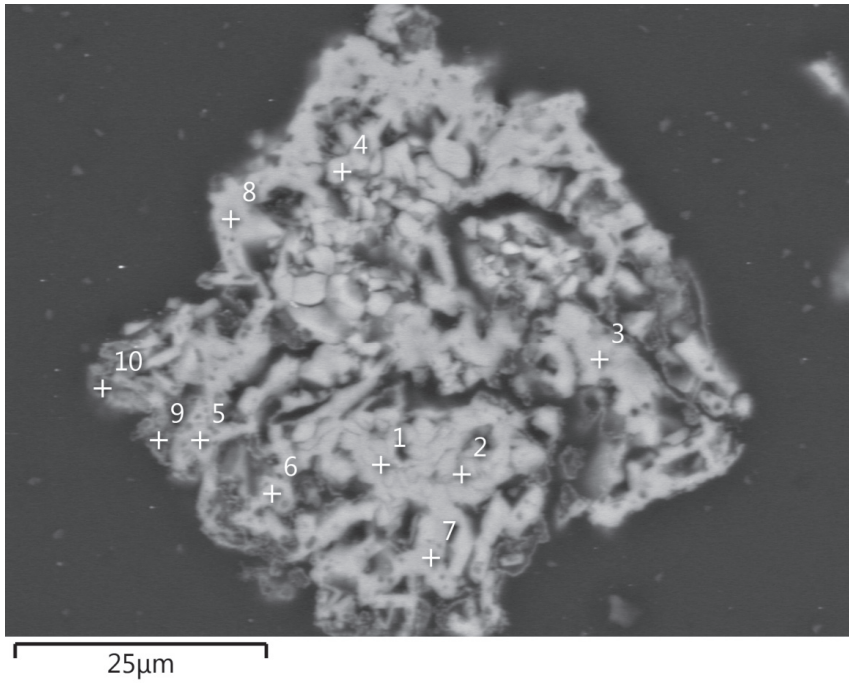

Figure 77. EDS analysis of experiment Fz_S_1.2, showing an intermediate phase between $MgSO_4$ and MgO.

Table 19. Theoretical composition of $MgSO_4$ and EDS analysis points relating to the SEM image in Figure 77.

	O	Mg	S	Total
Theoretical composition of $MgSO_4$	53.17	20.19	26.64	**100**

Spectrum	O	Mg	S	Total
1	53.92	17.96	28.12	100
2	53.02	20.62	26.35	100
3	53.59	18.94	27.48	100
4	53.45	19.34	27.21	100
5	50.01	29.6	20.39	100
6	49.74	30.4	19.86	100
7	51.79	24.28	23.93	100
8	51.77	24.37	23.87	100
9	44.74	45.28	9.98	100
10	46.94	38.72	14.34	100

Processing option : All elements analyzed (Normalized)
All results in weight%

Table 20 shows the calculated mineralogical composition of the spectra analyzed in Table 19, assuming that all sulfur is present as magnesium sulfate, or as elemental sulfur when there is an excess present. The remaining magnesium is assumed to be magnesium oxide.

Spectra 1-4 in Table 20 have a mineralogical composition of $MgSO_4$ with a minor amount of sulfur (spectra 1, 3 and 4) or MgO (spectrum 2). This minor amount of MgO or sulfur may actually be there or it may be calculated because of a measurement error in EDS. In spectra 5 and 6 there is approximately 25% MgO and 75% $MgSO_4$ and in spectra 7 and 8 there is 10% MgO and 90% $MgSO_4$. In spectra 9 and 10 there is clearly more MgO present. It needs to be noted that these numbers are not exact; the earlier mentioned measurement errors in EDS analysis and the fact that some material around or below the spectrum may have been measured may influence the results. Nevertheless, these results clearly show that the theory of partial decomposition within a crystal grain fits the mineralogy calculated from the EDS analysis well.

Table 20. Calculated mineralogical composition of the spectra from Table 19.

Spectrum	$MgSO_4$	MgO	S	Total
1	98.92	-	1.08	100
2	98.92	1.07	-	100
3	99.39	-	0.62	100
4	99.57	-	0.43	100
5	76.55	23.45	-	100
6	74.55	25.45	-	100
7	89.79	10.20	0.01	100
8	89.59	10.41	0.01	100
9	37.45	62.55	0.01	100
10	53.79	46.20	0.01	100

The structural change within the magnesium sulfate crystals prior to decomposition can also be observed from the powder samples that were analyzed with SEM. Figure 78 shows magnesium sulfate grains that have started cracking on the surface. A magnesium sulfate particle composed of several of these grains is shown in Figure 79, where some decomposition of magnesium sulfate into magnesium oxide also took place on the outer layer of the particle.

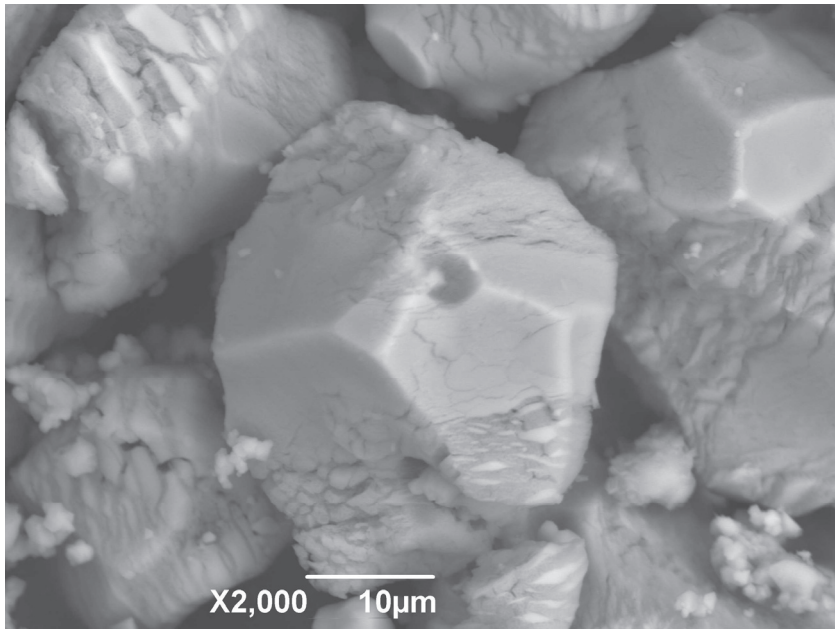

Figure 78. Magnesium sulfate grains which show cracking prior to decomposition.

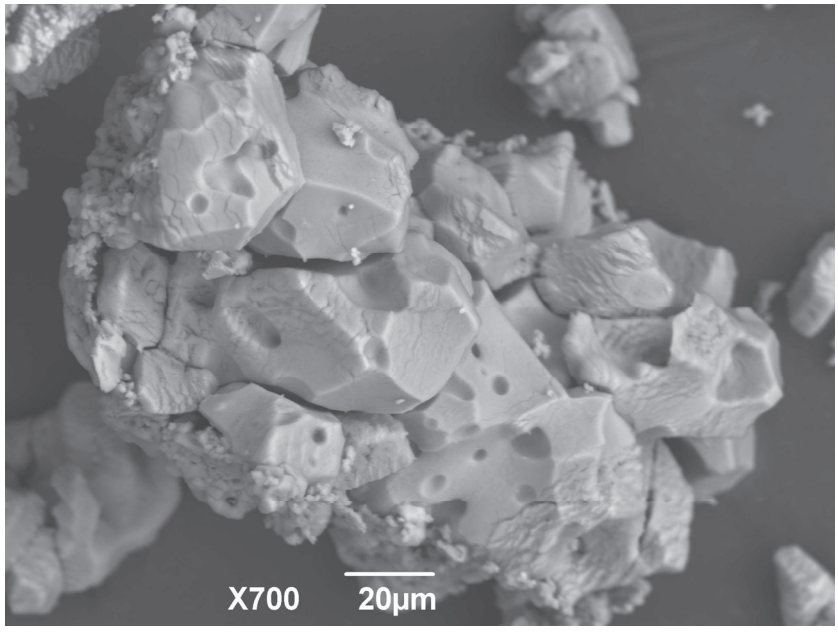

Figure 79. Magnesium sulfate particle with cracked grains and a minor amount of decomposition on the outer layer of the particle.

Structural changes due to decomposition

The structure clearly changes when magnesium sulfate decomposes to magnesium oxide. Comparing Figure 78, which shows magnesium sulfate grains, with Figure 80, which shows magnesium oxide grains, reveals that the magnesium oxide grains are much finer and the porosity between the grains is higher. The difference in structure can also be observed from the cross section samples, shown for example in Figure 87. The cross section in Figure 87 also shows that not only does the porosity between the grains increase, but also that the individual magnesium sulfate crystals decompose, forming magnesium oxide shells, due to the large difference in molar volumes, as described in section 2.2.2.

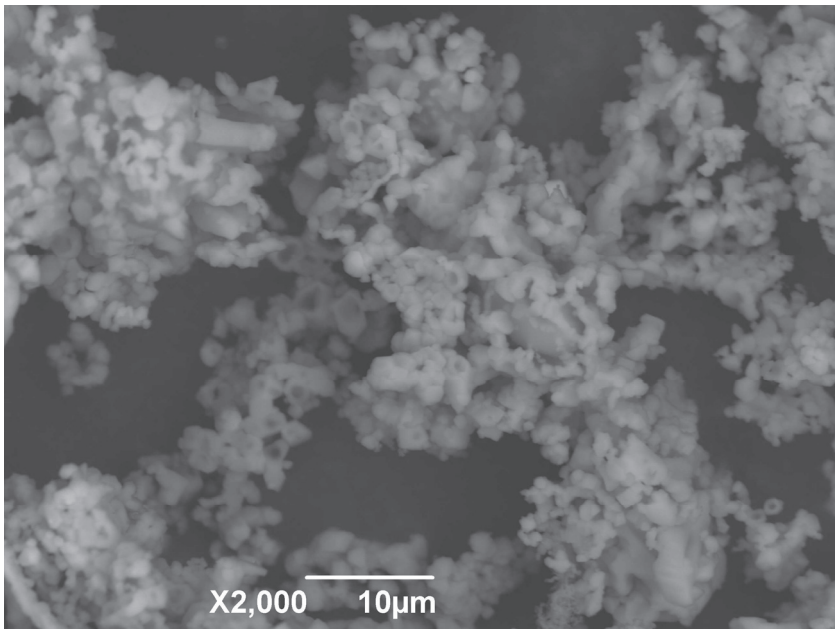

Figure 80. Powder sample of the magnesium oxide product.

5.1.5 The effect of the type of reductant on the overall $MgSO_4$ decomposition

The type of reductant has an effect on the overall decomposition mechanism of magnesium sulfate in the fluidized bed reactor. The feed material is hydrated magnesium sulfate and it will thus start to dehydrate when entering the fluidized bed reactor. A solid sulfur reductant will burn immediately on entering the bed, which causes a short increase in the sulfur gas partial pressure. The decomposition of magnesium sulfate starts to take place as soon as the particles enter the bed. A magnesium sulfate core was often found in the product samples from the experiments where sulfur was used as the reductant. This can be explained by the fact that the sulfur burns fast and after all the sulfur has burnt, the partial pressure of sulfur gas decreases significantly. The sulfur gas partial pressure has a large influence on the reaction kinetics, as can be seen from the gas analysis in Figure 66, where the sulfur dioxide concentration decreased immediately down to <0.4 vol% once the sulfur had been burnt. Figure 81 shows that dehydration and decomposition of particles takes place simultaneously at the initial stage of the reaction, according to the overall reactions (14) and (15).

$$MgSO_4 \cdot H_2O + S \rightarrow MgSO_4 + H_2O + S_2(\mathrm{g}) \quad (14)$$

$$MgSO_4 + \frac{1}{2}S \rightarrow MgO + \frac{3}{2}SO_2(g) \quad (15)$$

The rapid formation of a magnesium oxide outer layer prevents fluidization problems in the bed, which is especially of importance when particles with a small particle size (-150 μm) are used, as the surface area of these particles is large, and in addition, cohesion between the particles may play a role.

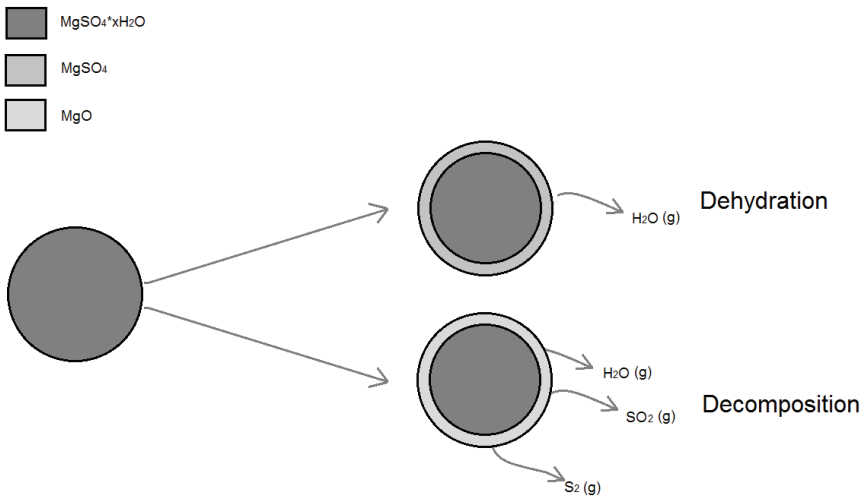

Figure 81. Illustration of reaction mechanism of magnesium sulfate decomposition with sulfur as the reductant.

The overall reaction with carbon as the reductant depends on the particle size of magnesium sulfate; fluidization problems did not occur with particle size groups 420-595 μm, 297-420 μm, and some defluidization occurred with particle size group 105-210 μm. In the experiments without fluidization problems, the formation of sulfur dioxide off-gas as a result of magnesium sulfate decomposition commenced as early as during the feeding period. Dehydration and decomposition took place in the initial stage of the reaction in which a magnesium oxide outer layer was formed, which prevented fluidization problems, as was also the case when sulfur was used as the reductant.

With particle size group -150 μm, however, fluidization problems occurred in the initial stage of the experiment, and as a result, no protective magnesium oxide layer was formed as it did with sulfur as the reductant. The fluidization problems were caused by softening of the magnesium sulfate particles, as well as by inter-particle cohesion, which is typical for finer particles. This resulted in sintering and thus agglomeration, which reduced the gas-solid contact interface. The decomposition reaction only started after a period of dehydration and sintering, as illustrated in Figure 82. Reaction (16) thus takes place alone first, followed by reactions (16) and (17) which take place simultaneously. The predominant reduction reaction with carbon is through

gaseous intermediates, as shown in reaction (17); the direct reaction of solid carbon with magnesium sulfate is minimal.

$$MgSO_4 \cdot H_2O \rightarrow MgSO_4 + H_2O(g) \quad (16)$$

$$MgSO_4 + CO(g) \rightarrow MgO + CO_2(g) + SO_2(g) \quad (17)$$

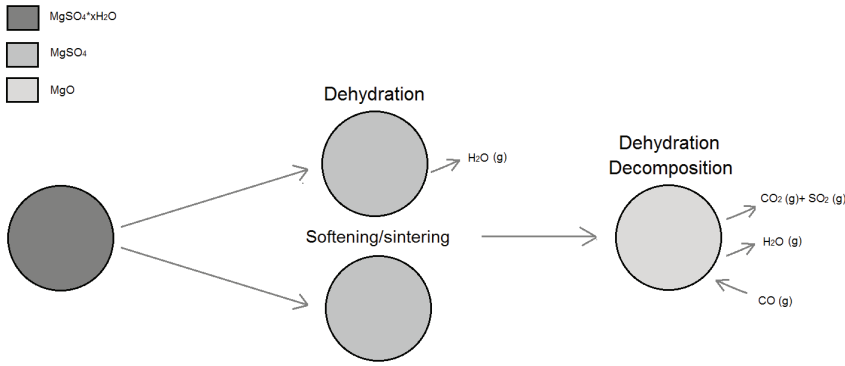

Figure 82. Illustration of reaction mechanism of magnesium sulfate decomposition with carbon as the reductant.

With carbon monoxide as the reductant, some decomposition of magnesium took place initially, but the reaction with carbon monoxide caused fracturing of the particles, so that many fines were produced. As a result, inter-particle cohesion caused fluidization problems, which in turn caused sintering due to softening of the magnesium sulfate material and a reduced magnesium sulfate reaction rate. The bed was refluidized only after enough of the surface of the particles had decomposed, after which the reaction rate increased again.

5.1.6 The reaction rate steps for a single $MgSO_4$ particle

A large number of sub-processes play a role in the decomposition of magnesium sulfate. Three main processes take place: heating up of the particles when entering the fluidized bed, dehydration, and decomposition. The different steps involved in these main processes are described below. These steps do not occur in sequence, thus more than one process may occur at a time. In addition to these processes, sintering of material also takes place, as well as the breaking of particles (especially with carbon monoxide as the reductant), crystal growth, and increase in porosity.

The following sub-processes take place during the heating up of the magnesium sulfate particles entering the bed and are illustrated in Figure 83:

a) Heat transfer (+) from the bulk gas to the gas film around the particle
b) Heat transfer (+) from the gas film to the particle surface
c) Heat transfer (+) from the particle surface into the particle
d) Heat transfer (-) from the particle to the particle surface
e) Heat transfer (-) from the particle to the gas film
f) Heat transfer (-) from the gas film to the bulk gas

Each particle is composed of several crystal grains and, as a result, there is some porosity in the particles.

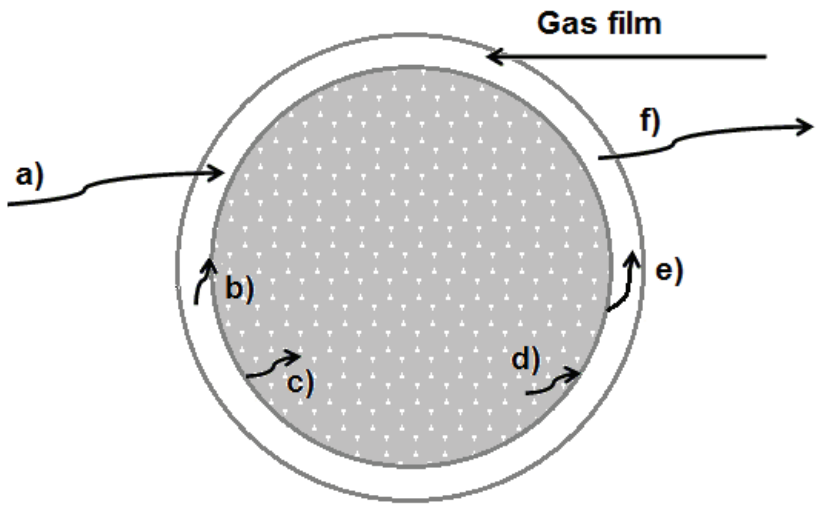

Figure 83. Sub-processes that take place during heating up of (hydrated) magnesium sulfate particles entering the bed.

The following sub-processes are related to the dehydration of magnesium sulfate and are illustrated in Figure 84:

g) Detachment of H_2O from the magnesium sulfate hydrate crystal structure
h) Mass transfer of H_2O from the particle to the interface
i) Mass transfer of H_2O from the interface to the gas film
j) Mass transfer of H_2O from the gas film to the bulk gas
k) Heat transfer (-) from the particle to the interface
l) Heat transfer (-) from the interface to the gas film
m) Heat transfer (-) heat transfer from the gas film to the bulk gas
n) Heat transfer (+) from the bulk gas to the gas film
o) Heat transfer (+) from the gas film to the particle interface
p) Heat transfer (+) from the particle interface into the particle

The particles are cooled during dehydration of magnesium sulfate, as this is an endothermic process. The particle needs to be heated up again for the dehydration to continue, which will slow down the dehydration reaction. In addition to these sub-processes, the porosity is also increased due to dehydration of magnesium sulfate hydrate, which is also illustrated in Figure 84.

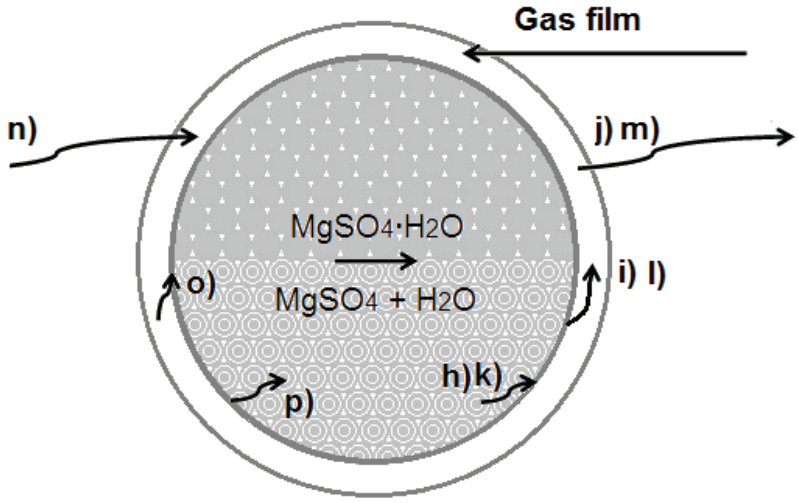

Figure 84. Sub-processes that take place during dehydration of magnesium sulfate particles.

The decomposition of magnesium sulfate is composed of the following sub-processes, which are illustrated in Figure 85:

q) Mass transfer: gaseous reductant from the bulk gas to the gas film around the particles
r) Mass transfer: gaseous reductant from the gas film through the ash* layer to the particle interface
s) Reaction at the particle interface: $MgSO_4$ → MgO**
t) Mass transfer of $SO_2/SO_3/CO_2$ from the particle interface through the ash layer to the gas film
u) Mass transfer of $SO_2/SO_3/CO_2$ from the gas film to the bulk gas
v) Heat transfer (-) from the particle interface into the particle
w) Heat transfer (-) from particle interface to the ash layer and gas film
x) Heat transfer (-) from the gas film to the bulk gas
y) Heat transfer (+) from the bulk gas to the gas film
z) Heat transfer (+) from the gas film to the particle interface
aa) Heat transfer (+) from the particle interface into the particle

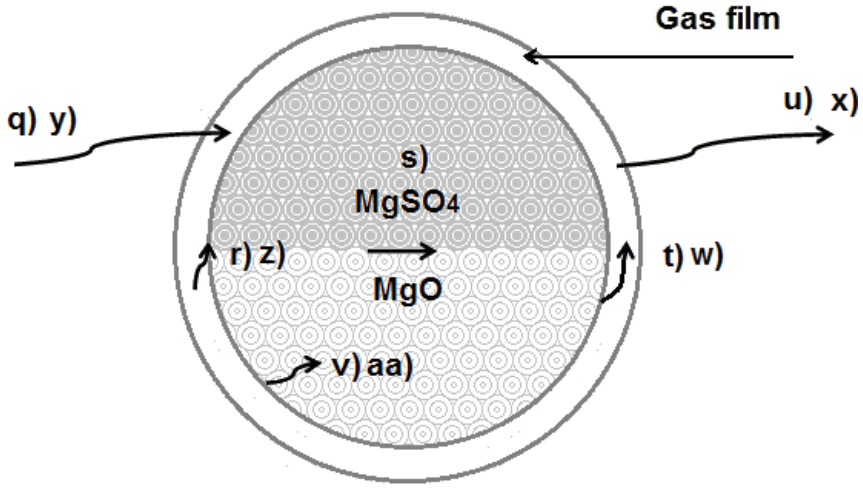

Figure 85. Sub-processes that take place during decomposition of magnesium sulfate particles.

* Initially, no ash layer is formed and the thickness of the ash layer increases as the reaction proceeds.

**The reductant is also involved in the decomposition reaction, according to reaction equations (4)-(6) in section 2.2.1.

The porosity increases strongly when magnesium sulfate decomposes to magnesium oxide, as illustrated in Figure 85. In reality, the decomposition takes place from the outer layers of the particles towards the center. The reaction at the interface causes cooling of the particles due to the endothermic character of the decomposition reaction; the particles need to be heated up every time a thin layer of magnesium sulfate has decomposed, in order for the reaction to continue. Under fluidizing conditions, the heat and mass transfer coefficients are much higher than in a stagnant gas, as for example in a chamber furnace. Not only the heat transfer steps, but also the mass transfer steps q) and r), in which the reductant is transported from the bulk gas to the gas film and from the gas film to the particle interface, respectively, are more rate-determining in a reactor where the entire gas phase is more or less stagnant, than in a fluidized bed reactor.

5.1.7 The rate-controlling step for $MgSO_4$ decomposition

Determination of the rate-controlling step can be done by fitting the experimental data with mathematical kinetic models. Commonly used reaction models include nucleation models, such as the Avrami, Erofeyev and powder law models; phase boundary models, diffusion models, including the Jander equation and ash layer diffusion/Ginstling-Brounshtein model [58, 71-74].

SEM micrographs of the intermediate sample and products showed that the majority of the partially decomposed particles have a clear reaction front, as shown for example in Figure 86. This reaction front was not only visible on the particle scale, but also the individual crystals within the particle, as can be seen in Figure 87, where the upper part of the material is composed of magnesium sulfate and the lower part of magnesium oxide. The individual crystals at the reaction front are partially decomposed; the outer layer is composed of MgO and the core is composed of magnesium sulfate. In addition to these particles, a minor amount of particles decomposed more evenly, as for example shown in Figure 88 (left), whereas for some particles there was no clear reaction front, nor was the particle evenly decomposed, as shown in Figure 88 (right). The reaction front for the decomposition of porous particles, however, may not always be clear, due to local decomposition ahead of the reaction front due to the porosity [75].

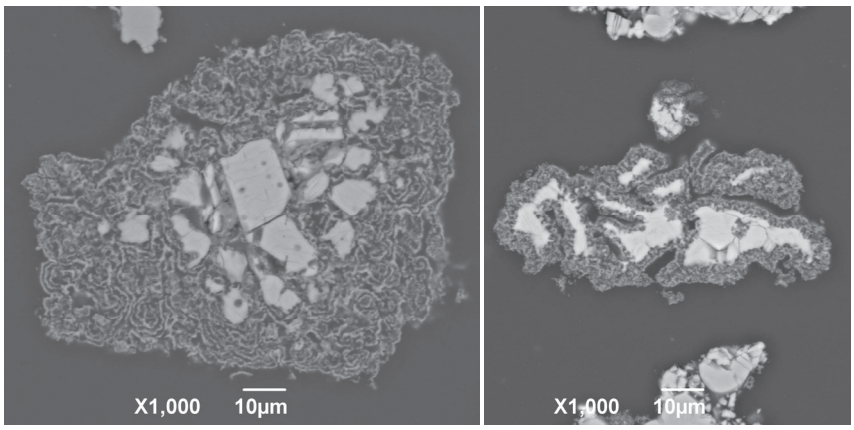

Figure 86. Partially decomposed magnesium sulfate particles in accordance with the shrinking core model with a magnesium oxide outer layer and magnesium sulfate core.

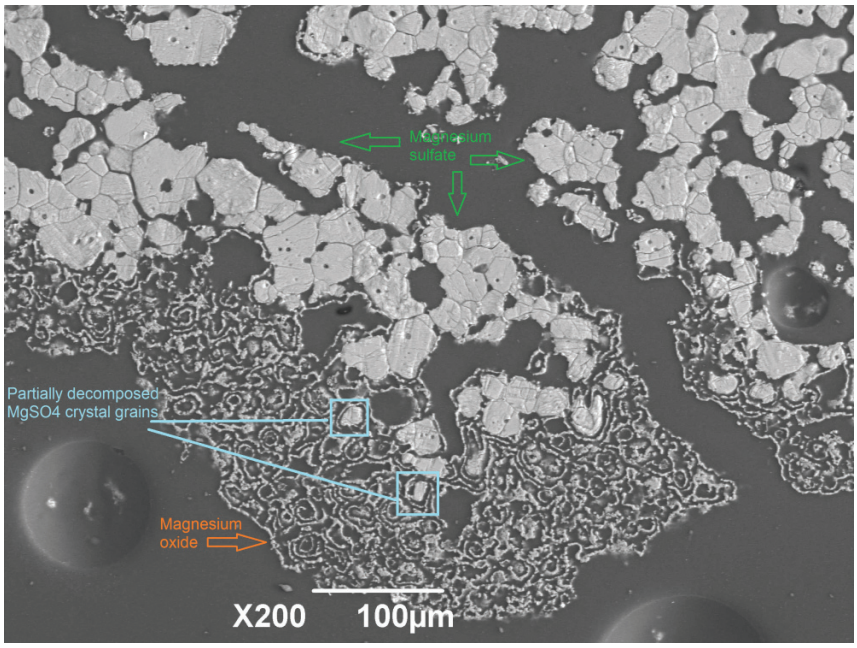

Figure 87. Decomposition of magnesium sulfate with a clear reaction front and partially decomposed individual crystals.

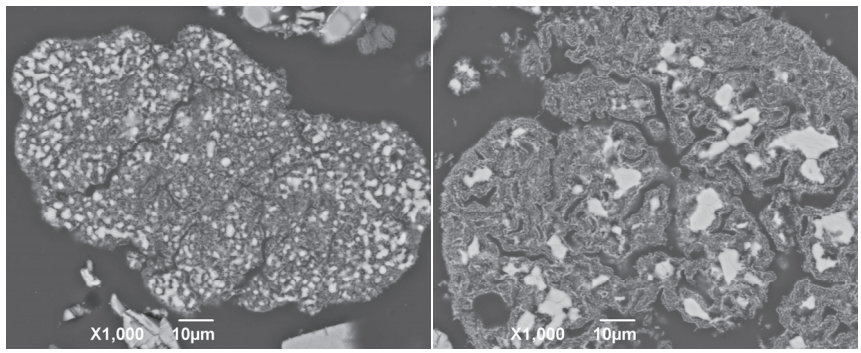

Figure 88. Magnesium sulfate particles decomposing in accordance with the uniform reaction model (left) or by mixed control (right).

As SEM analysis showed that the particles are spherical and the majority of the particles decomposed with a clear reaction front, only such kinetic models were considered. The experimental data from FTIR off-gas analysis and the final solid sample were used for determining the rate-controlling step of magnesium sulfate decomposition. This method was preferred over using only data from solid samples, as the number of samples was limited and most magnesium sulfate already decomposed during the feeding period when sulfur was used as the reductant. The off-gas analysis was converted to conversion of magnesium sulfate, taking the feeding period into account, by calculating the theoretical maximum decomposition at each measurement point. It was assumed that the feeding rate was constant, except for short breaks during the feeding periods when the analyzer tube was changed due to blockage. The conversion graphs for experiments M_S_4_G, M_C_4_G, M_CO_4_G and H_S_4 are shown in Figure 89. The model fitting calculations were carried out with Microsoft Excel, using the non-linear least squares method and the Solver add-in. A macro was created to calculate the optimal solution. The integrated functions of the shrinking core model as well as the Jander equation that are presented in section 2.2.2.were used.

The results in Table 21 show that the best fit (R^2 = 0.95) was obtained with the chemical reaction at the unreacted interface for experiment M_S_4_G, in which magnesium sulfate monohydrate was used as the feed material and sulfur as the reductant. This is in agreement with the strong temperature dependence that was found in section the experiments carried out at different temperatures in section 4.3.3, which indicates chemical reaction control at the interface rather than at the gas film or ash layer, according to Levenspiel [54].

The strong temperature dependence of the decomposition reaction, under different conditions, however, was also found by Hulbert [45] and Plewa and Steindor [49]. The use of dried magnesium sulfate heptahydrate instead of monohydrate shifts the rate-controlling mechanism; the reaction rate is determined by diffusion through the ash layer (R^2 = 0.96), as shown in Table 22. The change in rate-controlling step could be expected, as a dense outer layer or even hollow spheres were formed when heptahydrate was dried.

The curves for the experiments with carbon and carbon monoxide have a different shape than the curves with sulfur as the reductant, as shown in Figure 89. During both experiments defluidization occurred; in the experiment with carbon as the reductant the bed defluidized during the entire feeding period (0-25 minutes) and in the experiment with carbon monoxide defluidization occurred after feeding had already started (at t=6:30-32:46). The periods in which defluidization occurred and thus no reaction took place were omitted from model fitting, but were taken into account when calculating τ, the total time for completion of the reaction. The gas film diffusion model best fitted the data from both the experiment with carbon and carbon monoxide (R^2 =0.99), as shown in Table 23 and Table 24, respectively. A reasonably good fit was also obtained for chemical reaction control at the unreacted interface: R^2 =0.95 and 0.96 for carbon and carbon monoxide, respectively. It was not expected that gas film diffusion would be the rate-determining step, as the gas film resistance is always smaller than ash layer resistance when an ash film is being formed, according to Kunii and Levenspiel [55]. In addition, other authors [49, 76] found that the decomposition of magnesium sulfate in the presence of carbon or carbon monoxide was chemically controlled at the unreacted interface. However, those experiments were carried out under different conditions, using TG/DSC instead of a fluidized bed reactor. The number of kinetic models that was tested in [76] was limited. It was observed that all particles (including the bed material) had turned gray after the experiments with carbon and carbon monoxide as the reductant. The deposition of a thin layer of carbon on the surface of the particles can explain that the reaction seems to be controlled by gas film diffusion. It, however, also needs to be taken into account that the period of defluidization may have influenced the reliability of the results.

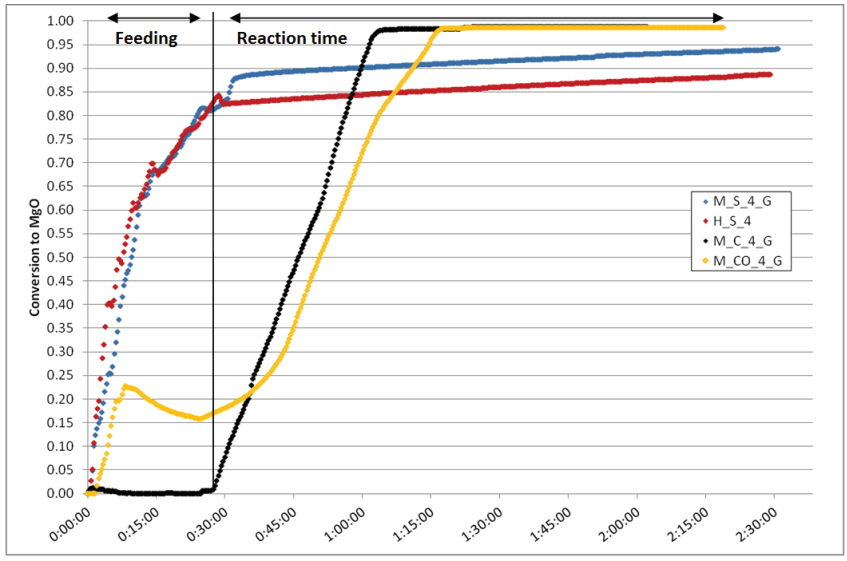

Figure 89. Decomposition of magnesium sulfate in the presence of sulfur, carbon and carbon monoxide as the reductant, experiments M_S_4_G, H_S_4, M_C_4_G and M_CO_4_G, conversion calculated from gas analysis.

Table 21. Results of kinetic model fitting with the off-gas analysis from the experiment with magnesium sulfate monohydrate and sulfur as the reductant (experiment M_S_4_G).

M_S_4_G	SS	R^2	τ (min)	k (s^{-1})
Chemical reaction at the interface	0.258	0.946	51.9	3.21E-04
Ash layer diffusion	0.355	0.926	73.4	2.27E-04
Gas film diffusion	1.305	0.726	25.5	6.54E-04
Jander	0.490	0.897	176.0	9.47E-05

Table 22. Results of kinetic model fitting with the off-gas analysis from the experiment with dried magnesium sulfate heptahydrate and sulfur as the reductant (experiment H_S_4).

H_S_4	SS	R^2	τ (min)	k (s^{-1})
Chemical reaction at the interface	0.568	0.848	49.2	3.39E-04
Ash layer diffusion	0.152	0.959	68.1	2.45E-04
Gas film diffusion	1.873	0.499	24.2	6.90E-04
Jander	0.209	0.944	160.9	1.04E-04

Table 23. Results of kinetic model fitting with the off-gas analysis from the experiment with magnesium sulfate monohydrate and carbon as the reductant (experiment M_C_4_G).

M_C_4_G	SS	R^2	τ (min)	k (s^{-1})
Chemical reaction at the interface	0.403	0.949	106.5	1.57E-04
Ash layer diffusion	1.952	0.754	156.8	1.06E-04
Gas film diffusion	0.016	0.998	63.8	2.61E-04
Jander	2.237	0.719	359.8	4.63E-05

Table 24. Results of kinetic model fitting with the off-gas analysis from the experiment with magnesium sulfate monohydrate and carbon monoxide as the reductant (experiment M_CO_4_G).

M_CO_4_G	SS	R^2	τ (min)	k (s^{-1})
Chemical reaction at the interface	0.543	0.957	120.9	1.38E-04
Ash layer diffusion	2.772	0.782	164.5	1.01E-04
Gas film diffusion	0.134	0.989	71.8	2.32E-04
Jander	3.309	0.739	372.2	4.48E-05

5.1.8 Summary

Good gas-solid contact and mixing are a requirement for the decomposition of magnesium sulfate with sulfur as the reductant to take place. Fluidization problems are caused both by cohesive forces between the particles as well by the softening of magnesium sulfate. The latter is avoided, especially with fine particles, when sulfur is used as the reductant, because with this reductant an MgO layer is formed around the magnesium sulfate core. Particles do not decompose evenly as a function of time: even with a short feeding time the particles are in different stages of decomposition, from unaffected to fully decomposed. A structural change takes place before decomposition occurs, which is caused by local decomposition within the crystal. Magnesium sulfate decomposes according to the shrinking core model, both on grain scale and single crystal scale. Decomposition and dehydration take place simultaneously during the initial stage of the reaction with sulfur as the reductant, whereas with carbon and carbon monoxide dehydration occurs first, followed by decomposition together with further dehydration. It was found that chemical reaction at the unreacted surface is the rate-controlling step for decomposition of magnesium sulfate monohydrate in the presence of sulfur, whereas gas film diffusion is the rate-controlling step in the presence of carbon or carbon monoxide. The reaction is controlled by ash layer diffusion when dried

magnesium sulfate heptahydrate was used instead of monohydrate in the presence of sulfur.

5.2 Operating window for successful decomposition of hydrated magnesium sulfate

The experiments of which the results are presented in section 4.3 were carried out to determine the overall reaction kinetics and the operating window for successfully decomposing hydrated magnesium sulfate. Successful decomposition is defined as having low residual sulfur content and a large surface area of the magnesium oxide product. The magnesium oxide can be utilized as a neutralizing agent in the leaching process, as described in more detail in the introduction (section 1.1).

5.2.1 Operating window with sulfur as the reductant

Magnesium sulfate heptahydrate, dried magnesium sulfate heptahydrate, and magnesium sulfate monohydrate were tested as the feed materials. It was not possible to use magnesium sulfate heptahydrate due to the large amount of crystal water that was liberated when the material was fed to the reactor, causing defluidization of the bed. Similar levels of residual sulfur were achieved with magnesium sulfate monohydrate and dried heptahydrate. The bed was, however, more stable with magnesium sulfate monohydrate than with dried heptahydrate, regardless of the fact that both materials contained approximately the same amount of crystal water. It is therefore preferable to use magnesium sulfate monohydrate.

Experiments carried out at 850, 900, and 950°C showed that the reaction kinetics are significantly affected by the temperature. At 850°C, only partial decomposition took place and this temperature is therefore considered too low for successful decomposition. At both 900°C and 950°C full decomposition (>98% of the magnesium sulfate decomposed) took place, but this point was reached faster at 950°C. From the kinetic viewpoint, the preferred decomposition temperature would therefore be 950°C. It is, however, important not only to take the kinetics into account, but also the effect of temperature on the surface area of the magnesium oxide produced. SEM

analysis of the powder samples taken after each experiment (section 4.3.3, Figure 36) showed that a reduced surface area was formed due to diffusion when magnesium sulfate was decomposed at 950°C. The preferred operating temperature is therefore 900°C, in order to ensure fast reaction kinetics without creating a surface area that is too reduced.

The amount of sulfur used as the reductant has a similar effect on the surface area of the magnesium oxide produced: the product had a large surface area when one time the stoichiometric amount of sulfur required to decompose magnesium sulfate was used. The surface area is slightly less when twice the stoichiometric amount of sulfur was used, but the single crystals can still easily be distinguished. With four times the stoichiometric amount of sulfur the surface area is highly reduced due to diffusion. More than 90% of the magnesium sulfate decomposed after a two-hour reaction time. The main difference is that the more sulfur used, the higher the reaction rate in the initial phase of the reaction. The use of twice the stoichiometric amount is preferred when taking the reaction rate and the surface area into account.

The reaction kinetics for decomposition of magnesium sulfate with sulfur as the reductant is fast: during the feeding time of 30 minutes >80% of magnesium sulfate decomposed. The reaction rate then decreases sharply after feeding is completed which is followed by a period with a low reaction rate. The optimum residence time is therefore two hours, in order to achieve >95% decomposition of magnesium sulfate. However, if, in a real process, a high conversion of magnesium sulfate is less important than ensuring a short residence time, a minimum residence time of 30 minutes in the bed would be required.

The experiments with sulfur as the reductant showed that the particle size was a limiting factor. The surface area-to-volume ratio or in other words, the specific surface area, increases with a decreased particle size and it is therefore desirable to have a smaller particle size. The relationship between the surface area to volume ratio and particle size for spherical, non-porous particles is shown in Figure 90, where the different particle sizes used in the powder experiments are highlighted.

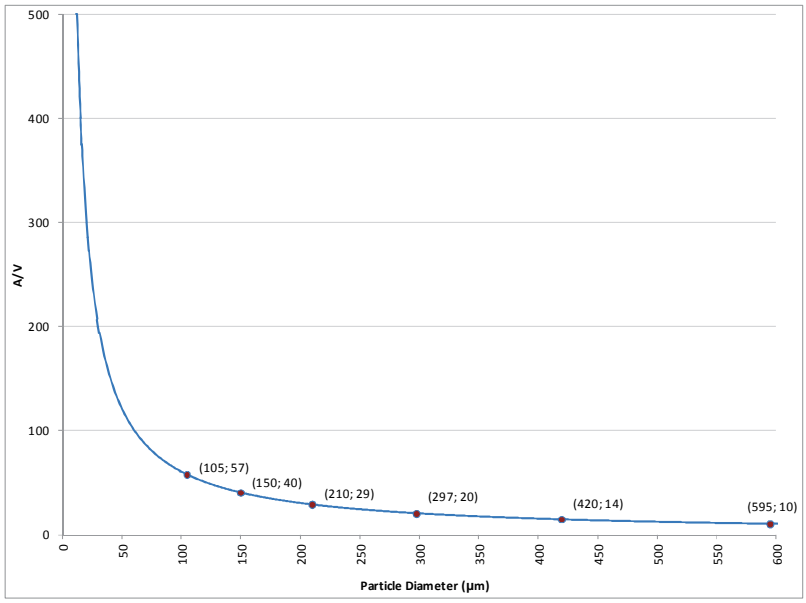

Figure 90. Surface area to volume ratio as a function of particle diameter for spheres, (particle size; surface to volume ratio).

Hydrated magnesium sulfate can only be decomposed successfully with particle size group -150 µm when sulfur was used as the reductant. With the larger particle size groups only partial decomposition was achieved.

Impurities were used in some of the experiments. The mechanism of decomposition of magnesium sulfate is different from the sulfate impurities that were used in this work: iron sulfate and manganese sulfate were first reduced to sulfide, which was followed by decomposition. Calcium sulfate did not decompose under the experimental conditions used in this work. Formation of intermediate sulfides during the decomposition of manganese, calcium, and iron sulfate under reducing conditions has also been found by other authors [77- 81]. Magnesium sulfate, on the other hand, decomposes directly to magnesium oxide with any of the reductants; no intermediate forms such as magnesium sulfide, magnesium sulfite, or magnesium carbonate when using a carbonaceous reductant, were observed under the experimental conditions used in this work.

The predominance diagrams in Figure 91 show that under the initial experimental conditions, where the sulfur partial pressure is increased due to burning of the solid sulfur reductant, metal sulfide is the stable compound in

the systems Fe-S-O, Mn-S-O and Ca-S-O, but for Mg-S-O magnesium oxide is the stable compound. In the course of the experiment, the sulfur partial pressure as well as the sulfur dioxide partial pressure decreases. This will move the operating conditions of all Me-S-O systems into the Me-O region, except for the system Ca-S-O.

The presence of iron sulfate enables the use of larger particle sizes; in the absence of iron sulfate there was still 12.8% sulfur in the product of the test with particle size group 105-210 μm, whereas this was only 0.82% in the presence of iron sulfate. It was found by Knittel et al. [44] that the presence of Fe_2O_3 promotes the decomposition of SO_3 into SO_2 and O_2 and thus acts as a catalyst. This is in agreement with the findings of this work, as Fe_2O_3 is the decomposition product of iron sulfate under the experimental conditions used in this work. The effect of 5 wt% Fe_2O_3 is claimed to shorten the total reaction time by 2.5 times when magnesium sulfate is decomposed in the absence of any reductants using TG/DSC [69].

Calcium sulfate, on the other hand, has a negative effect on the final sulfur content because the decomposition temperature of calcium sulfate is higher than the operating temperature, as shown in the predominance diagram in Figure 91. Additionally, calcium sulfate forms compounds with magnesium sulfate, which was expected beforehand, as it was reported by Kaljuvee et al. [82] and Rowe et al. (described in the paper by Du, [29]) that in the $MgSO_4$-$CaSO_4$ system the compound $CaMg_3(SO_4)_3$ may be stable.

The effect of manganese sulfate is minimal; the manganese does not form any compounds with magnesium sulfate. Fluidization problems were expected to occur due to melting of the manganese sulfate, which has a melting point of 700°C. The manganese particles, however, did not melt. The particles were composed of MnS directly after feeding, according to the SEM/EDS analysis and the stability diagram in Figure 91. The rapid conversion of manganese sulfate to manganese sulfide may explain why the particles did not melt: manganese sulfide has a melting point of 1530°C. In addition to this, the amount of manganese sulfate was relatively low and fluidized bed operations allow a minor amount of sticky particles without causing fluidization problems. The manganese was present as manganese oxide with minor amounts of sulfur in the sample taken after two hours and in the product sample.

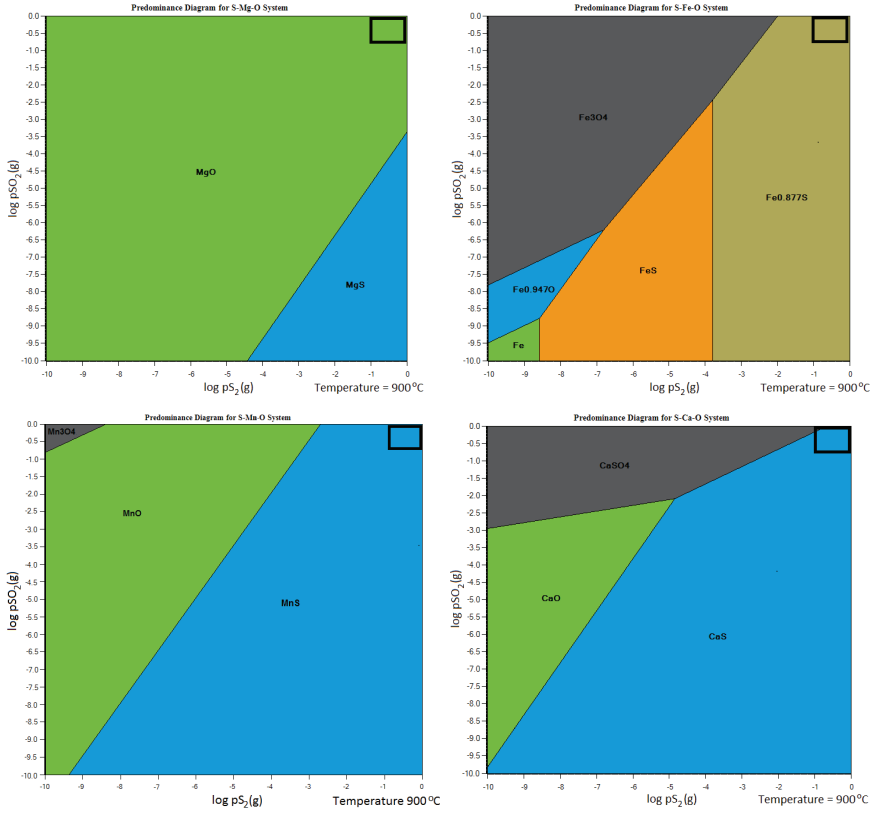

Figure 91. Predominance diagrams of Mg-S-O (top, left), Fe-S-O (top, right), Mn-S-O (bottom, left) and Ca-S-O (bottom, right) at 900°C, with experimental conditions during the initial phase of the experiment.

5.2.2 Operating window with carbon or carbon monoxide

Dried magnesium sulfate heptahydrate and magnesium sulfate monohydrate were tested as the feed materials in the presence of carbon or carbon monoxide as the reductant. Magnesium sulfate heptahydrate was not tested as the raw material, as the preliminary tests showed that it was not possible to use this raw material due to the large amount of crystal water that was liberated during feeding, causing defluidization of the bed. Some fluidization problems occurred at the beginning of the experiments with monohydrate and dried heptahydrate with both reductants, due to the slower reaction kinetics with these reductants compared with sulfur. This is discussed in more detail in section 5.1.2. The bed agglomerated when dried magnesium sulfate heptahydrate was used as the feed material; this behavior was not observed with magnesium sulfate monohydrate as the feed material. Fragmentation

took place due to the weakened structure of the dried heptahydrate; this was not the case with monohydrate. An example of the agglomeration and fragmentation of dried magnesium sulfate heptahydrate is shown in Figure 92. The amount of reductant required for decomposition of magnesium sulfate was dependent on the raw material that was used; with monohydrate, a CO partial pressure of 0.1 was required to achieve successful decomposition, whereas a CO partial pressure of 0.2 was needed to decompose dried magnesium sulfate heptahydrate. Due to fewer fluidization problems and the possibility to use a lower amount of reductant, magnesium sulfate monohydrate is the preferred raw material. If carbon is used as the reductant instead of CO, twice the stoichiometric amount of carbon is needed; one time the stoichiometric amount resulted in incomplete decomposition.

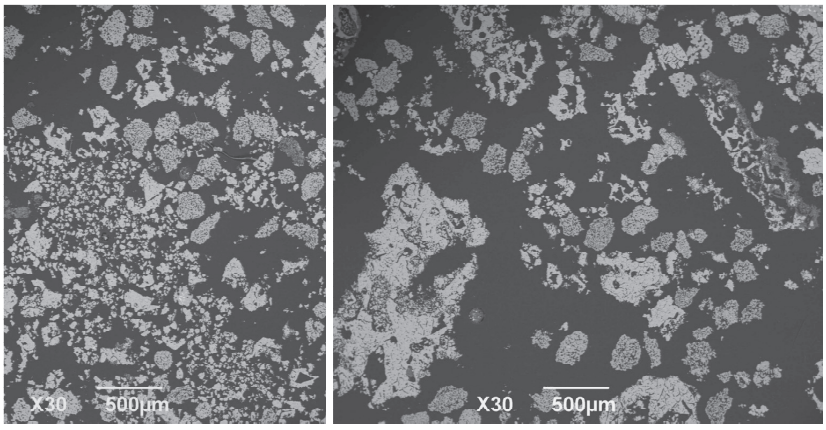

Figure 92. Fragmentation and agglomeration during experiment H_CO_3.

The effect of temperature was only tested with carbon monoxide as the reductant and not with carbon. The results for the experiments carried out at 850°C and 900°C are very similar when comparing the reaction kinetics, final sulfur content and structure of the product; therefore it is preferred to use a temperature of 850°C.

The rate of the decomposition reaction is lower with carbon or carbon monoxide compared with sulfur as the reductant. Whereas with sulfur >80% is decomposed directly after feeding, only >60% of the magnesium sulfate is decomposed when carbon or carbon monoxide is used as the reductant. Gas analysis showed that a residence time of at least one hour and 30 minutes is needed after feeding is completed with carbon as the reductant and one hour

and 40 minutes with carbon monoxide. In the samples taken after two hours, a decomposition of >98.8% can be achieved. A residence time of two hours is therefore preferred.

A wider range of particle sizes can be used with carbon and carbon monoxide as the reductant than with sulfur as the reductant. Successful decomposition was achieved for all the particle size groups that were tested, as can be seen for carbon in Figure 93. Successful decomposition was also achieved with carbon monoxide for all particle size groups.

The effect of impurities on the decomposition of magnesium sulfate with carbon monoxide as the reductant was tested also tested. Manganese sulfate does not have any influence on the final sulfur content, nor does calcium sulfate. The sulfur content in the presence of iron sulfate was slightly lower than in comparable experiments without any impurities. The main difference between using sulfur and carbon monoxide as the reductant is that calcium sulfate can be decomposed with carbon monoxide but not with sulfur. This can be explained by the formation of a CaS-containing intermediate, which may form in the temperature range of 850-950°C [80, 81]. SEM/EDS analysis indicates that such a compound may have formed in the presence of carbon monoxide, but not with sulfur as the reductant.

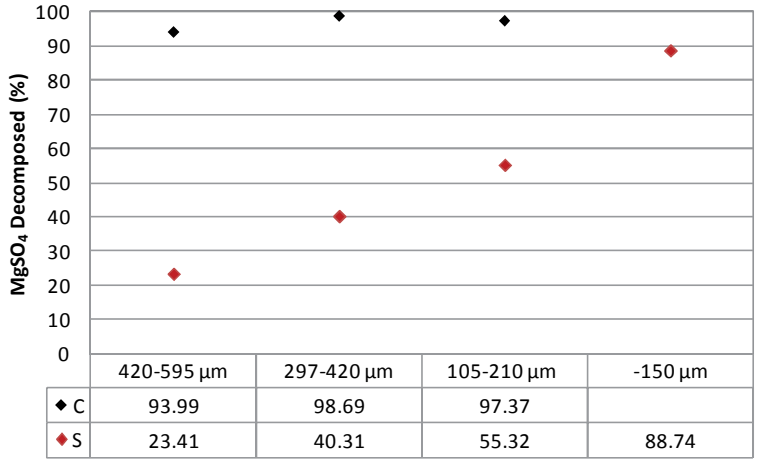

Figure 93. Decomposition of magnesium sulfate in different particle size groups with sulfur and carbon as the reductant, carried out at 900°C, experimental time: two hours, except for the test with particle size of 420-595 µm and carbon, where the reaction time was one hour.

5.2.3 Summary

The preferred conditions for decomposing magnesium sulfate in the presence of a reductant are summarized in Table 25. The operating window with carbon and carbon monoxide as the reductant is more flexible than with sulfur, as larger particle size groups can be used, which reduces the energy requirement for size reduction and fluidization problems due to the cohesion of fine particles are less likely. The presence of impurities, especially calcium sulfate, does not have a detrimental effect on the decomposition of magnesium sulfate. In addition to this, lower residual sulfur concentrations can be reached in the product with carbon or carbon monoxide as the reductant. The use of sulfur may also cause practical problems, as elemental sulfur may deposit on colder surfaces. There are, however, some drawbacks with the use of carbon and carbon monoxide as the reductant. Firstly, these reductants will produce an off-gas that contains carbon dioxide and possibly carbon monoxide. Carbon monoxide needs to be combusted in order to prevent problems in the off-gas line, requiring a post-combustion chamber or other auxiliary equipment. Carbon dioxide is an unwanted by-product because it is a greenhouse gas and the carbon dioxide emission regulations are becoming increasingly stringent. Secondly, operation of the fluidized bed may be difficult, because fluidization problems occur more with a carbonaceous reductant than with sulfur. This is due to the lower reaction rate of carbon and carbon monoxide compared with sulfur, which results in the softening of magnesium sulfate, which in turn causes fluidization problems. As a final point, the fragmentation of magnesium sulfate, especially that of dried magnesium sulfate heptahydrate which occurs with carbon monoxide, leads to more fines, which may be entrained with the gas stream and make gas cleaning more difficult in practice.

Table 25. Comparison of the operating windows with sulfur and with carbon/carbon monoxide as the reductant.

	Sulfur	Carbon/Carbon monoxide
Raw material	Monohydrate	Monohydrate
Amount of reductant	Two times the stoichiometric amount	10% CO, two times the stoichiometric amount of carbon
Temperature	900°C	850°C (CO)
Particle size	<150 micron	up to particle size group 420-595 µm
Residence time	>80% Decomp. During feeding, >95% after 2 hours	>60% Decomp. During feeding, >95% after 2 hours
Effect of impurities	Calcium sulfate: negative, iron sulfate: positive, manganese sulfate: neutral	Calcium and manganese sulfate: neutral, iron sulfate: positive (less clear than with sulfur)

6. Conclusions

Reaction mechanism

The decomposition of hydrated magnesium sulfate at 900°C requires a reductant, as it is not possible to fluidize the material without one. The reductant should react quickly with the outer surface of the sulfate particles, in order to create an outer layer of magnesium oxide, which prevents fluidization problems due to the softening of magnesium sulfate. This is of particular importance when particles under 150 microns are used, as cohesion between particles plays a role with these finer particles. Sulfur, carbon monoxide, and carbon were tested as reductants in this work and it was found that only sulfur reacts fast enough to prevent fluidization problems due to the softening of magnesium sulfate for particles below 150 microns.

The type of reductant has an effect on the fluidizing behavior of the material: sulfur reacts very fast and consequently, no fluidization problems occur. The particles will dehydrate and decompose simultaneously in the initial stage of the reaction. In the presence of carbon and carbon monoxide, defluidization of the bed took place during the feeding period. As a result, dehydration only took place at the beginning, after which the bed was refluidized and decomposition at a high reaction rate commenced. Magnesium sulfate continues to decompose in a nitrogen atmosphere when there is no reductant present, but at a much lower rate than in the presence of a reductant. Fluidization problems especially occurred during the experiments with a particle size below 150 microns, due to inter-particle cohesion.

Magnesium sulfate decomposes directly to magnesium oxide without any intermediate forms, such as magnesium sulfite or magnesium sulfide under the experimental conditions used in this work. However, iron sulfate and manganese sulfate that were used as impurities did form an intermediate

sulfide. The structure of magnesium sulfate changes before it is fully decomposed, due to local decomposition within the crystal. A clear reaction front was observed with SEM/EDS analysis, both on grain and on single crystal scale. The decomposition reaction is strongly endothermic and therefore cools down the particle and surrounding gas significantly when the reaction occurs. The reaction can only continue after the particles and surrounding gas film are heated up again.

Kinetic modeling was used to determine the rate-controlling step for the decomposition of magnesium sulfate in the presence of a reductant under fluidizing conditions. It was found that the decomposition of magnesium sulfate monohydrate with sulfur as the reductant is controlled by chemical reaction at the unreacted interface. The rate-controlling step shifted to ash layer diffusion when dried magnesium sulfate heptahydrate was used as the reductant, due to the formation of a dense outer layer during drying. The rate-controlling step is gas film diffusion in the presence of carbon or carbon monoxide, due to the deposition of carbon on the surface of the particles. Fluidization problems may have influenced the results with these experiments. It needs to be taken into account that these findings are only valid under the experimental conditions that were used; different rate-controlling steps may be found under different conditions.

Operating window with sulfur as the reductant

The preferred raw material is magnesium sulfate monohydrate with a particle size of below 150 microns in order to achieve low sulfur concentrations in the final sample. Inter-particle cohesion, however, starts to play a role with particles below 150 microns, especially when dried magnesium sulfate heptahydrate is used as the feed material. The operating temperature should be 900°C; the reaction rate is too slow at 850°C and the surface area is considerably reduced at 950°C. The residence time should be two hours in order to reach 95% decomposition; >80% had decomposed when feeding was completed. Two times the stoichiometric amount of sulfur should be used, as only one time the stoichiometric amount would lower the reaction rate and four times would reduce the surface area of the particles. The presence of calcium sulfate should be avoided, as it does not decompose and forms compounds with magnesium sulfate. Small amounts of manganese sulfate do not have any effect on the decomposition of magnesium sulfate. Iron sulfate has a positive effect on the decomposition of magnesium sulfate: low sulfur

concentrations can be achieved with larger particle size groups of magnesium sulfate compared with decomposition of pure magnesium sulfate.

Operating window with carbon/carbon monoxide

The preferred raw material is magnesium sulfate monohydrate, with a particle size of up to 420-595 μm. The use of small particles, below 150 microns, should be avoided as cohesion between these fines causes defluidization of the bed. The preferred operating temperature is 850°C with carbon monoxide; the effect of temperature was not tested with carbon as the reductant. The carbon monoxide partial pressure should be 0.1 or twice the stoichiometric amount should be used when carbon is the reductant. With a residence time of two hours, 95% decomposition can be reached and directly after feeding >60% will have decomposed. Iron sulfate as the impurity has a slightly positive effect; manganese sulfate and calcium sulfate have neither a positive nor a negative effect on the decomposition of magnesium sulfate in the presence of carbon monoxide.

The operating window for the decomposition of magnesium sulfate is quite narrow, especially with sulfur as the reductant. The feed material should preferably be magnesium sulfate monohydrate, which may be difficult to control when the material comes from a process waste stream. This work is, however, a first step towards considering increased internal circulation of waste streams and thus a reduction of both waste streams and raw materials.

Future work

The results of this work have shown that it is possible to decompose hydrated magnesium sulfate in the presence of sulfur as the reductant, but that the operating is quite narrow. The presence of iron sulfate made it possible to use larger particle size groups of magnesium sulfate. It would be of interest to investigate further, what the particle size limits of magnesium sulfate are, as well as the minimum amount of iron sulfate to have any effect. The effect of the presence of iron sulfate on the reaction mechanism could also be further studied.

The magnesium oxide product, which can be used as a neutralizing agent in the leaching process, is very likely to contain impurities. The effect of these impurities on the leaching process can be evaluated, in order to determine

their possible maximum levels. In addition, methods to remove impurities either from the stage where magnesium sulfate is crystallized from the waste acid or after decomposition in the fluidized bed can be studied further.

References

1. Amundsen, K.; Aune, T. K.; Bakke, P.; Eklund, H. R.; Haagensen, J. Ö.; Nicolas, C.; Rosenkilde, C.; Van den Bremt, S.; Wallevik, O. Magnesium. In: *Ullmann's Encyclopedia of Industrial Chemistry, Vol. 22*; Electronic Release; Wiley-VCH: Weinheim, 2003.
2. Whittington, B. I.; Muir, D. Pressure Acid Leaching of Nickel Laterites: A Review. *Min. Pro. Ext. Met. Rev.* **2000**, *21*, 527-600.
3. Senanayake, G.; Childs, J.; Akerstrom, B. D.; Pugaev. Reductive Acid Leaching of Laterite and Metal Oxides – A Review with New Data for Fe(Ni,Co)OOH and a Limonitic Ore. *Hydrometallurgy* **2011**, *110*, 13-32.
4. Bunjaku, A.; Kekkonen, M.; Pekkarinen, S.; Taskinen, P. Effect of Sulphur Addition on Roasting Reduction of Saprolitic Nickel Ores in CO/CO_2 Gas Mixture. *Trans. Inst. Min. Metall. C.* **2013**, *122*, 15-24.
5. McDonald, R. G.; Whittington, B. I. Atmospheric Acid Leaching of Nickel Laterites Review. Part I. Sulphuric Acid Technologies. *Hydrometallurgy*. **2008**, *91*, 35-55.
6. Harris, G. B.; Magee, T. J.; Lakshmanan, V. I.; Sridhar, R. The Jaguar Inc. Sechol Laterite Project Atmospheric Chloride Leach Project. In: Imrie, William P.; Lane, David M. (eds.) International Laterite Nickel Symposium – 2004, TMS Annual Meeting, Charlotte, North Carolina, March 14-18, 2004.
7. Kay, H. Treatment of Nickeliferous Oxidic Materials for the Recovery of Nickel Values. U.S. Patent 3,466,144, 1969.
8. Bailey, R. P. Method for Extracting Nickel from Laterite Ores. U.S. Patent 2,899,300, 1959.
9. Lailach, G.; Gerken, R. Process for the Preparation of Sulfur Dioxide. U.S. Patent 4,824,655, 1989.

10. Cross, H. E., Krieger, W.; Anschutz, E.; Reh, L.; Hirsch, M. Process of Producing Magnesia with Sulfuric Acid Recycle. U.S. Patent 4,096,235, 1976.

11. Kobayash, S. Process for Reductive Calcining of Magnesium Sulfate. U.S. Patent 4,225,573, 1979.

12. Schoubye, P. C. S.; Hansen, O.E. A Process for the Regeneration of Mixtures Containing Sulphuric Acid and Metal Sulphates into Sulphuric Acid and Metal Oxides. E.P. Patent 0,125,142, 1984.

13. Roche, E. G.; Prasad, J. Magnesium Oxide Recovery. W.O. Patent 2007070973, 2007.

14. MinDat website for Mineralogical Data. Link: http://www.mindat.org/min-2204.html, accessed 09-06-2011.

15. MinDat website for Mineralogical Data. Link: http://www.mindat.org/min-1393.html, accessed 09-06-2011.

16. Nickel, E. H.; Nichols, M. IMA/CNMNC List of Mineral Names. Link: http://pubsites.uws.edu.au/ima-cnmnc/IMA2009-01%20UPDATE%20160309.pdf http://pubsites.uws.edu.au/ima-cnmnc/IMA2009-01%20UPDATE%20160309.pdf, accessed on 06.08.2013.

17. Genzelli, F. E. Scaling-Up Eutectic Freeze Crystallization. PhD Thesis, TuDelft, the Netherlands, 2008.

18. Grevel, K.-D.; Majzlan, J. Internally Consistent Thermodynamic Data for Magnesium Sulfate Hydrates. *Geochim. Cosmochim. Acta*. **2009**, *73*, 6805-6815.

19. Bonello, P.; Perthet, P.; d'Hendecourt, L. Identification of Magnesium Sulfate Hydration State Derived from NIR Reflectance Spectrography, Lunar and planetary science XXXVI, 2005. Link: http://www.lpi.usra.edu/meetings/lpsc2005/pdf/1996.pdf, accessed 09-04-2010.

20. Phadnis, A. B.; Deshpande, V. V. On the Dehydration of $MgSO_4 \cdot 7H_2O$. *Thermochim. Acta*. **1981,** *43*, 249-250.

21. Emons, H. H.; Ziegenbalg, G.; Naumann, R.; Paulik, F. Thermal Decomposition of the Magnesium Sulfate Hydrates under Quasi

Isothermal and Quasi Isobaric Conditions. *J. Therm. Anal.* **1990**, *36*, 1265-1279.

22. Seeger, M.; Otto, W.; Flick, W.; Bickelhaupt, F.; Akkerman, O. S. Magnesium Compounds. In: *Ullmann's Encyclopedia of Industrial Chemistry, Vol. 22*; Electronic Release; Wiley-VCH: Weinheim, 2011.
23. Chipera, S. J.; Vaniman, D. T. Experimental Stability of Magnesium Sulfate Hydrates that may be present on Mars. *Geochim. Cosmochim. Acta*. **2007***, 71,* 241-250.
24. Grevel, K.-D.; Majzlan, J.; Benisek, A.; Dachs, E.; Steiger, M.; Fortes, A. D.; Marler, B. Experimentally Determined Standard Thermodynamic Properties of Synthetic $MgSO_4 \cdot 4H_2O$ (Starkeyite) and $MgSO_4 \cdot 3H_2O$: A Revised Internally Consistent Thermodynamic Data Set for Magnesium Sulfate Hydrates. *Astrobiology*. **2012,** *12,* 1042-1054.
25. Steiger, M.; Linnow, K.; Ehrhardt, D.; Rohde, M. Decomposition Reactions of Magnesium Sulfate Hydrates and Phase Equilibria in the $MgSO_4$-H_2O and Na^+-Mg^{2+}-Cl^--SO_4^{2-}-H_2O System with Implications for Mars. *Geochim. Cosmochim. Acta*. **2011**, *75,* 3600-3626.
26. Fortes, A. D.; Wood, I. G.; Vocadlo, L.; Brand, H. E. A.; Knight, K. S. Crystal Structures and Thermal Expansion of α-$MgSO_4$ and β-$MgSO_4$ from 4.3-300K by Neutron Powder Diffraction. *J. Appl. Cryst*. **2007**, *40*, 761-770.
27. Donnay, J. D. H.; Ondik, H. M. Crystal Data Determinative Tables. Third Edition, Volume 2; Inorganic Compounds. NBS and JCPDS: Washington, D.C., 1973.
28. Rowe, J.; Morey, G. W.; Silber, C. C. The Ternary System K_2SO_4-$MgSO_4$-$CaSO_4$. *J. Inorg. Nucl. Chem.* **1967**, *27*, 925-942.
29. Du, H. Thermodynamic Assessment of the K_2SO_4-Na_2SO_4-$MgSO_4$-$CaSO_4$-System. *J. Phase Equilib*. **2000**, *21*, 6-18.
30. Powder Diffraction File. CD for XRD software. International Center for Diffraction Data, Pennsylvania, USA, 2001.
31. Binnewies, M.; Milke, E. *Thermochemical Data of Elements and Compounds;* Wiley-VCH: Weinheim, 2002.

32. Landolt-Börnstein. Thermodynamic Properties of Inorganic Materials: Pure Substances. Part 4, Compounds from HgH to ZnTe. Compiled by SGTE; Springer-Verlag: Berlin, 2001.

33. Chase, M. W. NIST-JANAF Thermochemical Tables, (4th ed.). *J. Phys. Chem. Ref. Data* **1998**, *9*, 1961.

34. Pankratz, L. B. *Thermodynamic Properties of Carbides, Nitrides, and other Selected Substances;* U.S. Dept. of the Interior: Washington, D.C., 1995.

35. Barin, I. *Thermochemical Data of Pure Substances, Part II*; VCH Verlags Gesellschaft: Weinheim, 1993.

36. Ko, H. C.; Daut, G. E. Enthalpies of Formation of α- and β-Magnesium Sulfate and Magnesium Sulfate Monohydrate. Report of Investigations 8409; United States Department of the Interior, Bureau of Mines: Washington, D.C., 1979.

37. Parker, V. B.; Wagman, D.D.; Evans, W.H. *Selected Values of Chemical Thermodynamic Properties, Tables for the Alkaline Earth Elements*. U.S. NBS. Tech. Note 270-6; U.S. GPO: Washington, D.C., 1971.

38. Rossini, F. D.; Wagman, D. D.; Evans, W. H.; Levine, S.; Jaffe, I. *Selected Values of Chemical Thermodynamic Properties*. NBS Circular 500, U.S. GPO: Washington, D.C., 1961.

39. Davies, R. H.; Dinsdale, A. T.; Gisby, J. A.; Robinson, J.; Martin, S. Thermodynamic and Phase Equilibrium Software from National Physical Laboratory. *Calphad*. **2002**, *26,* 229-271.

40. Gmelin, L. Gmelins Handbuch der Anorganischen Chemie, 8. Auflage. System nr. 27, Magnesium, Teil B, Lieferung 2. 1938, Verlag Chemie GmbH.

41. Patnaik, P. Magnesium Sulfate. In: *Handbook of Inorganic Chemicals*; McGraw-Hill: New York, 2003.

42. Lau, K. H.; Hildenbrand, D. L.; Cubicciotti, D. Thermal Decomposition of some Metal Sulfates. In: Proceedings of the Conference of the Fuels Division, ACS, New York, USA, 1976. p. 48-54.

43. Lau, K. H.; Cubicciotti, D.; Hildenbrand, D. L. Effusion Studies of the Thermal Decomposition of Magnesium and Calcium Sulfates. *J. Phys. Chem,* **1977,** *66*, 4532-4539.

44. Knittel, D. R.; Lau, K. H.; Hildenbrand, D. L. Effusion Studies of the Catalyzed Decomposition of Magnesium Sulfate. J. Phys. Chem. **1980**, *84*, 1890-1894.

45. Hulbert, S. F. Effect of Processing Parameters on the Kinetics of Decomposition of Magnesium Sulphate. Materials Science and Engineering, **1968**, *2*, 262-268.

46. Roine, A. HSC Chemistry 8.0 User's Guide. Report 14024-ORC-J. Outotec Research Center. Finland 2014.

47. Roine, A. HSC Chemistry 7.0 User's Guide. Report 09006-ORC-J; Outotec Research Oy: Finland, 2009.

48. Zambrano, A. Production of High Purity and High Surface Area Magnesium Oxide. W.O. Patent 8102153, 1981.

49. Plewa, J.; Steindor, J. Kinetics of Reduction of Magnesium Sulfate by Carbon Oxide. *J. Therm. Anal.* **1987**, *32,* 1809-1820.

50. Griessbach, R.; Bitterfeld, K.; Sutterlin, W.; Zirngibl, H.; Duisberg, W. H. Process of preparing magnesia and sulfur dioxide. U.S. Patent 2,230,592, 1939.

51. Wynn, N. P. Procédé d'Extraction du Nickel de Minerais Latéritiques. Patent FR 24485771980 (in French).

52. Lide D. R. (ed.). CRC Handbook of Chemistry and Physics, 77th edition. CRC Press, Cleveland, Ohio, 1996, pp. 5-20. ISBN 0-8493-0477-6.

53. Sohn, H. Y. Gas-Solid Reactions in Extractive Metallurgy, In: Metallurgical Treatises: Presentations at the USA-China Bilateral Conference. Tien, J. K., Elliott, J. F (eds), TMS, Warrendale, 1981, p. 23-39.

54. Levenspiel, O. *Chemical Reaction Engineering*, *third edition*. John Wiley and Sons, 1999. ISBN 0-471-25424-X.

55. Kunii, D.; Levenspiel, O. *Fluidization Engineering, second edition*. Butterworth-Heinemann, 1991. ISBN 0-409-90233-0.

56. Szekely, J.; Evans, J. W.; Sohn, H. Y. *Gas-solid reactions*. Academic Press Inc, New York. 1976. ISBN: 0-12-680850-3.

57. Geldart, D. Gas Fluidization Technology. John Wiley and Sons Ltd, Great Britain, 1986. ISBN: 0-471-90806-1.

58. Khawam, A.; Flanagan, D. R. Solid-State Kinetic Models: Basics and Mathematical Fundamentals. *J. Phys. Chem. B.* **2006**, *110*, 17315-17328.

59. F. Habashi. *Kinetics of Metallurgical Processes*. Metallurgy Extractive Quebec, 1999.

60. Botterill, J.S.M. *Fluidized Bed Behavior. In: Fluidized Beds, Combustion and Applications, eds. Howard,* J. Applied Science Publishers Ltd, 1983. ISBN: 0-85334-177-X.

61. Werther, *J. Fluidized Bed Reactors.* In: *Ullmann's Encyclopedia of Industrial Chemistry*. Electronic Release; Wiley-VCH: Weinheim, 2007.

62. Orth, A.; Kerstiens, B. Calcination and Reduction of Laterite Nickel Ores. In: Imrie, William P.; Lane, David M. (eds.) International Laterite Nickel Symposium – 2004, TMS Annual Meeting, Charlotte, North Carolina, March 14-18, 2004.

63. Trans Temp Furnace Home Page, link: http://www.thermcraftinc.com/transtemp-furnaces.html, accessed 04-02-2011.

64. TransTemp brochure: http://www.thermcraftinc.com/umages/pdf/TransTemp.pdf, accessed 21-02-2013.

65. NETZSCH Home Page. link: http://www.netzsch-thermal-analysis.com/en/products/detail/pid,13.html , accessed 21-04-2011.

66. Carbolite Home Page, link: http://www.carbolite.com/DocGallery2.asp, accessed 10-10-2012.

67. Carbolite Home Page, link: http://www.carbolite.com/doclib/rwf%20spec%20details.pdf accessed 21.02.2013.

68. Paulik, J.; Paulik, F.; Arnold, M. Dehydration of Magnesium Sulphate Heptahydrate Investigated by Quasi Isothermal-Quasi Isobaric TG. *Thermochim. Acta.* **1981,** *50*, 105-110.

69. Ducarroir, M.; Romero-Paredes, H.; Steinmetz, D.; Sibieude, F.; Tmar, M. On the Kinetics of the Thermal Decomposition of Sulfates Related with Hydrogen Water Splitting Cycles. *Int. J. Hydrogen Energy*. **1984**, *9,* 579-585.

70. Koopmans, K.; Voncken, J.H.L. *Fysische Chemie van de Vaste Stof*. Faculteit Civiele Techniek en Geowetenschappen, Afdeling Technische Aardwetenschappen, Sectie Grondstoffentechnologie, Delft, 2000.

71. Straszko, J.; Olszak-Humienik, M.; Mozejko, J. Kinetics of Thermal Decomposition of $ZnSO_4 \cdot H_2O$. *Thermochim. Acta*. **1997,** *292*, 145-150.

72. Gabal, M. A. Kinetics of the Thermal Decomposition of CuC_2O_4-ZnC_3O_4 Mixture in Air. *Thermochim. Acta*, **2003**, *402*,199-208.

73. Devia, M.; Wilkomirsky, I.; Parra, R. Roasting Kinetics of High-Arsenic copper contcentrates; a Review. *Miner Metall Proc*, **2012**, *29*, 121-128.

74. Yan, Z.; Wang, Z.; Liu, H.; Tu, Y.; Yang, W.; Zeng, H.; Qiu, J. Decomposition and Solid Reactions of Calcium Sulfate doped with SiO_2, Fe2O3 and Al_2O_3. *J. Anal Appl Pyrol,* **2015,** article in press.

75. Turkdogan, E. T.; Olsson, R. G.; Wriedt, H. A.; Darken, L. S. Calcination of limestone. *SME Transactions*. **1973**, *254*, 9-21.

76. Yan, L. Y.; Lu, X. F.; Guoi, Q.; Wang, Q. H.; Ji, X. Y. Research on the Thermal Decomposition and Kinetics of Byproducts from MgO Wet Flue Gas Desulfurization. *Adv Powder Technol*, **2014**, *25,* 1709-1714.

77. Yang, X.; Zhang, Z.; Wang, X.; Yang, L.; Zhong, B.; Liu, J. Thermodynamic study of Phosphogypsum decomposition by Sulfur. *J. Chem. Thermodynamics*. **2013,** *57,* 39-45.

78. McWilliams, J. P.; Hixson, A. N. Thermal Decomposition of Manganese Sulfate. *Ind. Eng. Chem. Process Des. Dev.,* **1976**, *15*, 365-371.

79. Linde, van der, B. J. An Experimental Study on the Use of Manganese Oxide on γ-Alumina Acceptors for Flue Gas Desulfurization. Delft University Press, 1982.

80. Zheng, M.; Shen, L.; Xiao, J. Reduction of $CaSO_4$ Oxygen Carrier with Coal in Chemical-Looping Combustion: Effect of Temperature and Gasification Intermediate. *Int. J. Greenh. Gas Control,* **2010***, 4*, 716-728.

81. Swift, W. M.; Panek, A. F.; Smith, G. W.; Vogel, G. J.; Jonke, A. A. Decomposition of Calcium Sulfate: A Review of the Literature, Argonne National Laboratory, Illinois, 1973.

82. Kaljuvee, T.; Trikkel, A.; Kuusik, R.; Bender, V. The Role of MgO in the Binding of SO_2 by Lime-Containing Materials. *J. Therm Anal Calorim,* **2005**, *80,* 591-597.

Aalto-DD 120/2015

ISBN 978-952-60-6346-1 (printed)
ISBN 978-952-60-6347-8 (pdf)
ISSN-L 1799-4934
ISSN 1799-4934 (printed)
ISSN 1799-4942 (pdf)

Aalto University
School of Chemical Technology
Department of Materials Science and Engineering
www.aalto.fi

BUSINESS +
ECONOMY

ART +
DESIGN +
ARCHITECTURE

SCIENCE +
TECHNOLOGY

CROSSOVER

**DOCTORAL
DISSERTATIONS**